Michigan Technological University

Digital Commons @ Michigan Tech

2022

THE PHOTO-TRANSFORMATION OF FREE METHIONINE IN THE PRESENCE OF SURROGATE AND STANDARD ISOLATE DISSOLVED ORGANIC MATTER UNDER SUNLIT IRRADIATION

Benjamin J. Mohrhardt
Michigan Technological University, bjmohrha@mtu.edu

THE PHOTO-TRANSFORMATION OF FREE METHIONINE IN THE PRESENCE
OF SURROGATE AND STANDARD ISOLATE DISSOLVED ORGANIC MATTER
UNDER SUNLIT IRRADIATION

By

Benjamin J. Mohrhardt

A THESIS

Submitted in partial fulfillment of the requirements for the degree of

MASTER OF SCIENCE

In Environmental Engineering

MICHIGAN TECHNOLOGICAL UNIVERSITY

2022

This thesis has been approved in partial fulfillment of the requirements for the Degree of MASTER OF SCIENCE in Environmental Engineering.

Department of Civil, Environmental, and Geospatial Engineering

Thesis Advisor: *Dr. Daisuke Minakata*

Committee Member: *Dr. Paul V. Doskey*

Committee Member: *Dr. Sarah Green*

Department Chair: *Dr. Audra Morse*

Table of Contents

List of Figures

List of Tables

Acknowledgements

Abstract

Sulfur (S)-containing amino acids are key sources of carbon, nitrogen, and sulfur involved in protein synthesis, protein function, and providing energy for microbial growth. Dissolved free and combined methionine is one of two S-containing amino acids incorporated into proteins and has been attributed to their stability and function. The oxidation of methionine has received considerable attention given its ubiquitous presence in most biological systems and has been associated with losses in protein function and pathological disorders. In natural waters, methionine is rapidly and selectively taken up by microorganisms to achieve cellular requirements of carbon, nitrogen, and sulfur. The abiotic transformation of methionine is ultimately a sink of key macronutrients and attributed to cycling across environmental compartments. In particular, the photochemical transformation of methionine in the presence of dissolved organic matter (DOM) is an important component of cycling in sunlit surface waters globally, yet knowledge is lacking on the fate and transformation of methionine in the environment.

In this study, we investigated the photo-transformation products involved in the photochemical fate of dissolved free methionine in the presence of surrogate and standard isolate dissolved organic matter (DOM). Temperature-dependent, bench-top photolysis experiments under simulated sunlight at 10, 20, and 30 $^{\circ}$C were conducted and a wide array of analytical analyses were employed to elucidate transformation products and provide insights into reaction mechanisms. Two surrogate DOM compounds structurally unique and relevant to complex mixtures of DOM were employed, including 1,4-naphthoquinone and 2-naphthaldehyde. The two surrogate DOM have common base structures and critical

functional groups known to be important photosensitizers in the natural environment generating photochemically-produced reactive intermediates including excited triplet-state chromophoric DOM, singlet oxygen, and hydroxyl radicals. The quinone and carbonyl functionalities in 1,4-naphthoquinone and aldehyde and naphthalene functionalities in 2-naphthaldehyde generated unique transformation pathways for methionine and novel photo-transformation products were identified, providing key insights into the mechanisms of transformation. Photolysis experiments were expanded to two unique standard isolate DOM (Suwannee River Humic Acid, Elliott Soil Humic Acid) and previously identified transformation products were quantified to validate results in environmentally-relevant solutions of DOM. Mass balance analyses were performed to assess the transformation of key macronutrients including carbon, nitrogen, and sulfur present in methionine.

1 Introduction

In natural waters, amino acids (AAs) and AA-based molecules are vital sources of carbon (C), nitrogen (N), and sulfur (S) that provide the building blocks for protein synthesis and energy for microbial growth.[1] AAs and AA-based molecules enter the environment naturally from allochthonous (e.g., terrestrial and vegetative debris in runoff) and autochthonous (e.g., algal exudates) sources of dissolved organic matter (DOM) and anthropogenic inputs such as wastewater effluents.[1,2] The discharge of wastewater effluents to surface waters results in high concentrations of effluent organic matter (EfOM), primarily consisting of soluble microbial products and assimilable organic matter (AOM), such as dissolved organic nitrogen (DON) and dissolved organic sulfur (DOS).[3,4] Considering that nearly half of the United States' drinking water treatment plants are impacted by upstream wastewater discharges and increasing potable reuse applications, human health and ecological impacts of EfOM will become more apparent.[5] Dissolved free amino acids (DFAAs) and combined amino acids (DCAAs) comprise a significant fraction of DON in wastewater EfOM. Contributions to total DON ranges from 1 to 7% for DFAAs and up to 20% for DCAAs.[6,7] Rapid and selective uptake of DFAAs and DCAAs has been reported, accounting for 20-65% of bacterial nitrogen demand.[8-10] In addition to bacterial nitrogen demand, S-containing DFAAs (e.g., methionine, cysteine) and DCAAs have been shown to be rapidly and selectively taken up to achieve cellular requirements of S.[11] Concentrations of individual S-containing amino acids are low; however, higher concentrations in cells further indicate rapid cycling in biota.[1,11] Although DFAAs only account for a few percent of total AAs, they are considered expensive in terms of energy

and rare considering abundance.[1] In particular, S-containing amino acids (i.e., methionine and cysteine) account for less than 5% of the total AA pool.[1,11] Thus, understanding the fate and transformation of S-containing amino acids in natural waters is a key component of the global cycling of essential macronutrients, including C, N, and S. Considering the low abundance of DFAAs and their rapid and selective bacterial uptake, abiotic transformations pathways play an important role for the fate of DFAAs.[1,12,13]

In sunlit surface waters, photochemical transformation is a key abiotic transformation pathway for DFAAs and a sink for DON.[6] Out of the 20 proteinogenic DFAAs, only five are susceptible to photochemical oxidation, including: tryptophan, tyrosine, histidine, cysteine, and methionine.[6,12-14] Photochemical transformation occurs via direct photolysis and indirect photolysis by photochemically produced reactive intermediates (PPRIs).[1] Tryptophan and tyrosine have been shown to undergo direct photolysis; however, direct photolysis is not considered the dominant degradation pathway for these DFAAs.[1,6] Consequently, indirect photolysis is the primary degradation pathway for all photo-viable DFAAs by the reactions with PPRIs, including excited triplet state chromophoric dissolved organic matter ($^3CDOM^*$), singlet oxygen ($^1O_2$), hydroxyl radicals ($HO^{\bullet}$), and hydrogen peroxide (H_2O_2).[1,6] In particular, the presence of chromophoric constituents in DOM (CDOM) play a critical role (Figure 1). The production of $^3CDOM^*$ plays an important role in natural waters as it has been shown to sensitize production of PPRI and the degradation of DFAAs.[6,15] Briefly, ground state CDOM absorbs light producing its singlet excited state ($^1CDOM^*$), which may undergo two major pathways: (1) non-radiative relaxation to the ground state or (2) intersystem-crossing (ISC) to the $^3CDOM^*$.[16-18]
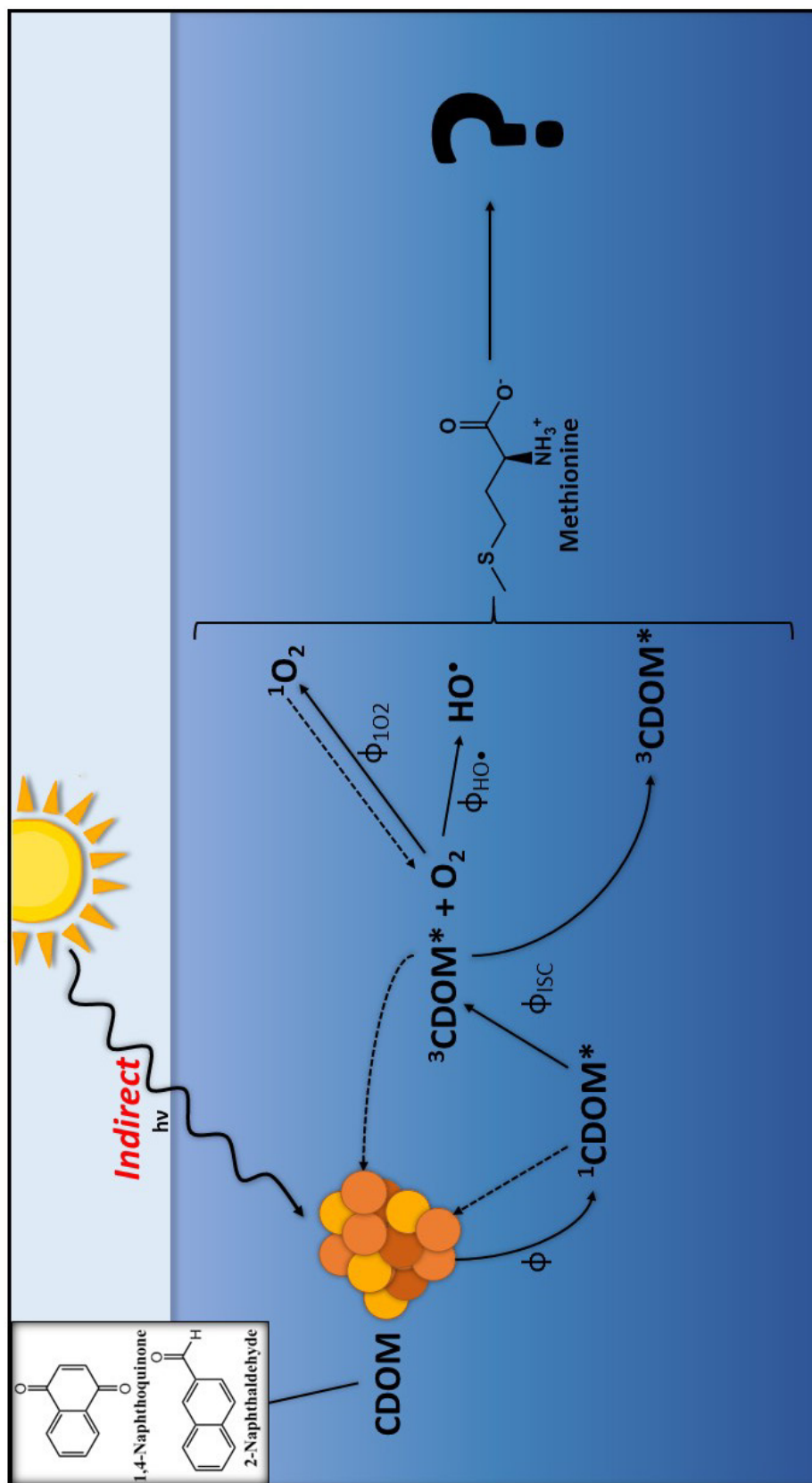
Figure 1. Schematic illustrating the CDOM photo-sensitized degradation of methionine in sunlit surface waters.

The first order rate constants of ^{3}CDOM* relaxation range from $(0.6 – 1.2) \times 10^5$ s^{-1}.[16] The

ISC process is rapid and the first order rate constant is estimated on the order of 10^{11} s^{-1}.[17]

The ^{1}O$_2$ is generated by temperature-dependent energy-transfer reaction of ^{3}CDOM* with

dissolved ground state molecular oxygen (^{3}O$_2$) and has been known to contribute to the

transformation of DFAAs.[11,12-16] The rates constant for production of ^{1}O$_2$ has been

previously estimated for well-defined sensitizers on the order of 10^9 M^{-1}s^{-1}.[15,18] This

process is driven the difference in the energy between the ^{3}CDOM* (140 – 300 kJ/mol for

single molecule sensitizers) and singlet-state for ^{3}O$_2$ (94 kJ/mol).[15] ^{1}O$_2$ can similarly

undergo temperature-dependent, non-radiative relaxation to the ground state (2.7 - 2.9 x

10^5 s^{-1}).[16] In general, initial transformations of DFAAs have been studied both

experimentally and computationally; however, the subsequent reactions with PPRI that

determine the fate of DFAAs in natural waters has not been elucidated yet due to the

complex radical-involved aqueous-phase reaction mechanisms and unknown properties of

complex mixtures of DOM.

The complex and highly diverse nature of DOM intrinsically relates the cycles of key

macronutrients: C, N, P, and S. While multiple studies have focused on the photo-

production of low molecular weight (MW) compounds and the photo-mineralization of

dissolved organic carbon (DOC),[19] DON,[19,20] and dissolved organic phosphorus (DOP),[20]

less attention has been given the photo-transformation of DOS constituents of DOM (e.g.,

S-containing amino acids). S is often not limiting in freshwaters;[21,22] however, recent

estimates suggest that average cellular requirements are similar to that of phosphorus

(C:N:P:S = 124:16:1:1.3).[23,24] Mass spectrometry studies on the photochemical lability of

DOS in various environments demonstrated more selective and rapid degradation of

CHOS-containing formulas relative to CHO, with conversion of CHOS into CHO-containing formulas.[25-28] More recent studies have investigated the photo-production of low MW DOS compounds (e.g., dimethyl sulfide, dimethyl sulfoxide, methanesulfonic acid)[13,19,29,30] and inorganic S (e.g., carbonyl sulfide, carbon disulfide, sulfate)[13,19,29] in aquatic systems. Furthermore, a comparison of the mass spectra of a reference NOM sample with EfOM showed significantly more S-containing molecular formulas (CHOS) unique to EfOM.[4] While environmental DOS concentrations are relatively rare compared to inorganic S in the literature, existing data suggests DOS cannot be ignored in the study of S-cycling. For example, Houle et al. 1995 demonstrated that DOS accounted for 9 – 22% of total S in 59 lakes in Quebec, Canada.[32] In particular, the photo-transformation of DOS in sunlit surface waters cannot be ignored as it is likely a key component for the turnover of DOS and has global-scale implications for S-cycling. Considering the rarity, energy expense of formation, and ubiquitous biological importance of S-containing amino acids, it is crucial to understand their photo-transformation pathways and byproducts. Furthermore, there is a need to better understand the role of different chromophoric functional groups in photo-transformation given the complex and widely diverse nature of environmental DOM.

In this study, we investigate the photo-transformation pathways and byproducts of free methionine (MET) in the presence of two surrogate DOM (i.e., 2-naphthaldehyde, 1,4-naphthoquinone) under bench-scale solar irradiation at pH 7 with 3 different solution temperatures (10, 20, and 30ºC). The two surrogate DOM have common structures found in complex mixtures of DOM, including quinone and carbonyl functionalities in 1,4-naphthoquinone and aldehyde and naphthalene functionalities in 2-naphthaldehyde (Figure

1). We use laboratory bench-scale experiments and a wide array of analytical analyses to identify product formation, provide insight into reaction mechanisms and guide theoretical investigations using density functional theory quantum mechanical calculations. We then utilize findings from surrogate DOM to investigate the photo-transformation pathways and byproducts produced in two standard isolate DOM derived from the environment, including Suwannee River Humic Acid (SRHA) and Elliot Soil Humic Acid (ESHA) under environmentally relevant conditions.

1.1 Transformation of Methionine: Overview

Over the years, the transformation of MET has been studied in various aspects of chemistry. It has received considerable attention in biological studies given its presence in proteins and importance in most biological systems.[33] In proteins, the oxidation of MET has been linked to losses in protein functionality and pathological conditions such as biological aging, neurodegenerative diseases (e.g., Alzheimer's disease), and even some cancers.[33-35] The photo-transformation of MET in foods and beverages (e.g., dairy products, beer, wine) has been linked with the production of flavor defects (e.g., rotten egg smell, cooked cabbage) and discoloration induced by the presence of photo-sensitizers (e.g., riboflavin, chlorins, porphyrins).[36-39] In sunlit aquatic systems, the presence of CDOM (Figure 1) and other oxidants have been attributed to the photo-transformation of MET.[6,13,20] Despite research thrusts in various fields, few studies have comprehensively studied the byproducts which is key to unlocking reaction mechanisms and ultimately the fate of MET in various environmental and biological compartments.

Proteins are subject to modification by various oxidants, produced deliberately (e.g., enzymatic intermediates, pathological response) and accidentally (e.g., exposure to chemicals, solar irradiation, radiation, or drugs).[33] The oxidation of side-chain MET in proteins to methionine sulfoxide (MetO) has received considerable attention in both environmental and human health aspects.[6,13,20,34,35] MET residues in proteins have been attributed to protein translation and stability, typically forming the hydrophobic core of proteins.[11,34,35] The oxidation of MET to MetO yields a decrease in hydrophobicity which may lead to changes in protein conformation and loss of function.[35] Conversely, MET residues can also act as antioxidants on the surface of proteins, providing protection to residues essential for protein functionality.[35] The reversibility of the oxidation of MET to MetO is owed to the ability of cells to reduce MetO via MET sulfoxide reductases (MSRs), but depends on accessibility of MSRs to oxidized MET residues.[34,35] While the oxidation of MET to MetO has been extensively studied by various 2-electron oxidants (e.g., hypohalous acids, iodic species, chloramines, H_2O_2, etc.)[35,40-44], $^1O_2$ has specifically received considerable and increasing attention over the years due to its prevalence in aquatic systems under sunlit irradiation, engineered water oxidation systems, and biomedical systems.[45,46]

The $^1O_2$-mediated oxidation of MET has been extensively studied and it is commonly understood that the main byproduct is MetO.[6,35,40,41,44] In addition, the mechanisms of MetO formation have been investigated both experimentally and theoretically.[35,40,44] It is generally understood that MET undergoes $^1O_2$-addition to the S-atom (k_{1O2} = 4.00 x 10^7 $M^{-1}s^{-1}$),[45] yielding a persulfoxide intermediate (Figure 2).[35,40,44,45] The persulfoxide intermediate then undergoes pH-dependent reactions via: (A) encounter

with another Met to form two sulfoxide in acidic solution and/or (B) OH⁻ attack on the sulfur, forming sulfoxide and H_2O_2 in basic solutions (Figure 2; Pathway A and B).[35,40,44] Dehydromethionine (DHM), a cyclic azasulfonium salt, has also been attributed to the $^1O_2$-mediated oxidation of MET via intramolecular interaction (Figure 2; Pathway C).[40,44]
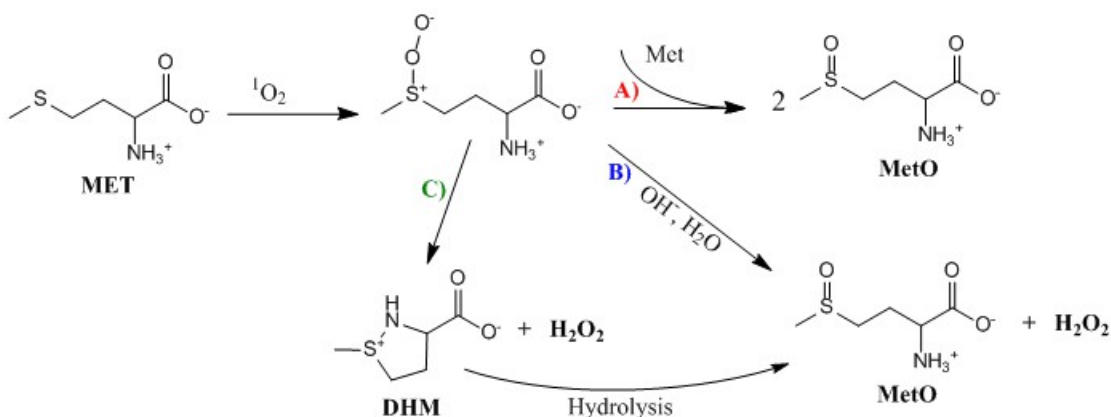
Figure 2. Schematic of the $^1O_2$-mediated oxidation of MET: A) encounter with another MET in acidic solution, B) OH- attack on the sulfur in basic solution, and C) intramolecular interaction with amine group.

DHM was first reported along with H_2O_2 and MetO as a co-products in the $^1O_2$-mediated oxidation of Met at pH 6-10 by Sysak et al. 1977,[40] then later in the reactive halogen (e.g., HOCl, HOBr, I_3^-, etc) induced oxidation of free MET and N-terminal MET residues in peptides and proteins by Peskin et al. 2009 and Beal et al. 2009.[42,43] Very recently, the works of Nascimento et al. 2022 demonstrated unequivocally that DHM is formed along with H_2O_2 and MetO by $^1O_2$ at pH 5.2, 7.4, and 9.2 with increasing amounts of DHM and H_2O_2 with increasing pH.[44] It is worth noting that the production of H_2O_2 as a reactive species has been associated with near full conversion to MetO.[43] At the neutral pH of 7, MET is in the zwitterionic form, where the carboxylic group (pK_a = 2.13) is deprotonated

with a negative charge and the amine group ($pK_b = 9.28$) is protonated with a positive charge, yielding a net neutral charge for the molecule.[35] As such, it is expected that mixture of mechanisms may occur with $^1O_2$-mediated degradation of MET as well as those described for the triplet-state-induced transformation in the remainder of this section.

While 2e-oxidants (e.g., $^1O_2$, H_2O_2, halogenated species) have received considerable attention in the oxidation of MET, the 1-electron oxidation (e.g., $^3CDOM*$, HO$^•$, other radical species) of MET is less understood despite potentially leading to irreversible biological damage.[34,47] This is primarily owed to the rapid production of highly reactive transients following 1e-oxidation and the subsequent complex degradation pathways.[47] In general, it is understood that the 1e-oxidation of MET produces radical cations of S and N as well as C-centered radical species.[37,47,48] Furthermore, the production and stabilization of these transient species is influenced by the nature of the oxidant, pH of solution, and neighboring functional groups, confounding the complexity of 1e-oxidation of MET.[47]

In the HO$^•$-mediated oxidation, the electrophilic nature of HO$^•$ lends itself to S-atom addition at diffusion-controlled rates.[47] The reaction steps that follow depend on pH. At neutral pH, it has been proposed that intramolecular interaction with the protonated amine group yields dihydroxylation and a three electron-bonded complex between the resulting –NH$_2$ and >S$^{+•}$, followed by opening of this complex to yield an N-centered radical cation (NH$_2^{•+}$).[47] The transfer of this electron to the unprotonated carboxylate group (-COO$^•$) promotes decarboxylation to form an α-amino-alkyl radical (α-N radical) with high reducing potential.[47]

Analogous mechanisms has been proposed for the carboxybenzophenone (CB)[47] and riboflavin[37] sensitized photo-transformation of MET; however, initial mechanisms of reaction for triplet state sensitizers (^{3}Sens*) involves the generation of charge transfer (CT)-complex with the S-atom at neutral and basic pH via single electron transfer (SET).[47] The summarized initial reaction pathways for CB are shown in Figure 3. Based on the CB-sensitized mechanisms, the CT complex ([CB$^{•-}$...>S$^{•+}$]) follows four major pathways for degradation: (1) charge separation producing CB$^{•-}$ and >S$^{•+}$ radicals, (2) proton transfer within complex to yield a ketyl radical (CBH$^•$) and a C-centered radical in the α-position relative to the S-atom (α-S), (3) transfer of a proton from the protonated amine group yielding a ketyl radical (CBH$^•$) and a >S$^{•+}$ radical with a deprotonated amine group, and (4) reverse electron transfer to restore the initial reactants (Figure 3).[47] The production of an unprotonated amine group in the >S$^{•+}$ radical stabilizes via formation of a three electron-bonded complex followed by decarboxylation to yield an α-N radical described in the HO$^•$ mechanism.[47] The >S$^{•+}$ radical with a protonated amine group can additionally be stabilized via intermolecular interaction with another MET, forming a three electron-bonded complex between two S-atoms ([S∴S]$^+$), or deprotonated to form an α-S radical.[47] The generation of these short-lived, transient species are simply the initial steps in the complex and predominantly irreversible transformation of MET and MET-containing proteins.[34] Such initial mechanisms have been proposed for other sensitizers, including pterins, flavins, and quinones.[41,47,50] Multiple studies on the photo-transformation of MET in food and beverages have described volatile byproducts such as methional,[36-39,47] methanethiol (MeSH),[35-39] dimethyl sulfide (DMS),[36] dimethyl disulfide (DMDS),[36-39] dimethyl trisulfide,[36] and acetaldehyde/CO_2.[36,47]
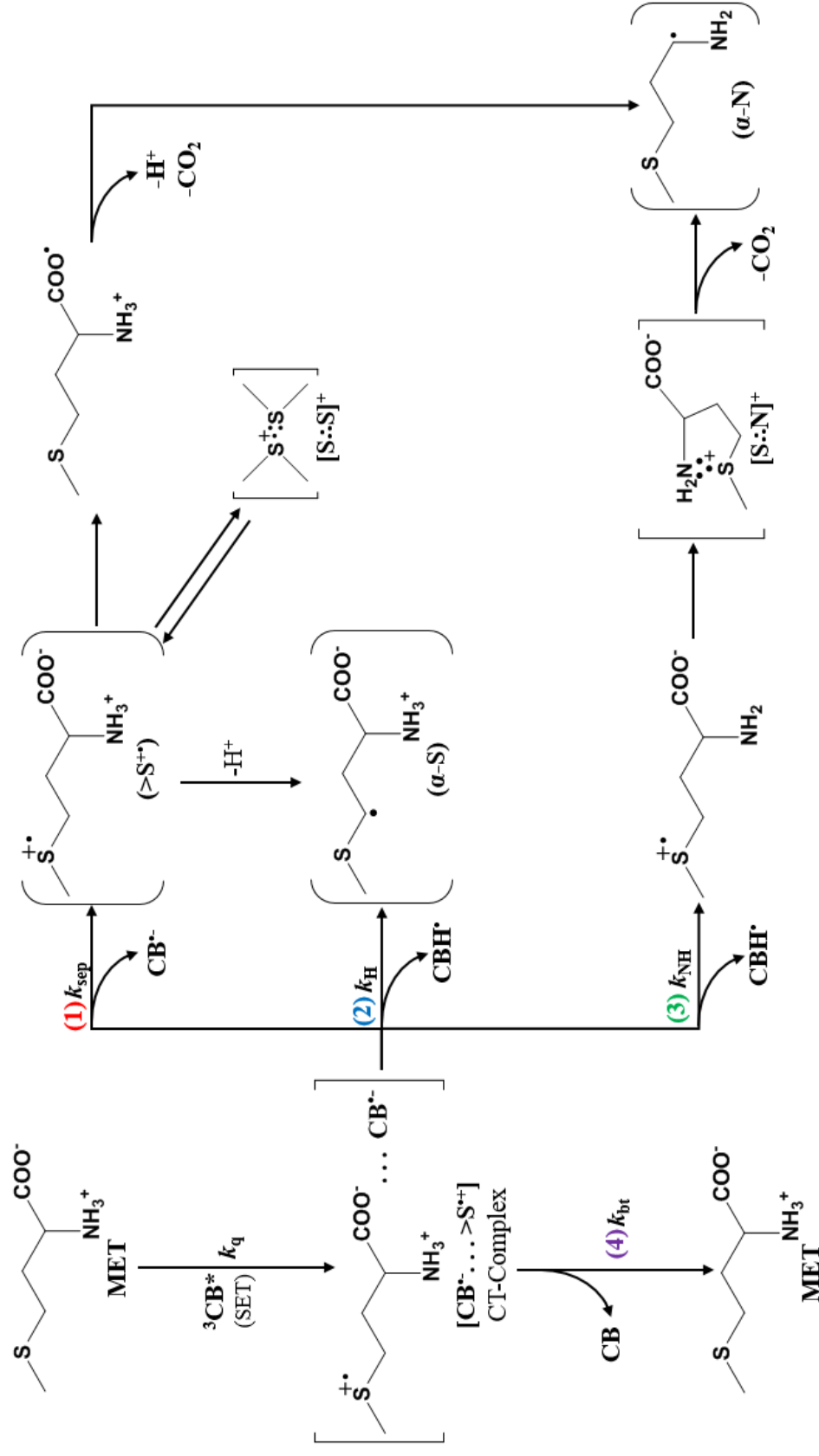
Figure 3. Schematic of photo-sensitized transformation of MET via triplet state single electron transfer in neutral, aqueous solutions. Based on the CB-sensitized mechanisms described by Marciniak & Bobrowski, 2022.

11

The production of methional from MET has been proposed to follow reaction pathways that form the decarboxylated α-N radicals, which reduce the ground-state sensitizer and hydrolyze to form methional and ammonium (NH_4^+).[47] The photo-ammonification of MET has been previously documented in the presence of surrogate DOM (i.e., anthraquinone-2-sulfonate, rose bengal),[49] standard isolate DOM (i.e. SRHA),[20] and in natural water samples.[49] The works by Zhang et al. 2021 utilized rose bengal (RB) to evaluate contribution of $^1O_2$ and anthraquinone-2-sulfonate (AQ2S) to evaluate the contribution of $^3CDOM^*$ to photo-ammonification of MET.[49] This group demonstrated significant photo-ammonification in AQ2S whereas little to none was observed in RB, suggesting the critical role of $^3CDOM^*$ in the photo-ammonification of MET.[49] The works by Ossola et al. 2019 described the photo-production of methanesulfonic acid (MSA) and sulfate from MET in the presence of a natural DOM sensitizer.[13] Evidently, the cleavage of the S – C bond in MET is of clear importance to 1e-induced oxidation and is likely associated with production of volatiles and photo-mineralization of C, N, and S. The formation of the $[S\therefore S]^+$ complexes has been proposed to produce DMDS via S – C cleavage of both MET molecules.[37] While methional is known to be unstable and further degrade to compounds such as MeSH, it is still not fully understood and three mechanisms have been proposed, including: (1) retro-Michael addition reaction to form MeSH and 2-propenal, (2) H abstraction followed by S – C cleavage, forming MeSH radical (MeS•) and 2-propenal, and (3) another SET between $^3Sens^*$ and methional, yielding MeSH, ethylene, and formic acid.[37] While production of methional is generally accepted, the works by Asaduzzaman et al. 2019 provided evidence that MeSH may also be formed directly from MET without methional as an intermediate.[36] They demonstrated rapid generation of MeSH and delayed

12

formation of methional, 2-propenal, and formic acid.[36] Utilization of a methional blocking

agent to mitigate degradation to MeSH further provided evidence of such a pathway.[36]

2 Materials and Methods

2.1 Chemicals

L-Methionine (≥99.5%), L-Methionine Sulfoxide (≥98%), L-Methionine Sulfone (≥98%), L-Aspartic Acid (≥99%), L-Serine (≥99%) were obtained from Sigma Aldrich. An aqueous working standard of 5 mM L-Aspartate 4-semialdehyde was obtained from GlycoFineChem. L-Homoserine (>98%) was obtained from Tokyo Chemical Industry (TCI). 3-methylthiolpropionaldehyde (Methional, 96%), dimethyl sulfide (≥99%), dimethyl disulfide (≥99%), thiophene (≥99%), ammonium sulfate (≥99%), methanesulfonic acid (≥99%), formic acid (≥96%), acetic acid (≥99%), and oxalic acid (≥99%) were obtained from Sigma Aldrich.

1,4- naphthoquinone (97%), 2-naphthaldehyde (98%), borax anhydrous (≥99.0%), sodium phosphate dibasic (≥99.0%), sodium phosphate monobasic (>99.0%), sodium azide (>99.8%), sodium hydroxide (≥ 98%), hydrochloric acid (37%), phosphoric acid (≥85%), sulfuric acid (99%), acetonitrile (UHPLC grade, ≥99.92), methanol (UHPLC grade, ≥99.92%), 2,4,6-trimethylphenol (97%), 4-chlorobenzoic acid (99%), furfuryl alcohol (98%), neocuproine (≥98%), copper (II) sulfate (≥99.99%), ferrous ammonium sulfate (≥99%), and ACS grade xylenol orange were obtained from Sigma Aldrich. O-phthaldehyde and 3-mercaptopropionic acid in a 0.4 M borate buffer and 0.4 N borate buffer (pH 10.2) were obtained from Agilent Technologies, Inc. Sodium chloride (≥99%) was obtained from Fisher Scientific and ACS grade ethanol was obtained from Pharmco-AAPER. Standard isolate DOM, including Suwannee River Humic Acid (SRHA; 3S101H)

and Elliott Soil Humic Acid (ESHA; 5S102H), were purchased from the International Humic Substances Society (IHSS).[51]

2.2 Experimental Methods

2.2.1 Temperature-Controlled Solar Irradiation Apparatus

Bench-top phototransformation experiments were conducted using an Atlas SunTest XLS+ (II) solar simulator equipped with a 1700 W xenon arc lamp and daylight filter to limit exposure of solutions to the ultraviolet-visible light range of 300 – 800 nm. Total irradiance was set to 500 W/m^2 in the solar simulator. Experimental irradiance measurements were collected with a Black Comet spectroradiometer (StellarNet Inc.) within the solar simulator and outside on our rooftop experimental platform at 47.12°N, 88.55° W on July 22nd, 2019 at 2 PM to validate the manufacturer-provided solar simulator irradiance with that of the solar spectrum (Figure 4).[52]
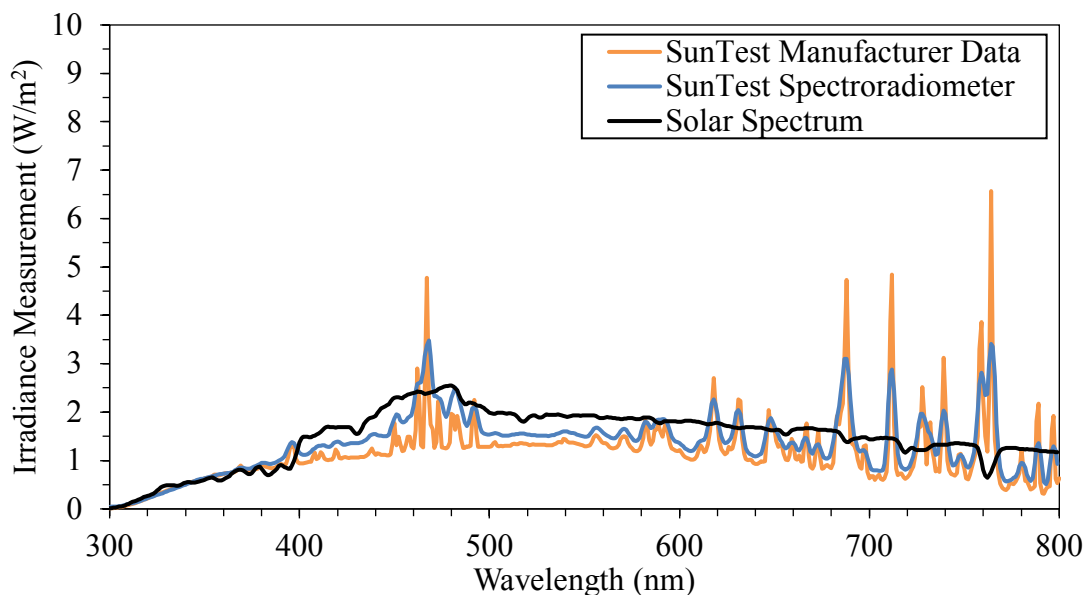
Figure 4. Irradiance Measurement for SunTest Simulator and Solar Spectrum.

Our group previously observed strong increases in solution temperature with exposure to solar irradiation (0.4 °C/min over first 15 minutes), indicating that circulating cooling air was not sufficient for strict temperature control. The solar simulator was fitted with a circulating water bath to control solution temperature throughout the experiments (Figure 5).
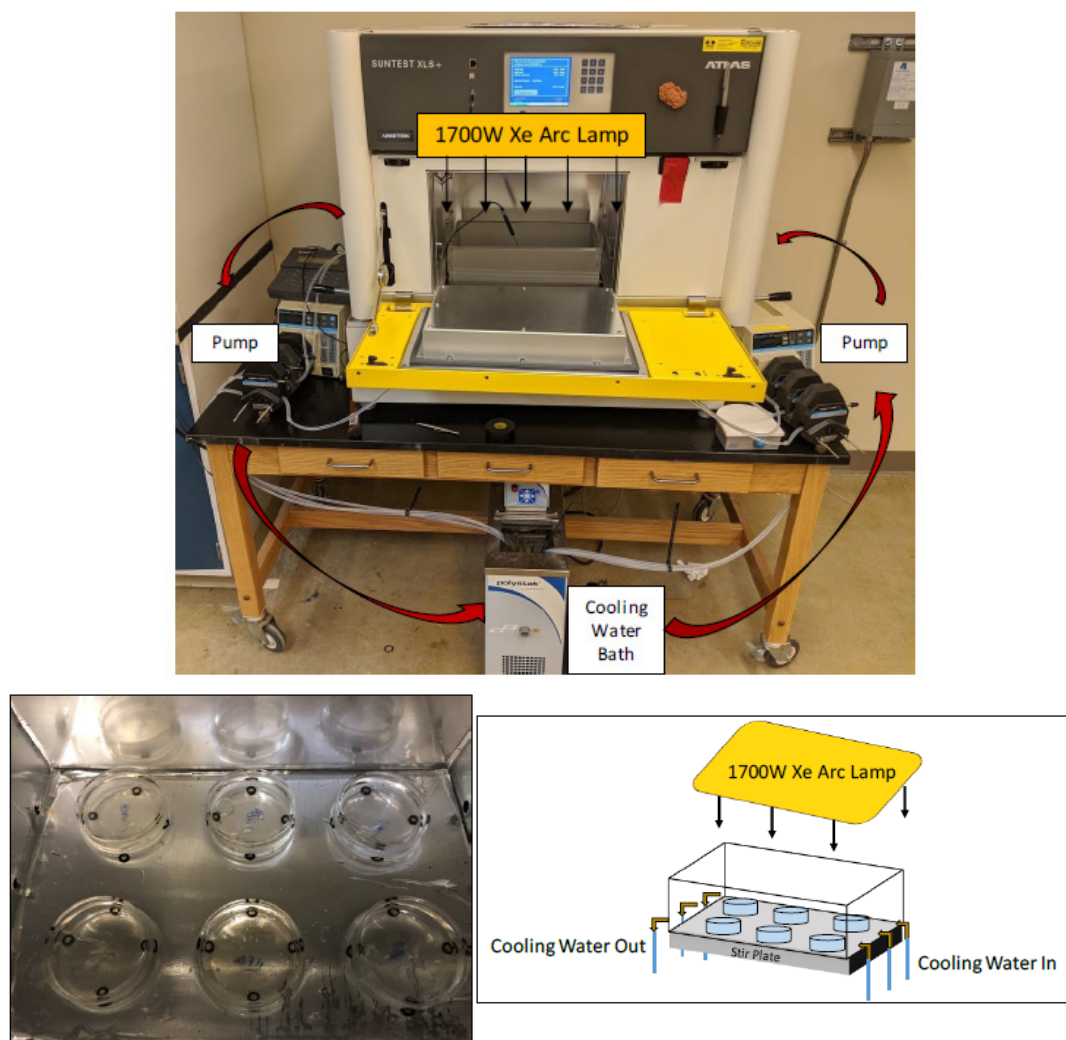
Figure 5. Experimental Setup for Solar-Simulated Transformation Experiments: Schematic of custom circulating water bath (top) and inner view of temperature-controlled water bath (bottom).

Briefly, two pumps circulate cooling water from the Cole Parmer Polystat Cooling/Heating Circulating bath to a custom built acrylic water basin on a six position magnetic stir plate within the simulator. Custom quartz photoreactors (50 mL) were placed on o-rings to maximize contact between reactors and cooling water during experiments (Figure 5). The temperatures studied included 10, 20, and 30 °C.

2.2.2 Photo-transformation Experiments

Bulk solutions were prepared containing 10 mg C/L of a single surrogate CDOM (i.e., 2-naphthaldehyde, 1,4-naphthoquinone) or standard isolate DOM (i.e., SRHA, ESHA) dissolved in a 1 mM phosphate buffer at neutral pH of 7. All solutions were prepared using Milli-Q grade water (resistivity > 18 MΩ, Millipore Milli-Q Gradient A10 purification system. Upon preparation, dissolution for 48 hours was allowed prior to using bulk solutions. All solutions were stored at 4°C while mixing. 24 hours prior to an experiment, approximately 600 mL of bulk CDOM solution was collected in a brown borosilicate bottle and placed in a Cole Parmer temperature-control bath to equilibrate the solution to the correct temperature. On the morning of experiments, methionine was spiked into solution and filtered through a 0.2 um polyethersulfone membrane filter. For photolysis of surrogate and standard isolate solutions, an equivalent volume of Milli-Q water was added in place of methionine stock solution. Solutions were transferred to clean brown bottles and placed in the water bath for an additional hour. The concentration of methionine was 30 μM in all experiments. 50 mL of solutions were transferred to photoreactors and placed in the solar simulator. A total of 6 photoreactors were used and to obtain enough volume to perform numerous analytical measurements, entire

photoreactors were pulled at specified times depending on the surrogate CDOM. For 2-naphthaldehyde, experiments were conducted for 60 minutes with sampling every 10 minutes. Experiments were conducted for 15 minutes with sampling every 2.5 minutes in 1,4-naphthoquinone due to its rapid photolysis. For photolysis of surrogate DOM, reduced time-steps were utilized. In standard isolate DOM solutions, experiments were conducted for 8 hours with sampling every 1 hour up to 4 hours, followed by every 2 hours up to 8 hours. Approximately 40 mL was collected and stored at 4°C immediately in amber vials. All analytical measurements were completed within two weeks of experiments.

Experiments were first conducted with surrogate DOM at 20°C to perform screening analyses of byproducts using UHPLC and direct infusion electrospray ionization mass spectrometry (ESI-MS). Once an idea of potential byproducts observed in experiments and literature was obtained, standards or high purity versions of commercially available compounds were purchased and utilized in calibration of analytical instruments for quantification. Experiments were then conducted at each solution temperature for surrogate CDOM then analyzed using the suite of analytical measurements described below. For standard isolate DOM, experiments were only conducted at 20°C.

2.2.3 Probe Compound Decay Experiments

Due to the typically low concentration and short-lived nature of PPRI (e.g., ^{3}CDOM*, $^1O_2$, HO•), probe compounds have been utilized extensively to provide indirect estimates of steady-state PPRI concentrations in both surrogate DOM solutions and standard isolate DOM.[15,46,53,54] We employed 2,4,6-trimethylphenol (TMP)[15,53,54] and furfuryl alcohol (FFA)[16,46,54] for the probing of ^{3}CDOM* and $^1O_2$, respectively. Estimation

of steady-state PPRI concentrations was completed using the observed pseudo-first-order decay rate constants (k'_{probe}) obtained in experiments and reported bimolecular reaction rates for FFA ($k^{FFA}_{^{1}O_2}$ = 1 x 10^8 $M^{-1}s^{-1}$)[54] and TMP ($k^{TMP}_{^{3}CDOM^*}$ = 2.0 x 10^9 $M^{-1}s^{-1}$)[54] in the following equations:

$$[^{3}CDOM^*]_{SS} = \frac{k'_{TMP}}{k^{TMP}_{^{3}CDOM^*}} \tag{2.1}$$

$$[^{1}O_2]_{SS} = \frac{k'_{FFA}}{k^{FFA}_{^{1}O_2}} \tag{2.2}$$

The preparation of experimental bulk solutions of surrogate and standard isolate DOM are described in the prior section (2.2.2 Photo-transformation Experiments). Stock solutions of FFA and TMP were prepared at concentrations of 1 mM. FFA stock solutions were stored at 4 °C and TMP was stored at room temperature, with constant mixing. The day prior to experiments, 250 mL of bulk surrogate or isolate DOM solution was collected in a brown borosilicate bottle and equilibrated to the desired temperature for 24 hours. On the morning of experiments, FFA or TMP were spiked into solution and filtered through a 0.2 um polyethersulfone membrane filter. The resulting solution was transferred to a fresh brown borosilicate bottle and allowed further temperature equilibration for an additional hour. The concentration of each probe compound was constant at 30 μM. Following equilibration, solutions were transferred to 50 mL photoreactors and placed in the solar simulator.

Our group previously investigated the temperature-dependent probe compound decay in 5 mg C/L surrogate DOM solutions[52] and for this reason, we only studied 20 °C at 10 mg C/L surrogate DOM concentrations. For surrogate DOM, previous investigations

into the temperature-dependent probe compound decay at 5 mg C/L over a two hour experiment revealed two-phase decay in 1,4-naphthoquinone, with a rapid initial phase up to 15 minutes followed by a much slower consumption of probe compounds up to 120 minutes.[52] In addition, full consumption of TMP was observed with 2-naphthaldehyde in the first 15 minutes.[52] For these reasons, we conducted experiments for only 10 minutes with sampling every 2 minutes to capture trends for surrogate DOM at 10 mg C/L. For standard isolate DOM solutions, we employed a 6 hour experiment with sampling every hour.

2.3 Analytical Methods

2.3.1 Ultra-High Performance Liquid Chromatography

2.3.1.1 Free Amino Acid Analysis

Free amino acids were detected and quantified using ultra-high performance liquid chromatography (UHPLC) via an online derivatization procedure using o-phthaldiadehyde/3-mercaptopropionic acid (OPA/3-MPA). This method was previously established in our laboratory and is based on methods and reagents described by Agilent Technologies.[55] The summary of the free amino acids used in calibration are listed in Table 1 along with structures, retention times, limits of detection (LOD), and limits of quantification (LOQ).

Table 1. Summary of free amino acids analyzed via UHPLC: structures, retention times, and detection limit parameters.

Name	Structure	Retention Time (min)	LOD (μM)	LOQ (μM)
L-Aspartic Acid (ASP)		1.05	0.02	0.05
L-Aspartate 4-Semialdehyde (ASA)		2.22	0.04	0.12
L-Serine (SER)		3.39	0.04	0.12
L-Methionine Sulfoxide (MetO)		4.59	0.04	0.12
L-Methionine Sulfone (MetOO)		5.00	0.03	0.10
L-Methionine (MET)		7.96	0.07	0.22

Free amino acids were separated using a gradient method consisting of A) 10 mM sodium phosphate dibasic: 10 mM borax anhydrous: 5 mM sodium azide (pH 8.20) and B) 45% acetonitrile: 45% methanol: 10% water by volume. The flowrate was 1.5 mL/min and the gradient program was as follows: 98% A: 2% B (0-0.35 min); 43% A: 57% B (0.35-13.4 min); 0% A: 100% B (13.5-15.7 min); 98% A: 2%B (15.8-18 min). Derivatization of free amino acids was achieved by mixing 52.5 uL of 0.4 N borate buffer (pH 10.2), 2.5 uL of OPA/3-MPA, and 1 uL of aqueous sample in the sample loop. To match mobile phase conditions, dilution with 15 uL of injection diluent (100 mL Mobile phase A + 0.4 mL 85% phosphoric acid) was performed and 2 uL was injected into the system. Amino acids were

separated on a reverse-phase Agilent AdvanceBio AAA column (4.6 mm x 100 mm, 2.7 um) at 40 ºC using a Dionex Ultimate 3000RS UHPLC. Detection was completed using fluorescence with excitation and emission wavelengths of 340 and 450 nm, respectively.

2.3.1.2 Probe Compound Analysis

2,4,6-trimethylphenol was employed as a triplet-state probe compound. Measurement was completed using an isocratic mobile phase and an Agilent AdvanceBio AAA column (4.6 mm x 100 mm, 2.7 µm). The flowrate was 1 mL/min and the column temperature was 40 C. The mobile phase composition was 45% water: 55% methanol. The injection volume was 50 uL and 2,4,6-trimethylphenol was detected using UV-detection at 220 nm. The retention time was 4.50 minutes. The limit of detection and quantification were 0.02 µM and 0.08 µM, respectively.

Furfuryl alcohol was employed as a probe compound for $^1O_2$ that was measured using an isocratic mobile phase and separated on an Agilent AdvanceBio AAA column (4.6 mm x 100 mm, 2.7 µm). The flowrate was 1 mL/min and the column temperature was 40 C. The mobile phase composition was 60% water: 40% methanol. The injection volume was 100 uL and 2,4,6-trimethylphenol was detected using UV-detection at 220 nm. The retention time was 1.50 minutes. The limit of detection and quantification were 0.13 µM and 0.40 µM, respectively.

2.3.2 Gas Chromatography combined with Mass Spectrometry
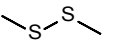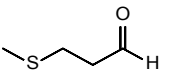
In order to measure volatile sulfur compounds (VSCs), gas chromatography combined with mass spectrometry (GC/MS) utilizing headspace solid-phase micro

extraction (HS/SPME). The method utilized was developed based on the studies reported in the literature for the same compounds of interest.[36-38,56] HS/SPME extraction was automated using the PAL3 autosampler, equipped with two heated agitation units and a SPME conditioning port. Briefly, samples were prepared by adding 5 mL of aqueous sample to a 20 mL headspace vial along with 1 g of sodium chloride (20% w/v) to improve analyte extraction to the headspace. The automated extraction procedure is as follows: equilibration to 50°C (20 minutes); extraction at 50°C (35 minutes); thermal desorption at 250°C (0.5 minutes). The agitation speed was kept constant at 500 rpm for equilibration and extraction. The SPME arrow employed was a PAL carbon-wide range/polydimethylsiloxane (C-WR/PDMS; dimensions). The SPME arrow was conditioned for 5 minutes pre- and post-desorption at 260°C in N_2 gas. To separate the VSCs, an Agilent 8890 gas chromatograph equipped with a Restek RXI-624Sil capillary column (30m x 0.25mm x 1.4μm) with an oven temperature as follows: 30°C (hold, 1.5 min); 120°C (25°C/min); 220° (45°C/min, hold 1 min). The GC inlet was maintained at a 10:1 split ratio to accommodate the wide range of compound boiling points and extraction efficiencies.

Detection of VSCs was completed using an Agilent 7010b triple-quadrupole mass spectrometer. First, standard solutions containing the relevant VSCs were analyzed in full-scan mode to obtain the total ion chromatogram (TIC). Fragmentation of ions was achieved using 70 electron volts and qualitative analysis was completed using Agilent MassHunter software. Mass spectra obtained from ion peaks were validated by comparing with fragmentation patterns observed in the NIST Mass Spectral database. Only matches with greater than 95% quality match were accepted. Standard solutions were then used to

develop a selected-ion-monitoring (SIM) method for quantification. Prior to analyzing standards using the SIM method, TIC's were collected from samples and NIST quality matches obtained for VSCs at each temperature. Detection was then optimized using time-segments for compounds that were expected in samples. Samples and standards were analyzed in triplicate. Thiophene was employed as an internal standard in calibration. Table 2 summarizes the detection parameters, NIST quality matches, and detection limits for each compound.

Table 2. Summary of volatile sulfur compounds analyzed via HS/SPME GC/MS: structures, retention times, NIST quality matches, and detection parameters.

Name	Structure	Retention Time (min)	NIST Quality Match	SIM Ions	LOD (µM)	LOQ (µM)
Thiophene*		6.11	98%	84, 56	n/a	n/a
Dimethyl Disulfide (DMDS)		9.15	98%	94, 78	0.06	0.18
Methional		7.12	97%	104, 76, 48	0.09	0.27
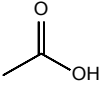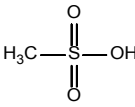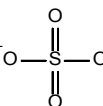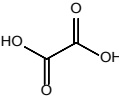
*Internal standard spiked at 1 µM for each standard and sample analyzed.

2.3.3 Anionic Chromatography and NH_4^+ Measurement

Anion chromatography was performed in the Chemical Advanced Resolution Methods (ChARM) Facility located at Michigan Tech University, as a part of the Chemistry Department and Michigan Tech's Micro-Analytical Facility (MAF). Briefly, a Dionex ICS-2100 equipped with an AS-17 column was utilized to separate and detect various anions via gradient elution. The mobile phase consisted of potassium hydroxide (KOH) and milli-Q water (MQ) and the gradient is as follows: 0 – 5 min (1 mM KOH,

isocratic), 5 – 10 min (1-10 mM KOH, gradient), 10 – 15 min (10 mM, isocratic), 15 – 25 min (10-40 mM, KOH gradient). The flowrate was 1 mL/min and the injection volume was 1 mL. Samples and standards were analyzed in triplicate. Anions quantified included: formate, acetate, oxalate, sulfate, and methanesulfonic acid (MSA). The structures, retention times, and detection parameters are summarized in Table 3. Samples and standards were analyzed in triplicate.

Table 3. Summary of anionic compounds analyzed via ion chromatography: structures, retention times, and detection limits.

Name	Structure	Retention Time (min)	LOD (μM)	LOQ (μM)
Acetic Acid		2.25	0.23	0.70
Formic Acid		2.61	0.30	0.90
Methanesulfonic Acid (MSA)		3.03	0.05	0.14
Sulfate		11.82	0.16	0.50
Oxalic Acid		12.42	0.49	1.48

Ammonium (NH_4^+) quantification was completed by the AQuatic Analysis (AQUA) lab and their employees located in the Great Lakes Research Center at Michigan Tech University, also a part of the Michigan Tech MAF. NH_4^+ was measured using a SEAL Analytical AQ-2 discrete analyzer under the Environmental Protection Agency (EPA)-approved method: AQ2 Method EPA-148-A Rev. 2.[57] Briefly, ammonia is reacted with hypochlorite previously released from dichloroisocyanurate, forming chloramine.

Salicylate is reacted with chloramine at alkaline pH of 12.6, forming indophenol blue dye. Colorimetric detection at 660 nm is used and related to the concentration of ammonium. The LOD and LOQ were 0.50 µM and 1.50 µM, respectively.

2.3.4 Non-Targeted Electrospray Ionization-Mass Spectrometry

Qualitative direct-infusion electrospray ionization-mass spectrometry (ESI-MS) was conducted in collaboration with the ChARM facility's technician. Briefly, standards and samples were diluted in methanol then injected directly to a ThermoScientific Ultrahigh Resolution Orbitrap Elite Mass Spectromer for ESI-MS. Samples were analyzed in both positive and negative polarity modes on the MS. The MS was operated in full scan mode with a mass range of 100 – 800 g/mol for screening of byproducts and mass spectra were collected by averaging 150 scans together. Mass spectra data was then input into a formula assignment software, MFAssignR, developed by the ChARM lab.[58] Molecular formula assignment was completed with allowable mass error of 2.5 ppm.

2.3.5 Spectrophotometric Measurements

2.3.5.1 Absorbance Measurement

All absorbance readings were conducted using a Hach DR 5000 spectrophotometer and a 1 cm quartz cuvette. Wavelength-scanning function was utilized to characterize the time-dependent absorption spectrums of surrogate and standard isolate DOM. Wavelength scans were obtained using a wavelength range of 280 – 800 nm, corresponding to the ultraviolet-visible (UV-VIS) range. For 1,4-naphthoquinone, time-dependent absorbance readings were taken at 0, 2.5, 5, 10, and 15 minutes. Measurements were taken every 20

minutes up to 60 minutes for 2-naphthaldehyde. For standard isolate DOM, measurements were taken every 2 hours up to 8 hours.

2.3.5.2 Hydrogen Peroxide Assays

Hydrogen peroxide (H_2O_2) was quantified using an adapted procedure with neocuproine (DMP) and copper (II) sulfate, followed by spectrophotometric measurement of absorbance at 454 nm.[59] Briefly, 10 mL of standard or sample was added to a 25 mL volumetric flask followed by 2.5 mL of 10 g/L DMP and 0.01 M Cu(II)SO$_4$. For the reagent blank and standards prepared in Milli-Q water, 10 mL of bulk surrogate DOM solution was added for background. The solutions were briefly mixed then diluted to the 25 mL mark on the flask. Micro stir-bars stirred solutions for an incubation time of 10 minutes. Immediate absorbance readings were taken at 454 nm in a 1 cm quartz cuvette. Absorbance measurements of surrogate DOM photolysis indicated that neither assay could not be used for 1,4-naphthoquinone due to production of hydroxylated forms that absorb light at and above 454 nm.[60] The established detections limits for this method were 0.20 μM and 0.60 μM for the LOD and LOQ, respectively.

For standard isolate DOM, H_2O_2 was quantified using an adapted procedure ferric xylenol orange (FOX) assay with spectrophotometric measurement at 580 nm.[61] Briefly, 10 mL of standard or sample was added to a 25 mL volumetric flask along with 10 mL of dilute sulfuric acid to achieve a concentration of 25 mM H_2SO_4. Next, 1 mL of 6250 μM ferrous ammonium sulfate and 1 mL of 2500 μM xylenol orange were added and mixed briefly. Milli-Q water was used to dilute reaction solutions to the 25 mL mark. The solution pH was approximately 1.8. Micro stir-bars were added and solutions were mixed for 30

minutes in the dark. Immediate absorbance readings were taken at 580 nm in a 1 cm quartz cuvette. The established detections limits for this method were 0.15 µM and 0.45 µM for the LOD and LOQ, respectively.

2.3.6 Dissolved Organic Carbon and Total Nitrogen

Dissolved organic carbon (DOC) and total nitrogen (TN) quantification was completed by the AQuatic Analysis (AQUA) lab and their employees located in the Great Lakes Research Center at Michigan Tech University, also a part of the Michigan Tech MAF. DOC and TN were quantified using a Shimadzu TOC-L$_{CPH}$ equipped with an inline TNM-L under Standard Methods for the Examination of Water and Wastewater: Method 5310-B (21st Edition).[62] Briefly, samples are acidified to promote conversion of inorganic carbon (IC) to CO_2 and sparged for removal. The remaining non-purgeable organic carbon (NPOC) is injected into a combustion tube where an oxidation catalyst is used to convert NPOC to CO_2 through combustion at 680ºC. The produced CO_2 is delivered in a carrier gas to a non-dispersive infrared gas analyzer for detection. Potassium hydrogen phthalate was utilized as a source for NPOC in standard solutions. All samples were measured in triplicate. The established LOD and LOQ for NPOC were 0.46 mg C/L and 1.39 mg C/L, respectively.

The inline TNM-L allows for subsequent measurement of TN in the same injection as for DOC. In the case of TN, samples injected are combusted at 720ºC promoting the decomposition of TN to nitrogen monoxide (NO) gas. NO is delivered via carrier gas to a chemiluminescence gas analyzer for detection. Potassium nitrate was utilized as a source

of TN in standard solutions. All samples were measured in triplicate. The established LOD and LOQ for TN were 0.05 mg N/L and 0.14 mg N/L, respectively.

2.4 Data Analysis

2.4.1 Conversion Calculations

For the conversion of MET to the measured byproducts in this study, concentration data was evaluated as the observed change in concentration relative to initial values for MET and products (Prod):

$$\Delta[\text{MET}]_t = [\text{MET}]_0 - [\text{MET}]_t \tag{2.3}$$

$$\Delta[\text{Prod}]_t = [\text{Prod}]_t - [\text{Prod}]_0 \tag{2.4}$$

For compounds detected in DOM photolysis and in the presence of MET, the contributions of DOM photolysis in measured byproducts was removed by subtracting the observed change in concentrations as shown in Equation 2.5:

$$\Delta[\text{Prod}]_{\text{corr, t}} = \Delta[\text{Prod}]_t - \Delta[\text{Prod}]_{\text{Photo, t}} \tag{2.5}$$

Where $\Delta[\text{Prod}]_{\text{corr, t}}$ represents the corrected change in concentration associated to the presence of is MET, $\Delta[\text{Prod}]_t$ is the change in concentration with MET present in DOM solutions, and $\Delta[\text{Prod}]_{\text{Photo, t}}$ is the change in concentration in background DOM photolysis experiments. The conversion of MET to each byproduct was then calculated at each time-step using equation 2.6:

$$\% \text{ Conversion} = \frac{\Delta[\text{Prod}]_{\text{corr, t}}}{\Delta[\text{MET}]_t} \times 100\% \tag{2.6}$$

% Conversion was averaged over the time-scale of the experiments at each solution temperature. In addition, an overall average and standard deviation was taken including all three temperatures to access differences in temperature.

2.4.2 Carbon and Nitrogen Mass Balance Calculations

DOC and TN measurements were performed to gain insight into changes in major elements during MET-sensitized degradation in all DOM solutions. MET degradation and byproduct formation were utilized to complete balances on both carbon and nitrogen. In order to assess the balance relative to measured values of DOC and TN, all the measured concentrations of byproducts were summed to obtain the calculated values (DOC_{calc}, TN_{calc}). Background experiments on DOM photolysis were included in the calculation as shown in equations 2.7 and 2.8 at each measured time-step for DOC and TN, respectively:

$$[DOC]_{calc,\,t} = [DOM]_t + [MET]_t + \Sigma[Prod]_t \qquad (2.7)$$

$$[TN]_{calc,\,t} = [DOM]_t + [MET]_t + \Sigma[Prod]_t \qquad (2.8)$$

Where $[DOM]_t$ represents the measured DOC or TN concentration from DOM photolysis, $[MET]_t$ is the measured MET concentration, and $\Sigma[Prod]_t$ is the sum of all byproduct concentrations at a specified time-step. For TN, the approach only differed for surrogate DOM in that background concentrations of TN were negligible and confirmed to be lower than the detection limit of the instrument. To further evaluate the calculations, we compared them with the measured values from MET degradation experiments at each time-step using the following equations:

$$\frac{[DOC]_{calc,t}}{[DOC]_{meas,t}} \times 100\% \qquad (2.9)$$

$$\frac{[\text{TN}]_{\text{calc,t}}}{[\text{TN}]_{\text{meas,t}}} \times 100\% \qquad\qquad (2.10)$$

This approach allows us to directly compare actual measured concentrations of specific compounds with changes observed in major elements. While there inherently exists errors in measurement and a potential confounding effect in such a calculation, a secondary evaluation of the % conversion in terms of DOC (mg C/L), TN (mg N/L), and S (mg S/L) was employed using equation 2.6. This provides a more direct measure of the conversion of C,N, and S from the parent MET molecule to products measured in experiments.

3 Results and Discussion

3.1 Dissolved Organic Matter (DOM) Photolysis

3.1.1 Surrogate DOM Photolysis

3.1.1.1 Photo-transformation of Absorption Spectra

The time-dependent absorption spectra was collected for each of the tested surrogate DOM to access significant changes in absorption in the UV-VIS range 300 – 800 nm. These time-dependent absorption spectra are depicted in Figure 6.
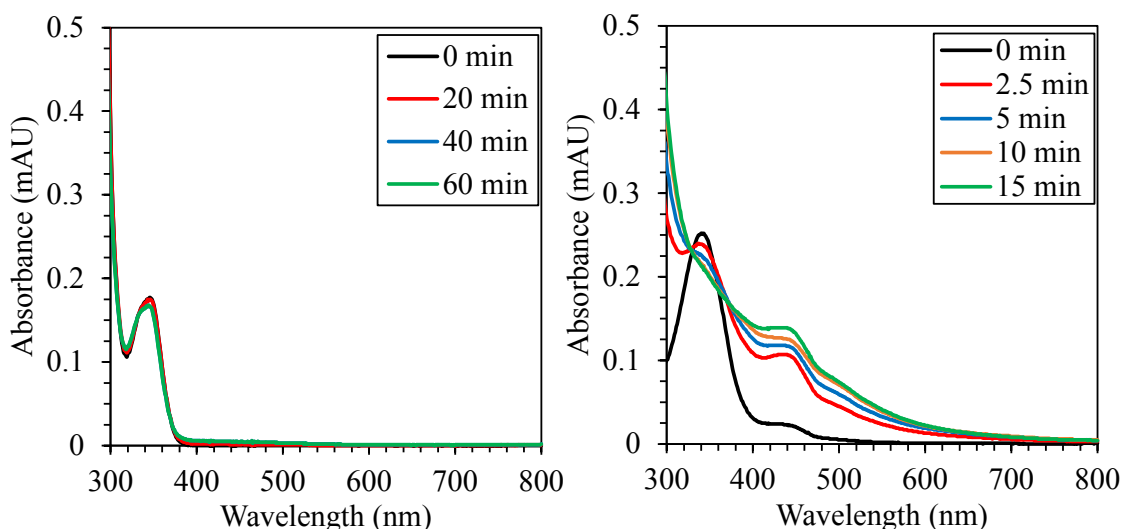
Figure 6. Time-dependent absorption spectra for 2-naphthaldehyde (left) and 1,4-naphthoquinone (right) at 20 ºC.

2-naphthaldehyde did not demonstrate significant changes in absorption spectra with time, indicating that it is not significantly photo-transformed when irradiated by sunlight. Conversely, significant changes in absorbance were observed in 1,4-naphthoquinone photolysis. Generally, increasing absorption was observed across the spectrum, with the exception of 330 – 360 nm where a decrease in absorption was observed. Furthermore, the

majority of changes in absorption occur in the first 2.5 minutes of 1,4-naphthoquinone photolysis, suggesting rapid photo-transformation.

McNeill & Canonica 2016 reported the triplet state energies and reduction potentials (E^{o*}) for both surrogate DOM tested.[15] The reported E_T for 2-naphthaldehyde is 249 kJ mol^{-1} and the E^{o*} is 1.48 V (SHE).[15] For 1,4-naphthoquinone, the reported E_T was 241 kJ mol^{-1} and the E^{o*} is 2.38 V (SHE).[15] The high reduction potential of triplet state 1,4-naphthoquinone (^{3}NQ*) indicates high reactivity that is associated with the significant photo-transformation observed in absorption spectra. Brahmia & Richard 2003 studied the photolysis of 1,4-naphthoquinone using 313 nm and 334 nm irradiation to elucidate influence of pH, photo-products, and transients.[60] Following irradiation at 334 nm, 1,4-naphthoquinone was completely consumed within 5 minutes supporting the rapid transformation that we have observed within 2.5 minutes. Several photo-products were identified, including: (1) 1,4-dihydroxynaphthalene (λ_{max} = 323 nm), (2) 7-hydroxy-1,4-naphthoquinone (7-OH-NQ; λ_{max} = 390 nm), (3) 5-hydroxy-1,4-naphthoquinone (5-OH-NQ; λ_{max} = 425 nm), and (4) 2-hydroxy-1,4-naphthoquinone (2-OH-NQ).[60] The observed increases in absorbance at 323 nm, 390 nm, and 425 nm indicate formation of a mixture of 1,4-dihydroxynaphthalene, 7-OH-NQ, and 5-OH-NQ in agreement with Brahmia & Richard 2003.[60] Based on observed transient species, Brahmia & Richard 2003 propose the rapid heterolytic addition of H_2O to the C_5 and C_7 carbons (k' = 2.25 x 10^6 s^{-1}) to ultimately form observed photo-products.[60] Very little literature information is available on the photolysis of 2-naphthaldehyde and our results suggest that relaxation pathways and energy-transfer with ground state molecular oxygen ($^3O_2$) are dominant, as indicated by little to no changes in absorption spectra.

3.1.1.2 Photochemical Production of Reactive Intermediates

The production of reactive intermediates was probed in surrogate DOM solutions using TMP for triplet states and FFA for $^1O_2$. The results for TMP decay are shown in Figure 7 for each surrogate DOM at 20 ^{o}C.

$$y = -0.087x$$
$$R^2 = 0.9662$$

$$y = -0.5823x$$
$$R^2 = 0.9559$$

10 mg C/L NA
10 mg C/L NQ
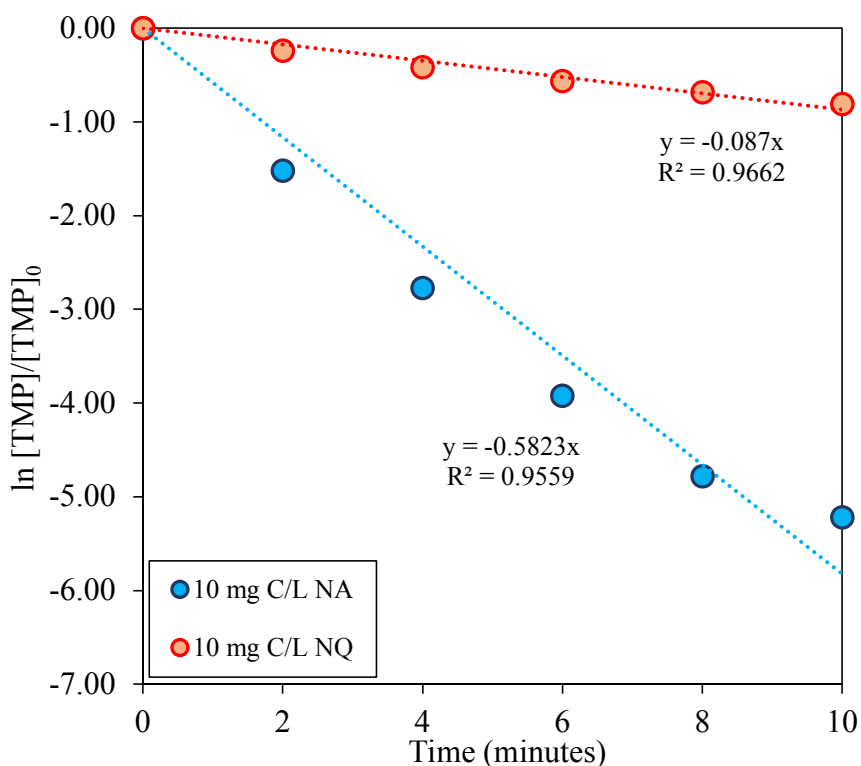
Figure 7. Time-dependent natural-log [TMP]/[TMP]$_0$ for both surrogate DOM at 20 ^{o}C.

TMP decay showed significant differences between the surrogates, with rapid decay of TMP observed in 2-naphthaldehyde solutions. The pseudo-first-order decay rates were 9.71×10^{-3} s^{-1} and 1.45×10^{-3} s^{-1} for 2-naphthaldehyde and 1,4-naphthoquinone, respectively. The corresponding [^{3}CDOM*]$_{ss}$ values were 4.85×10^{-12} M and 7.25×10^{-13} M for 2-naphthaldehyde and 1,4-naphthoquinone, respectively. The effectively complete consumption of TMP over 10 minutes in 2-naphthaldehyde suggest the highly efficient production of triplet state 2-naphthaldehyde (^{3}NA*). The lower TMP decay rates observed

34

in 1,4-naphthoquinone may be owed to competing reactions of TMP, H_2O, and $^3O_2$ with the $^3NQ^*$. The FFA decay is depicted in Figure 8 for the surrogate DOM at 20 °C.
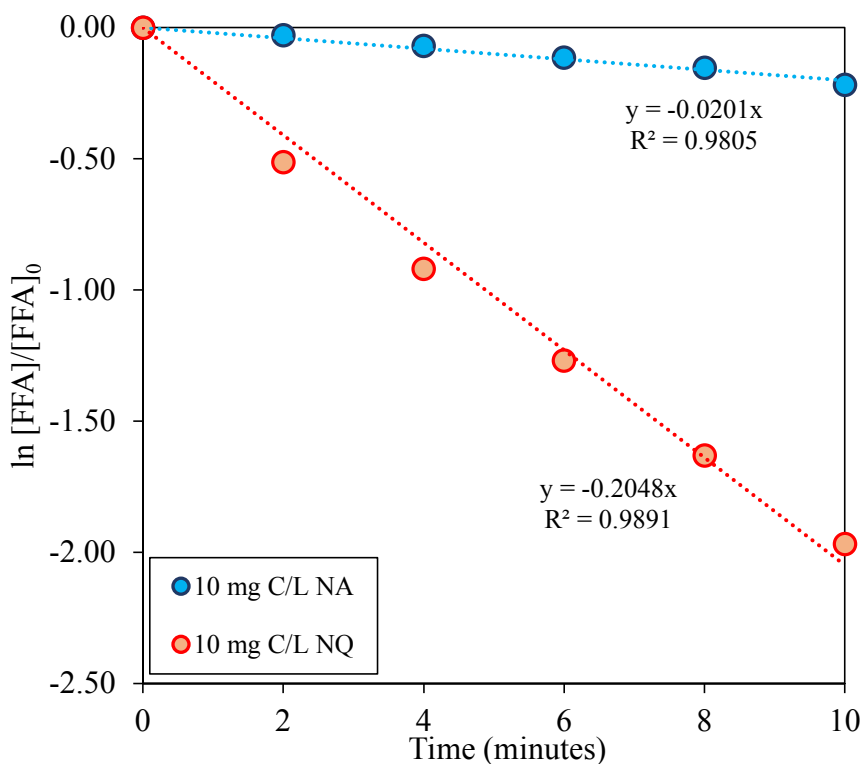
Figure 8. Time-dependent natural-log $[FFA]/[FFA]_0$ for both surrogate DOM at 20 °C.

Conversely to TMP, the decay of FFA was significant in 1,4-naphthoquinone compared to 2-naphthaldehyde solutions. Both pseudo-first-order rate constants and estimated $[^1O_2]_{ss}$ values were an order of magnitude higher in 1,4-naphthoquinone solutions. The pseudo-first-order decay rates were 3.35×10^{-4} s^{-1} and 3.41×10^{-3} s^{-1} for 2-naphthaldehyde and 1,4-naphthoquinone, respectively. The corresponding $[^3CDOM^*]_{ss}$ values were 3.35×10^{-12} M and 3.41×10^{-11} M for 2-naphthaldehyde and 1,4-naphthoquinone, respectively. This result suggests the highly efficient production of $^1O_2$ induced by $^3NQ^*$. This result suggests that energy transfer to O_2 may further be a competing reaction that yields the low rate of TMP decay and steady-state concentration

35

of ^{3}NQ*. In 2-naphthaldehyde, the steady-state concentrations of ^{3}NA* and ^{1}O$_2$ were on the same order of magnitude, which along with the minimal changes in absorption spectra may suggest that relaxation and energy transfer with ^{3}O$_2$ are the predominant decay pathways for ^{3}NA*. While the triplet energies of 2-naphthaldehyde (249 kJ mol^{-1}) and 1,4-naphthoquinone (241 kJ mol^{-1}) are sufficient to react with ^{3}O$_2$ (94 kJ mol^{-1}), it is hypothesized that the high reactivity of ^{3}NQ*(E^{o*} = 2.38 V) will lend itself single electron transfer (SET) with MET while also producing ^{1}O$_2$ as a reactive species.[15] The lower triplet reduction potential of ^{3}NA*(E^{o*} = 1.48 V)[15] may not be sufficient to induce significant SET of ^{3}NA* with MET, yet it is anticipated that ^{1}O$_2$ will be an active species in solution.

The production of H$_2$O$_2$ was also measured in surrogate DOM photolysis. Given the significant changes in absorption spectra for 1,4-naphthoquinone (Figure 6), the concentration of H$_2$O$_2$ could not be determined spectrophotometrically due to lack of available assay. Thus, only 2-napthaldehyde solutions were measured for H$_2$O$_2$ production in photolysis experiments. The time-dependent concentration profiles of H$_2$O$_2$ are shown in Figure 9 for 2-naphthaldehyde at 10, 20, and 30 ºC. The production of H$_2$O$_2$ was observed at all temperatures in 2-naphthaldehyde; however, little differences were observed between the different temperatures. On average between the temperatures, the amount of H$_2$O$_2$ formed in 2-naphthaldehyde photolysis was 1.10 ± 0.10 µM over the 60 minute irradiation. Overall, very little H$_2$O$_2$ is produced in 2-naphthaldehyde photolysis and is unlikely to contribute to the degradation of MET in these solutions.
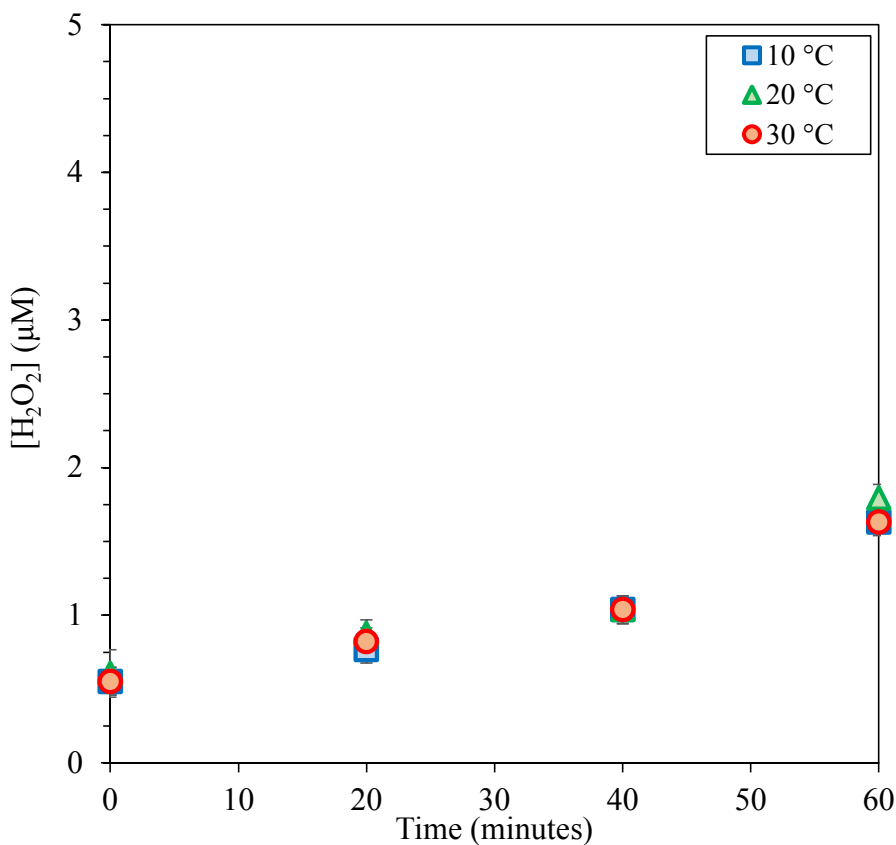
Figure 9. Time-dependent concentration profiles of H_2O_2 in 2-naphthaldehyde solutions at 10, 20, and 30 ºC. Error bars represent standard deviation of triplicate measurements.

3.1.1.3 Photo-production of Small Ionic Species

The photo-production of small ionic species (i.e., formic acid, acetic acid, oxalic acid) in photolysis background experiments was measured at 10, 20, and 30 ºC. Sulfate and ammonium were not measured in the photolyzed surrogate DOM solutions containing only carbon, hydrogen, and oxygen in their molecular formulas. The results for organic acid formation 2-naphthaldehyde are shown in Figure 10.
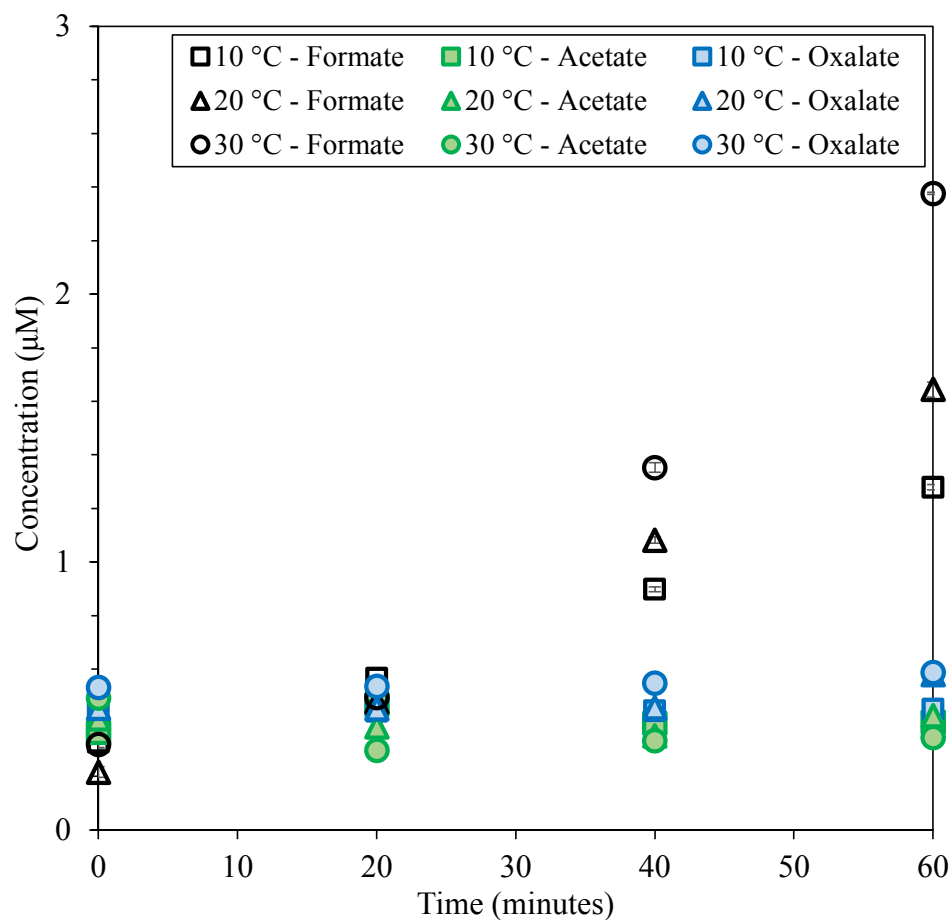
Figure 10. Time-dependent concentration profiles of organic acids in 2-naphthaldehyde photolysis at 10, 20, and 30 ℃. Error bars represent standard deviation of triplicate measurements.

The production of organic acids in the photolysis of 2-naphthaldehyde was only observed for formic acid. Temperature-dependent formation was apparent for formic acid, demonstrating increases of 1.00 μM, 1.40 μM, and 2.10 μM at 10, 20, and 30 ℃, respectively. Acetic and oxalic acids showed no significant changes in concentration with time. The organic acid formation in 1,4-naphthoquinone solutions is shown in Figure 11.
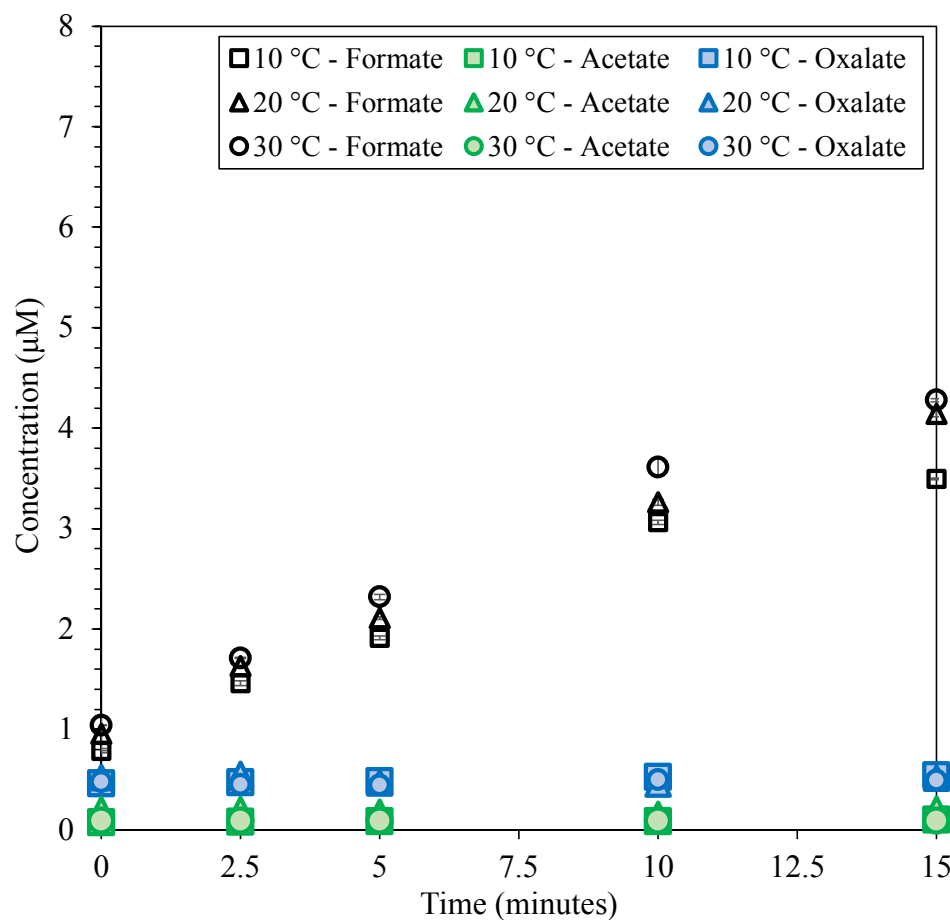
Figure 11. Time-dependent concentration profiles of organic acids in 1,4-naphthoquinone photolysis at 10, 20, and 30 °C. Error bars represent standard deviation of triplicate measurements.

Consistent with the significant photo-transformation depicted by the absorption spectra and in the literature, the production of formic acid was more significant in 1,4-naphthoquinone solutions. The concentration of formic acid increased by 2.70, 3.20, and 3.20 μM at 10, 20, and 30 °C, respectively. The production of acetic and oxalic acids was not significant in 1,4-naphthoquinone solutions.

3.1.2 Standard Isolate DOM Photolysis

3.1.2.1 Photo-transformation of Absorption Spectra

As with the surrogate DOM, the time-dependent absorption spectra of each standard isolate DOM was accessed for significant changes in absorption in the 300 – 800 nm range. The absorption spectra for Suwannee River Humic Acid (SRHA) and Elliott Soil Humic Acid (ESHA) are shown in Figure 12 at 20 °C.
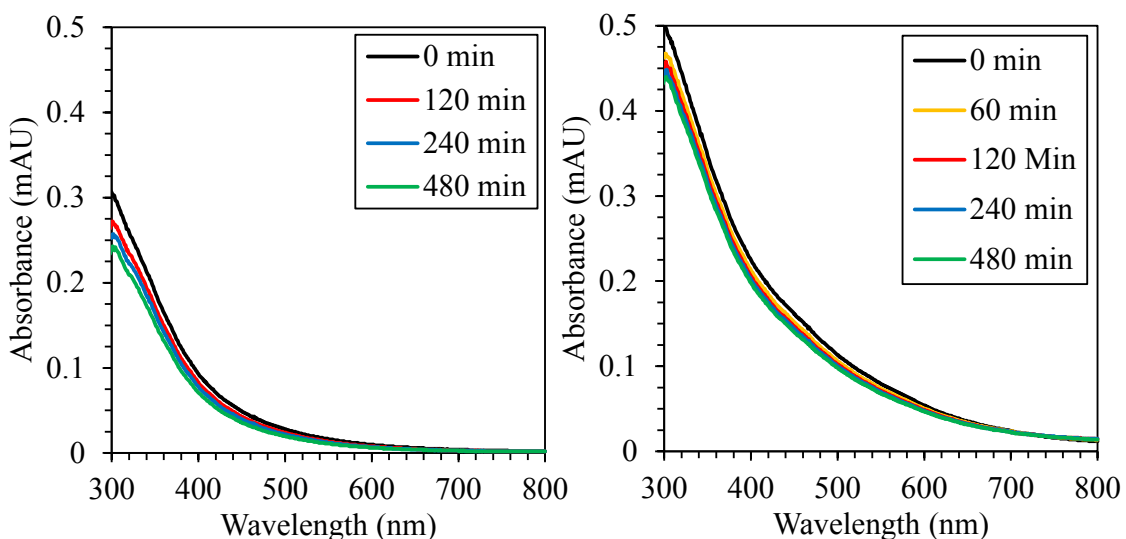
Figure 12. Time-dependent absorption spectra for SRHA (left) and ESHA (right) at 20 °C.

Comparing the two isolate DOM, ESHA demonstrates generally higher absorption than SRHA across the range of wavelengths relevant to sunlight. Both SRHA and ESHA demonstrated loss of absorbance, predominantly in the 300 – 600 nm range. These results do not show highly significant changes in absorption for either standard isolate DOM, indicating only minimal fractions of chromophores are transformed. In standard isolate DOM, the combination of different functional groups and their properties yield the macroscale properties that are observed.[15] Thus, estimates of triplet reduction potentials

and energies are lacking as natural DOM consists of multiple pools of ^{3}CDOM* with varying energy. Parker & Mitch estimated Suwannee River DOM to have triplet reduction potential in the range of 1.6 – 1.8 V (SHE),[63] which is comparable to that of 2-naphthaldehyde.

3.1.2.2 Photochemical Production of Reactive Intermediates

Probing of reactive species in standard isolate DOM yielded some key differences between the two isolate DOM tested. The time-dependent decay of TMP is depicted as the natural-log normalized concentration in Figure 13.
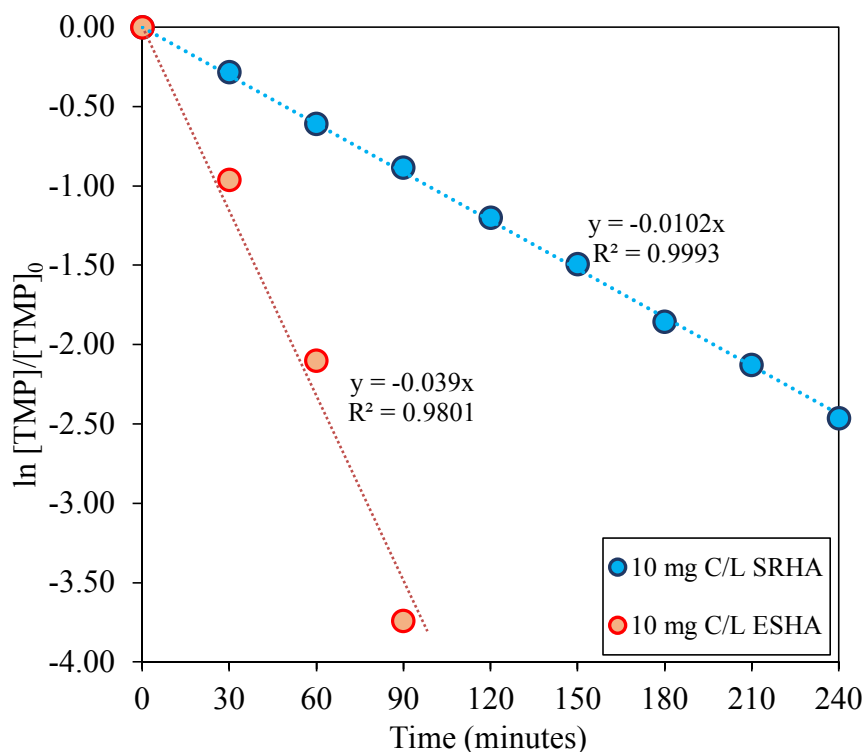
Figure 13. Time-dependent natural-log [TMP]/[TMP]$_0$ for standard isolate DOM at 20 ºC.

In ESHA solution, TMP decay was rapid and full consumption was observed within the first 90 minutes of irradiation. TMP remained available for quenching of triplet states throughout the 240 minute experiment in SRHA solution. The pseudo-first-order decay

rates were 1.70×10^{-4} s^{-1} and 6.50×10^{-4} s^{-1} for SRHA and ESHA, respectively. The corresponding estimates of $[^3CDOM^*]_{ss}$ were 8.50×10^{-14} M and 3.25×10^{-13} M for SRHA and ESHA, respectively. The increased rate of TMP decay and higher absorption spectra in ESHA suggest more efficient production of triplet states compared with SRHA. Thus, production of $^1O_2$ was anticipated to be significantly increased in ESHA solution. The time-dependent decay of FFA is depicted as the natural-log normalized concentration in Figure 14.
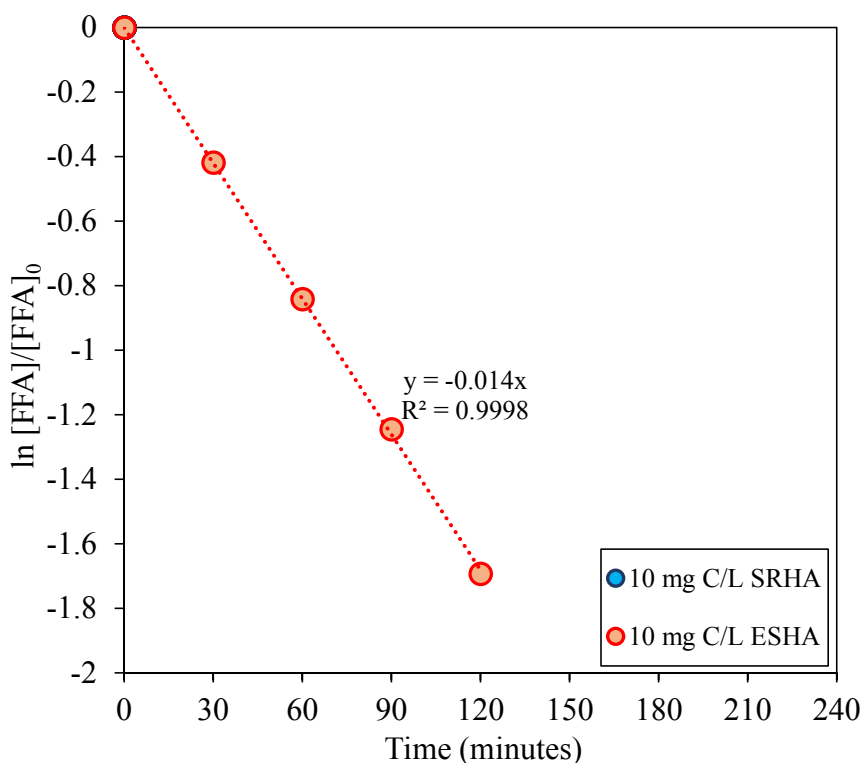
Figure 14. Time-dependent natural-log $[FFA]/[FFA]_0$ for standard isolate DOM at 20 ^oC.

Consistent trends with TMP were observed for the FFA decay in standard isolate DOM solutions. ESHA demonstrated more rapid decay of the $^1O_2$ probe compared to SRHA, decreasing to 18% of the initially added concentration over just 120 minutes. Once again, FFA remained available for quenching $^1O_2$ over the 240 minute experiment. The

pseudo-first-order decay rates were 0.38 x 10^{-4} s^{-1} and 2.30 x 10^{-4} s^{-1} for SRHA and ESHA, respectively. The corresponding estimates of $[^1O_2]_{ss}$ were 3.80 x 10^{-13} M and 2.30 x 10^{-12} M for SRHA and ESHA, respectively. For comparison, another study estimated the $[^1O_2]_{ss}$ on the order of 7.60 x 10^{-14} M for SRHA and 6.70 x 10^{-13} M for ESHA at 5 mg C/L each, which generally agree with our values determined at 10 mg C/L.[64] These results indicate the higher production of reactive species in ESHA solution will yield increased decay of MET, particularly by that of $^1O_2$. Based on the previous estimates of triplet reduction potential for SRNOM similar to that of 2-naphthaldehyde and the presence of low- and high-energy triplet pools in complex DOM, it is anticipated that $^1O_2$ will likely be the dominant reactive species.

The production of H_2O_2 was additionally quantified in each standard isolate DOM solution tested. The time-dependent H_2O_2 concentrations for SRHA and ESHA at 20 °C are shown in Figure 15. Both SRHA and ESHA demonstrated significantly more formation of H_2O_2 than in 2-naphthaldehyde solutions. Comparing the two isolates, the production of H_2O_2 was more significant in ESHA with higher background concentrations, consistent with higher production of $^3CDOM^*$ and $^1O_2$ indicated by probe compound decay. Specifically, the formation of H_2O_2 over the 480 minutes was 9.80 μM in SRHA and 12.00 μM in ESHA. Such concentrations of H_2O_2 may participate in the degradation of MET, either through direct reaction or indirectly through H_2O_2 photolysis, producing $HO^•$. While this cannot be ignored, it is not likely to compete with other reactive species that are expected to contribute significantly to the decay of MET in standard isolate DOM solutions (i.e., $^3CDOM^*$, $^1O_2$).
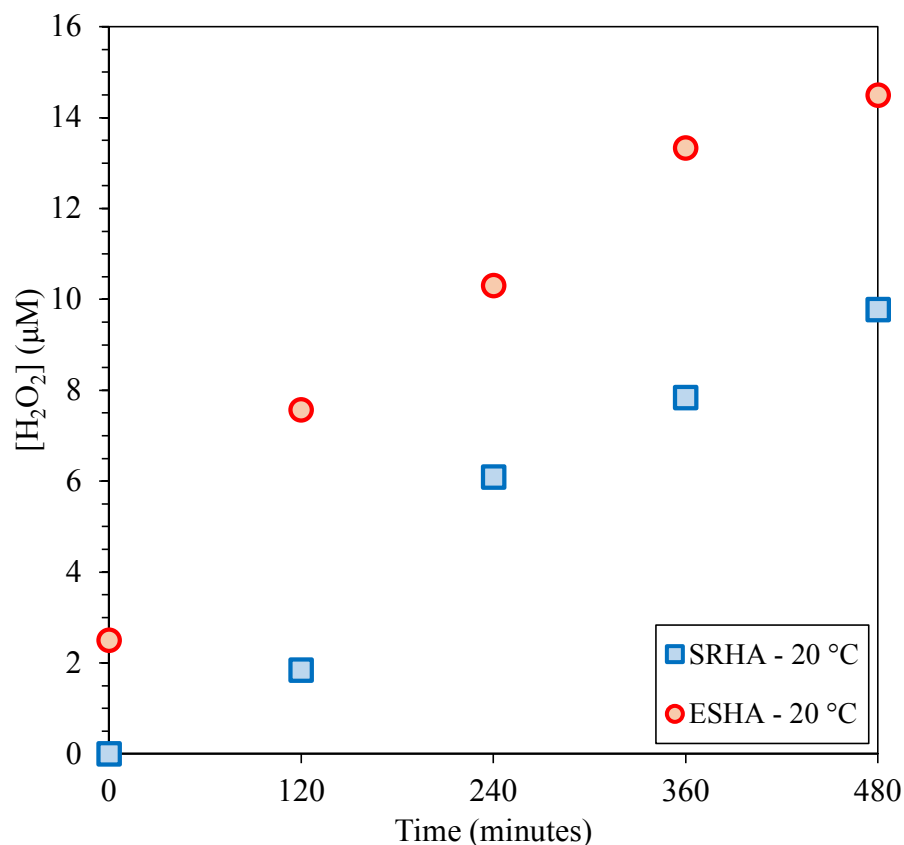
Figure 15. Time-dependent concentration profiles of H_2O_2 in standard isolate DOM photolysis at 20 ℃. Error bars represent standard deviation of triplicate measurements.

3.1.2.3 Photo-production of Small Ionic Species

The photo-production of organic acids (i.e., formic acid, acetic acid, oxalic acid, methanesulfonic acid) as well as inorganic constituents (i.e., sulfate, ammonium) were measured in standard isolate DOM solutions due to the presence of N and S-containing formulas in naturally-derived DOM. The time-dependent concentration profiles for each compound are shown in Figure 16 for SRHA photolysis at 20 ℃.
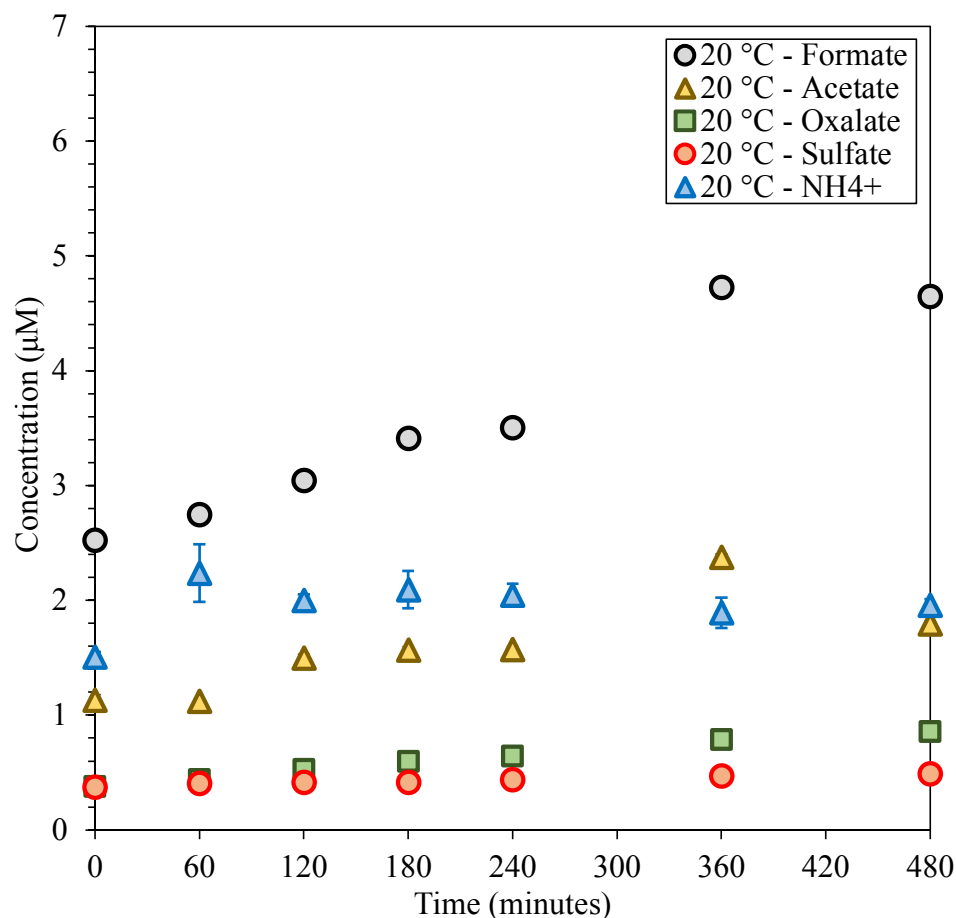
Figure 16. Time-dependent concentration profiles of organic acids and inorganic compounds in SRHA photolysis 20 °C. Error bars represent standard deviation of triplicate measurements.

Consistent with the results for surrogate DOM, the formation of formic acid was the most significant compound formed in SRHA photolysis. Comparing the organic acids, the amount of formation observed in order of decreasing significance was: formic acid (2.10 µM) > acetic acid (1.70 µM) > oxalic acid (0.60 µM). The photo-production of sulfate was minimal in SRHA photolysis, with a change in concentration of 0.12 µM over 480 minutes and an average concentration of 0.43 ± 0.04 µM. Photo-ammonification appeared to occur within the first 60 minutes of the experiment, followed by fairly stable concentrations of

NH$_4^+$ up to 480 minutes. The maximum change in concentration was 0.70 µM at 60 minutes while at 480 minutes it was only 0.45 µM. This result should be taken with caution as it may be a result of error in the initial measurement at 0 minutes. The time-dependent concentration profiles for each compound are shown in Figure 16 for ESHA photolysis at 20 ºC.
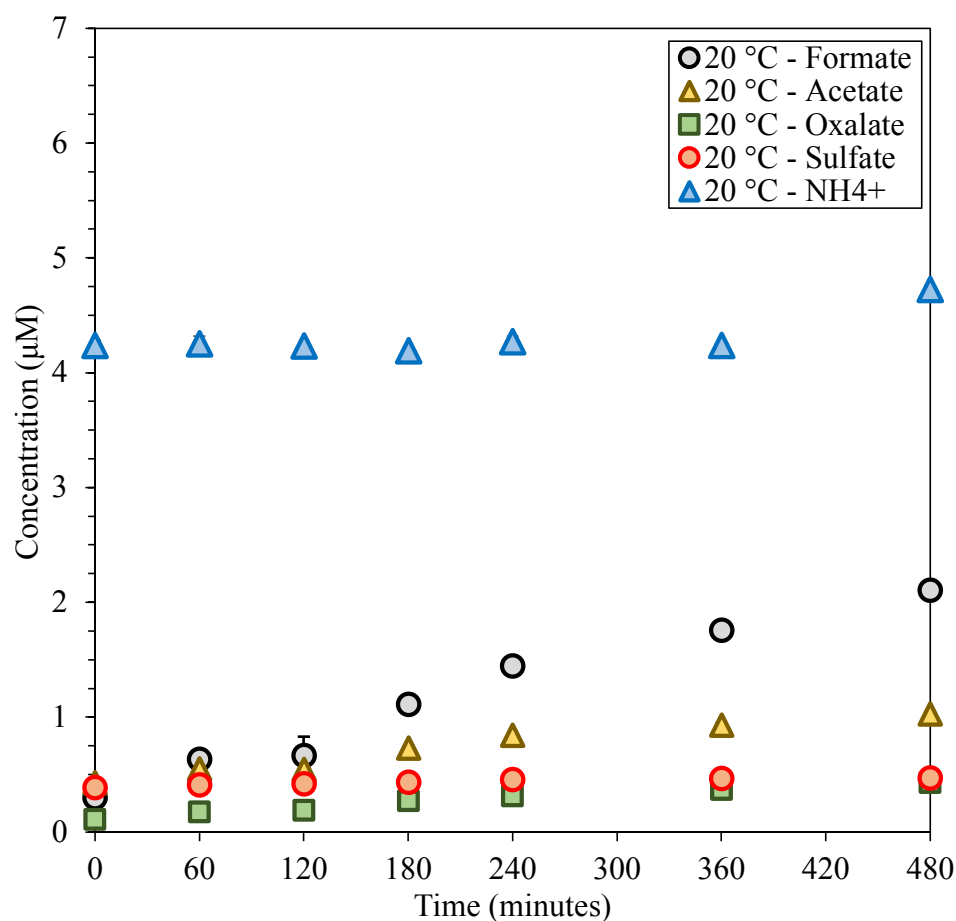
Figure 17. Time-dependent concentration profiles of organic acids and inorganic compounds in ESHA photolysis 20 ºC. Error bars represent standard deviation of triplicate measurements.

The formation of organic acids in ESHA photolysis followed similar trends as with SRHA. Organic acid formation was generally lower than what was observed in SRHA.

Over the course of the experiments, the amount of formation observed in order of decreasing significance was: formic acid (1.40 µM) > acetic acid (0.95 µM) > oxalic acid (0.30 µM). Furthermore, sulfate production was also minimal in ESHA solution, only demonstrating an increase of 0.08 µM and an average concentration of 0.43 ± 0.03 µM. Concentrations of NH_4^+ appeared relatively stable throughout the experiment, with the exception of 480 minutes where an increase of 0.50 µM was observed. Generally, it can be concluded that minimal amounts of photo-ammonification occur in the photolysis of both standard isolate DOM tested.

It should be noted that the photo-production of methanesulfonic acid (MSA) was not detected whatsoever in the photolysis of either SRHA or ESHA. Furthermore, the results depicted in this section contradict those presented in the literature for various small ionic compounds. Specifically, Ossola et al. 2019 reports the photo-production of both sulfate and MSA in the photolysis of various field-collected waters and standard isolate DOM.[13] Over a 5 hour irradiation, they observed sulfate formation of approximately 0.50 µM and 0.40 µM for 20 mg C/L SRHA and ESHA, respectively.[13] For MSA, the detected levels in SRHA and ESHA photolysis by Ossola et al. 2019 were below our detection limit (~10 – 20 nM), suggesting differences in analytical sensitivity may account for the lack of MSA production observed in our study.[13] One clear difference is the strict solution temperature-control we employed in our experimentation while Ossola et al. 2019 only controlled the air temperature (30 – 32 ℃) in the simulator.[13]

3.2 Photo-transformation of Methionine

3.2.1 Non-Targeted Screening in Surrogate DOM Solutions

3.2.1.1 2-naphthaldehyde

Direct-injection ESI-MS was performed on three samples collected at 20 °C (0, 30, 60 minutes) for initial screening of transformation in 2-naphthaldehyde. Both positive and negative polarity modes were analyzed; however, it was found that preferential ionization of sulfur-containing compounds in positive mode occurred, likely due in part to availability of sodium (Na^+) as a charge adduct. For this reason, the results presented here will focus on positive mode ESI. The comparison of the mass spectra with and without MET in solution yielded molecular formulas unique to the presence of MET. Mass spectra for carbon, hydrogen, nitrogen, oxygen, and sulfur (CHNOS)-containing formula detected are shown in Figure 18.

Two major formulas were detected in the photo-transformed solutions of MET ($C_5H_{11}NO_2S$) in the presence of 2-napthaldehyde. The first was $C_5H_{11}NO_3S$ corresponding to oxygen-addition to the S-atom (+16 Da) to form methionine sulfoxide (MetO). The second formula was $C_5H_9NO_2S$ indicating the loss of 2 hydrogen ions (-2 Da) and corresponding to dehydromethionine (DHM). The structures are shown in Figure 19. The pathways of formation have been previously investigated and described in Figure 2 (Section 1.1). We validated the production of MetO through matrix spikes of authentic standards into samples and analysis via UHPLC.

48
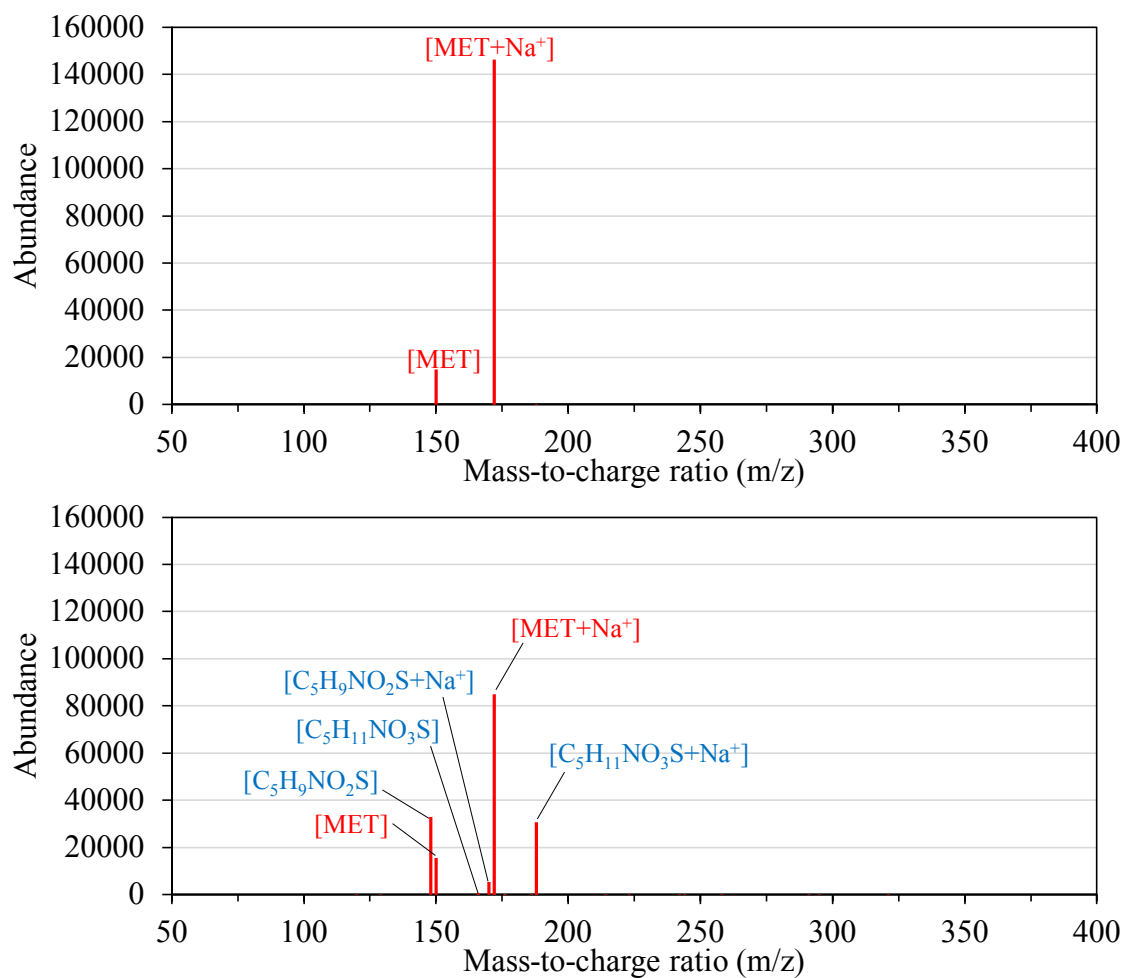
Figure 18. CHNOS-containing mass spectra for MET in 2-naphthaldehyde solutions at 20 °C: initial solution (top) and 60 minute irradiated solution (bottom). MET is indicated in red and suspected byproducts in blue. Charge adducts indicated with Na^+.

$C_5H_{11}NO_3S$
L-Methionine Sulfoxide (MetO)

$C_5H_9NO_2S$
Dehydromethionine (DHM)
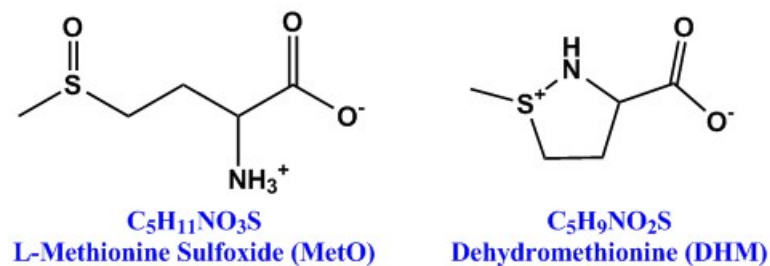
Figure 19. Photo-product structures and formulas detected in positive mode ESI-MS in 2-naphthaldehyde solution at 20 °C.

MS/MS fragmentation was performed on the suspected DHM ion observed at 148 m/z to verify the structure through comparison with the literature (Figure 20). Fragmentation of this ion yielded a major ion fragment at 120 m/z and minor fragments at m/z values of: 102, 90, 74, 64, and 60. These results are in agreement with fragmentation patterns reported in the literature, where the major ion fragment at 120 m/z represented the loss of ethylene ($-C_2H_4$) and the minor ion fragment at 102 m/z represented the loss of the thiol functionality ($-CH_3S$).[42,44] No significant formulas not associated to background were assigned in the CHNO formulas.
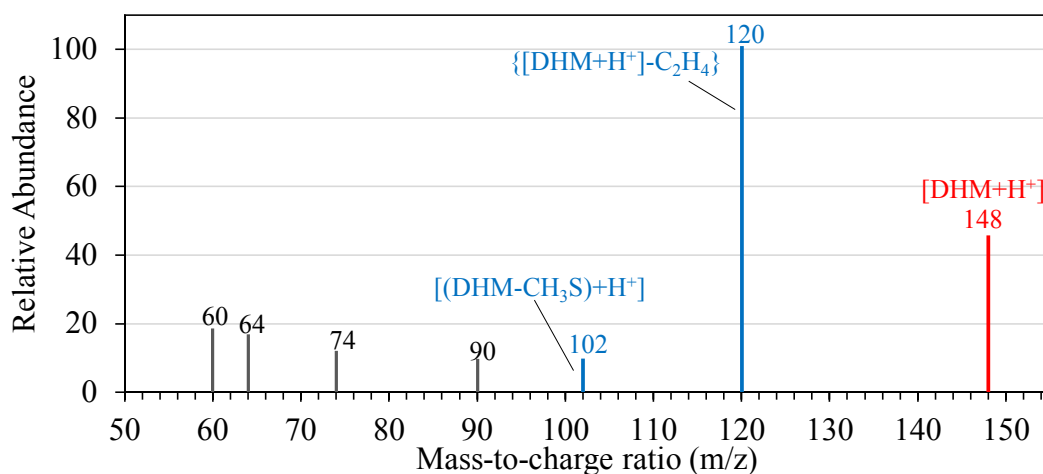
Figure 20. MS/MS fragmentation of suspected DHM ion at 148 m/z. Parent ion shown in red and ion fragments consistent with the literature shown in blue.

To visualize the importance of MetO and DHM as products in 2-naphthaldehyde solutions, the abundance values for products ($A_{t,Prod}$) were normalized to the initial MET abundance ($A_{0,MET}$), both taken as the sum of the protonated form (H^+) and the charge adduct form with sodium (Na^+). The time-dependent normalized abundances are shown in Figure 21 for each compound detected in ESI-MS screening.
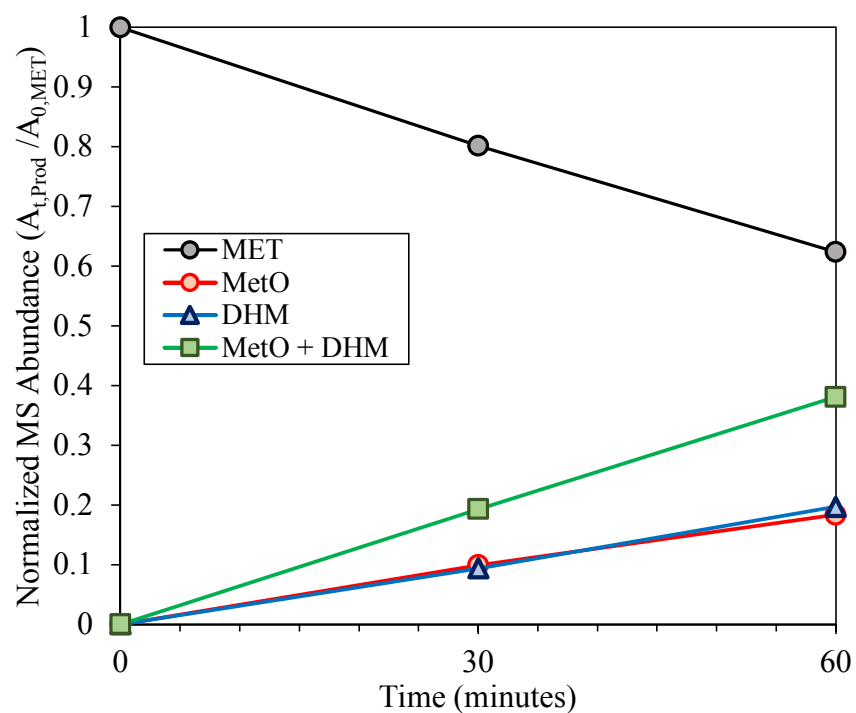
Figure 21. Time-dependent normalized abundance of MET, MetO, and DHM in 2-naphthaldehyde solution at 20°C.

In terms of MS abundance, MET decreased by 38% while MetO and DHM increased to 18% and 20% relative to the initial MET abundance. This yields a proportional change in MS abundance, where the sum of MetO and DHM yield a total 38% increase in abundance relative to the initial MET abundance. This result indicates that MetO and DHM represent major products produced in 2-naphthaldehyde. Furthermore, the literature-reported production of these compounds confirms our suspicions that $^1O_2$ is the primary reactive species responsible for the decay of MET in 2-naphthaldehyde solutions.[6,35,40,44]

3.2.1.2 1,4-naphthoquinone

Direct-injection ESI-MS was performed on three samples collected at 20 °C (0, 30, 60 minutes) for initial screening of transformation in 1,4-naphthoquinone solution.

51

Consistent with 2-naphthaldehyde, the most efficient ionization was observed in positive mode ESI and the results presented here will focus on this. The mass spectra of CHNOS-containing formula detected are shown in Figure 22.
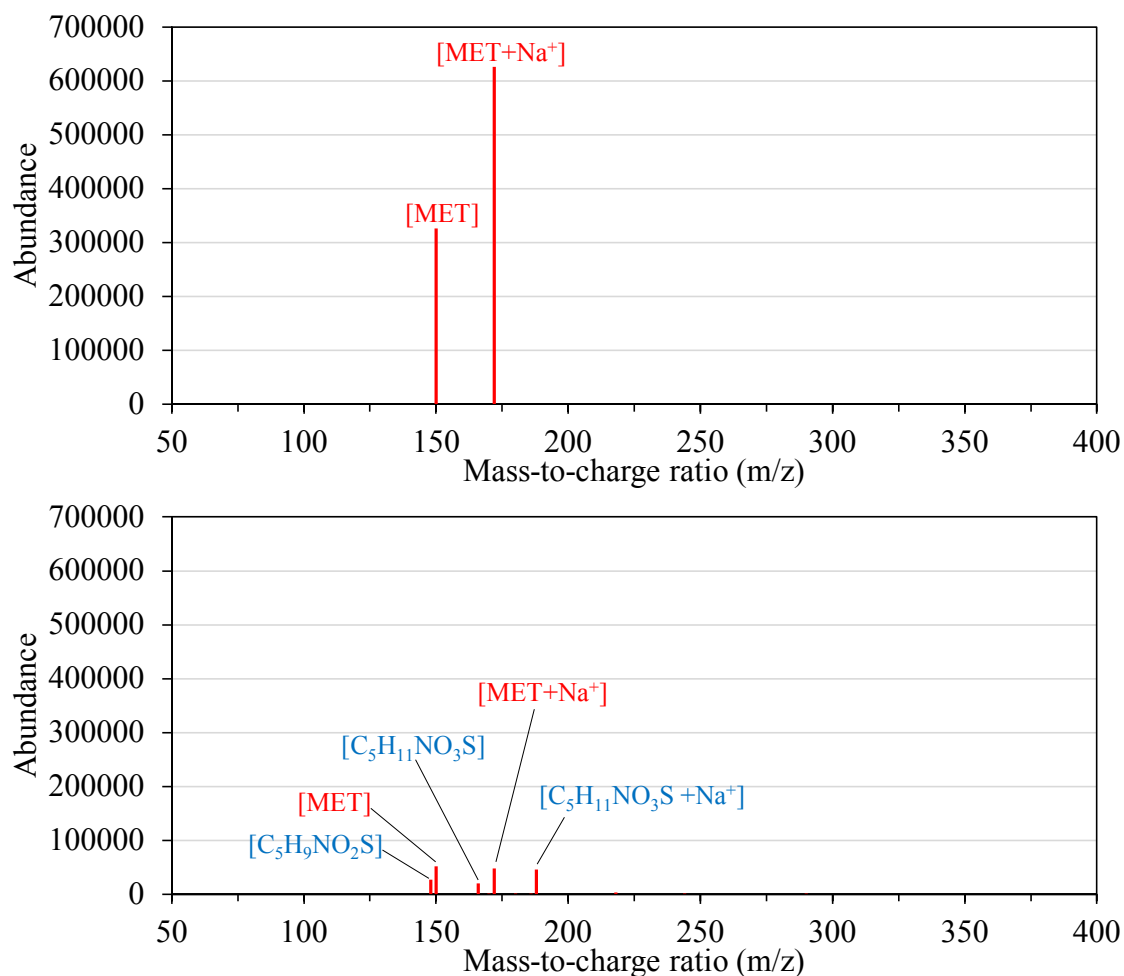
Figure 22. CHNOS-containing mass spectra for MET in 1,4-naphthoquinone solutions at 20 °C: initial solution (top) and 30 minute irradiated solution (bottom). MET is indicated in red and suspected byproducts in blue. Charge adducts indicated with Na^+.

As observed in 2-naphthaldehyde, the primary CHNOS formulas detected corresponded to that of MetO ($C_5H_{11}NO_3S$) and DHM ($C_5H_9NO_2S$); however, the abundances of these formulas were much less significant in 1,4-naphthoquinone solution despite increased

MET degradation. Applying the same approach as with 2-naphthaldehyde, the normalized abundances of CHNOS formulas were plotted to visualize the importance of MetO and DHM in 1,4-naphthoquinone (Figure 23).
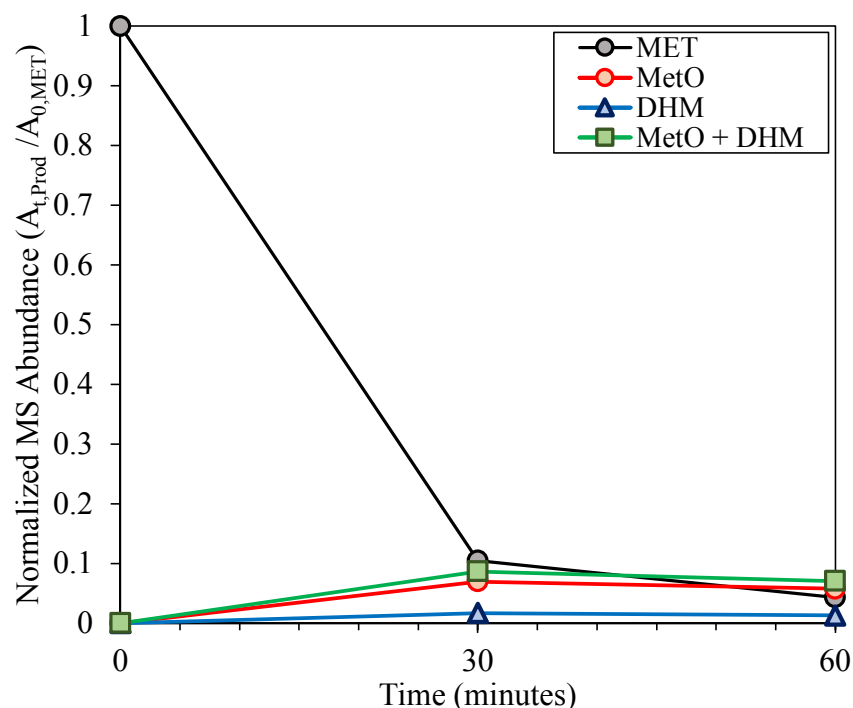
Figure 23. Time-dependent normalized abundance of MET, MetO, and DHM in 1,4-naphthoquinone solution at 20 °C.

Relative to the initial abundance, MET decreased by 90% in just 30 minutes and 94% over the 60 minute irradiation. Meanwhile, MetO and DHM increased to 6% and 1% of the initial MET abundance, demonstrating low conversion of MET to these products. As a whole, these products represent less than 10% of conversion based on abundance, which suggests that the rapid transformation of MET is likely owed to other reactive species, such as $^3NQ^*$. Furthermore, the rapid decrease observed in the first 30 minutes followed by significantly decreased rates up to 60 minutes indicate the consumption of 1,4-naphthoquinone and its photo-products are primary chromophores present in solution.

While the apparent $^1O_2$ production indicated by probe compound decay was significant, the low amounts of formation may suggest that MetO and DHM are intermediary products and subject to further degradation in 1,4-naphthoquinone solutions. Conversely to 2-naphthaldehyde, significant CHNO-containing formulas were assigned in positive mode ESI following irradiation. The mass spectra for CHNO-containing formulas are shown in Figure 24. The proposed structures are shown in Figure 25.
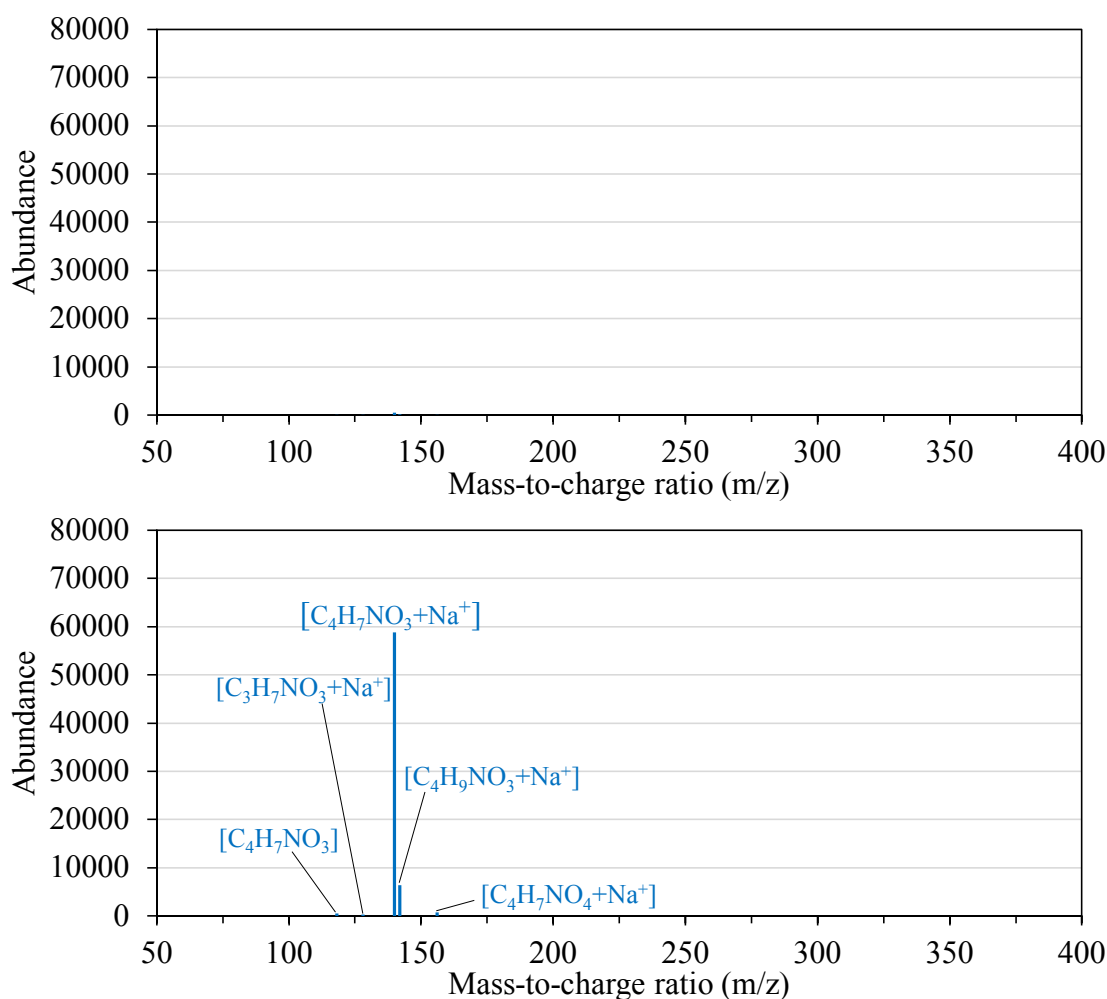
Figure 24. CHNO-containing mass spectra for MET in 1,4-naphthoquinone solutions at 20 °C: initial solution (top) and 30 minute irradiated solution (bottom). Suspected byproducts in blue. Charge adducts indicated with Na^+.
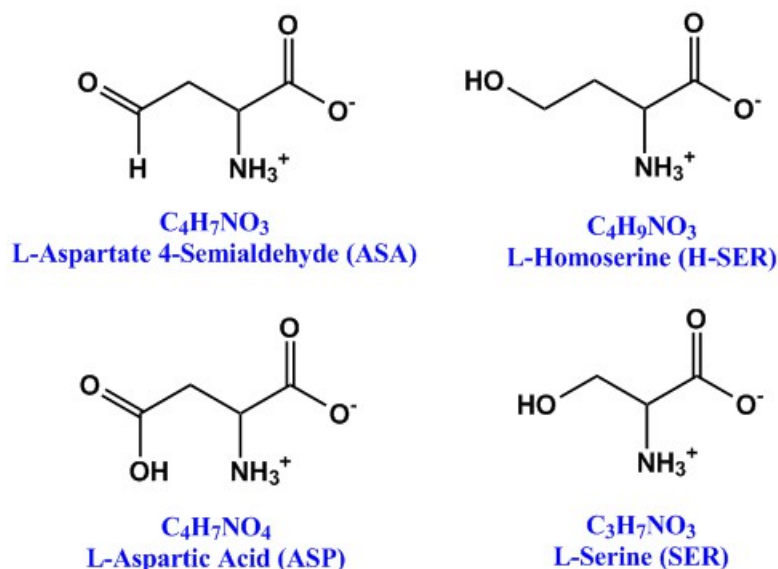
Figure 25. Proposed CHNO-containing product structures and formulas detected in positive mode ESI-MS in 1,4-naphthoquinone solution at 20 °C.

Two major formulas appear as sodium-adducts in photo-transformed solutions with 1,4-naphthoquinone. The most significant was $C_4H_7NO_3$ (-32 Da), indicating cleavage of the S − C bond in MET. Multiple studies on the light-induced oxidation of MET as a side-chains in proteins have reported the -32 Da species and it is commonly proposed to be an aldehyde, L-aspartate 4-semialdehyde (ASA).[33,65] This compound corresponds to a loss of CH_4S (-48 Da) and oxygen addition at the carbon in the γ-position (+16 Da). The second formula was $C_4H_9NO_3$ (-30 Da), indicating cleavage of the S − C bond as with ASA. This formula could correspond to two potential products, including L-Threonine (THR) or L-Homoserine (H-SER). Considering the formation of small CHNO-containing amino acids from MET, we further looked into the formulas for others similar amino acids and observed formulas $C_4H_7NO_4$ and $C_3H_7NO_3$, which are anticipated to correspond to L-aspartic acid (ASP) and L-serine (SER). ASP is the further oxidation product of ASA and its presence may indicate that ASP is the final stable oxidation byproduct in 1,4-naphthoquinone

solutions.[65] ASA, ASP, and H-SER exist as important reactants and/or intermediates in synthesis of amino acids such as MET, THR, lysine, and isoleucine in biological pathways.[65] It is clear that the products identified here parallel those observed as intermediates and products in biosynthetic pathways.

The formation of S – C cleavage byproducts is supported in the literature by the formation of small S-containing products such as MSA,[13] sulfate,[13] and volatile sulfur compounds (e.g., methanethiol, DMS, DMDS, etc.).[36-38,48] While the mechanisms are not understood fully, it is expected that ^{3}CDOM* plays a key role in this MET oxidation pathway via formation of a sulfur-radical cation resulting from single electron transfer (SET).[41,47] In the photo-sensitized cysteine oxidation, Ossola et al. 2019 proposes triplet-induced C – S cleavage of L-Cysteine (CYS) photo-oxidation byproduct, CYS sulfinic acid, to explain formation of sulfate.[14] For UHPLC screening, high purity versions or authentic standards were purchased and matrix spikes into experimental solutions helped verify their presence. In particular, only H-SER and THR did not produce a chromatogram peak that corresponded to any peaks observed in irradiated solutions.

3.2.2 Product Formation in Surrogate DOM Solutions

3.2.2.1 2-naphthaldehyde

The results from non-targeted screening indicated the predominant activity of $^1O_2$ and the major photo-transformation products were expected to be MetO, DHM, and H_2O_2 (Figure 2; Section 1.1). The time-dependent concentration profiles for MET and major products produced in 2-naphthaldehyde are shown in Figure 26 for 10, 20, and 30 °C.

Figure 26. Time-dependent concentration profiles for MET and the major photo-transformation products produced in 2-naphthaldehyde solutions at 10, 20, and 30 °C. Error bars represent the standard deviation of triplicate measurements.

MET demonstrated temperature-dependent degradation that followed linear pseudo-first-order kinetics. The pseudo-first-order decay constants (k') were 6.50×10^{-5} s^{-1} (R^2=0.96), 7.83×10^{-5} s^{-1} (R^2=0.99), and 10.5×10^{-5} (R^2=1.00) at 10, 20, and 30°C, respectively. Clear temperature-dependent formation of MetO is observed in accordance with the degradation of MET. Relative to the change in concentration for MET, the formation of MetO at 60 minutes accounted for 60%, 74%, and 73% of decay at 10, 20, and 30 °C, respectively. On

average over the time-scale of the experiment, MetO accounted for $82 \pm 22\%$, $85 \pm 6\%$, and $82 \pm 7\%$ of decay at 10, 20, and 30 °C, respectively. Similarly, the H_2O_2 demonstrated temperature-dependent formation most strongly observed at 30 °C, consistent with that of MET decay. Over the course of 60 minutes, the amount of H_2O_2 formed was 4.32 μM, 5.24 μM, and 8.32 μM for 10, 20, and 30°C, respectively. To calculate the percent of MET decay accounted for by H_2O_2 formation, the values were corrected by removing contributions from 2-naphthaldehyde photolysis (Figure 9; Section 3.1.1.3) and the procedure for this is described in section: 2.4.1 Conversion Calculations. Based on corrected values, H_2O_2 formation at 60 minutes accounted for 48%, 55%, and 77% of decay at 10, 20, and 30 °C, respectively On average over the time-scale, H_2O_2 formation accounted $29 \pm 19\%$, $38 \pm 19\%$, and $60 \pm 16\%$ of MET decay at 10, 20, and 30 °C, respectively. These results verify the significant activity of $^1O_2$ in 2-naphthaldehyde solutions. It is worth noting that methionine sulfone (MetOO) was not detected.

The formation of DHM could not be quantified due to the unavailability of authentic standards. The remaining 25 – 40% of decay unaccounted for at 60 minutes is expected to be associated with DHM due to its prevalence in non-targeted screening results and literature-reported $^1O_2$ decay pathways (Figure 2; Section 1.1). Nascimento et al. 2022 reported that approximately 30% of conversion was associated with DHM, which is consistent with the conversion unaccounted for in our results.[44] Furthermore, the production of H_2O_2 agrees with the formation of DHM in 2-naphthaldehyde; however, it typically exceeds the 25 – 40% of decay unaccounted for at 60 minutes. This indicates that some H_2O_2 formation is associated with the formation of MetO (Figure 2: Pathway B; Section 1.1) and agrees with the mixture of mechanisms occurring at neutral pH.[44]
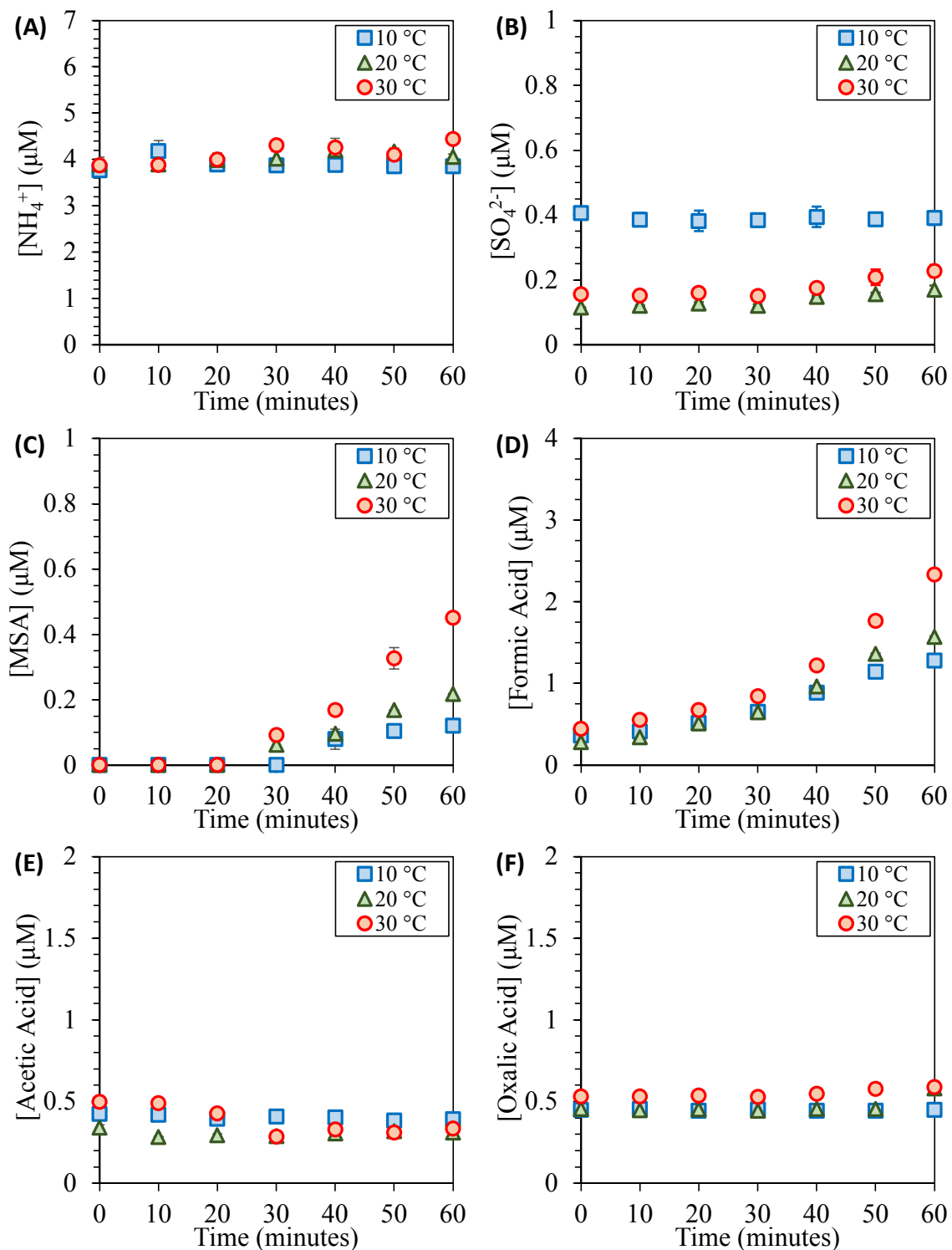
Figure 27. Time-dependent concentration profiles for inorganic compounds and organic acids measured in 2-naphthaldehyde at 10, 20, and 30 °C: (A) NH_4^+, (B) SO_4^{2-}, (C) MSA, (D) Formic Acid, (E) Acetic Acid, and (F) Oxalic Acid.

59

The time-dependent concentration profiles for inorganic compounds (i.e., NH_4^+, SO_4^{2-}) and organic acids (i.e., MSA, formic acid, acetic acid, oxalic acid) at all temperatures are shown in Figure 27. The time-dependent concentration profiles of NH_4^+ demonstrated very little formation with no significant trends (Figure 27A). On average, the minimal increases in $[NH_4^+]$ accounted for $3.0 \pm 3.0\%$, $3.0 \pm 2.0\%$, and $5.0 \pm 3.0\%$ of MET decay at 10, 20, and 30 ℃, respectively. Similarly, the time-dependent $[SO_4^{2-}]$ profiles demonstrated no formation at 10 ℃ and very little formation ($\Delta[SO_4^{2-}] < 0.1$ µM) at 20 and 30 ℃ (Figure 27B). On average between the temperatures that did show increases, SO_4^{2-} accounted for $0.5 \pm 0.4\%$ of MET decay. The results for NH_4^+ and SO_4^{2-} demonstrated that little photo-mineralization of N and S occur in 2-naphthaldehyde, consistent with the predominant activity of $^1O_2$.

For organic acids, the only compounds that showed increases in concentration were MSA (Figure 27C) and formic acid (Figure 27D). MSA formation was observed with temperature-dependence, although concentrations were relatively low. At 60 minutes, the [MSA] only increased by 0.12 µM, 0.22 µM, and 0.45 µM at 10, 20, and 30 ℃, respectively. On average, the formation of MSA accounted for $1.0 \pm 1.0\%$, $1.5 \pm 1.0\%$, and $2.2 \pm 2.0\%$ of MET decay at 10, 20, and 30 ℃, respectively. While temperature-dependent formation of formic acid was observed, its formation is effectively the same as what was observed in 2-naphthaldehyde photolysis (Figure 10; Section 3.1.1.3). For example, the Δ[Formic Acid] with MET present was 0.90 µM, 1.30 µM, and 1.90 µM compared to 1.00 µM, 1.40 µM, and 2.10 µM in 2-naphthaldehyde photolysis at 10, 20, and 30 ℃, respectively. This suggests that the slightly decreased formation of formic acid with MET present is predominantly associated with 2-naphthaldehyde photolysis and not MET decay.

Acetic acid (Figure 27E) and oxalic acid (Figure 27F) did not demonstrate increasing concentrations with time with MET present, consistent with the results demonstrated in 2-naphthaldehyde photolysis (Figure 10; Section 3.1.1.3).

The photo-transformation products of MET in 2-naphthaldehyde demonstrated the activity of $^1O_2$ as the predominant reactive species through the production of MetO and H_2O_2. The summarized reaction pathways and products are shown in Figure 28. The significance of the apparent DHM formation demonstrated in non-targeted screening and measured H_2O_2 further validated previously described $^1O_2$ reaction mechanisms. Generally, the results depicted here are in agreement with those reported in the literature for the $^1O_2$-mediated oxidation of MET.[35,40,41,44] The low photo-ammonification observed agreed with the lack of volatile sulfur compounds such as methional in 2-napthaldehyde. While a degree of MSA formation was observed, it was not a major product formed and indicates the low activity of $^3NA*$ as a reactive species.
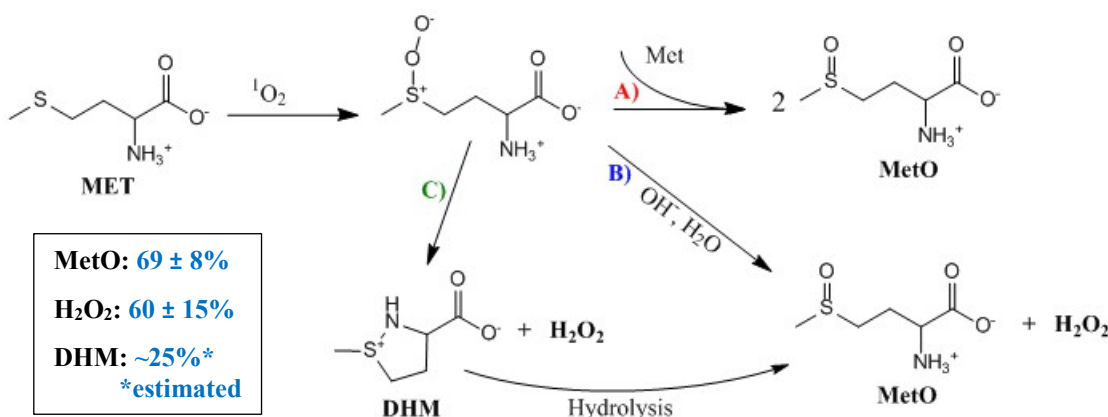
Figure 28. Summary of reaction pathways and products for MET in the presence of 2-naphthaldehyde. Percent conversion shown in blue along with standard deviations between temperatures.

3.2.2.2 1,4-naphthoquinone

The non-targeted screening results for 1,4-naphthoquinone indicated the predominance of fragmented amino acid compounds (i.e., ASA, ASP, SER), indicating the loss of the thiol functionality from MET and the products associated with $^1O_2$ (i.e., MetO, DHM) were expected to be of lesser importance in these solutions. The time-dependent concentration profiles for MET and the major photo-transformation products produced in 1,4-naphthoquinone are shown in Figure 29 at 10, 20, and 30 ^{o}C. MET demonstrated temperature-dependent decay with an initial rapid decay phase up to 7.5 minutes followed by decreasing rates up to 15 minutes, signifying the consumption and transformation of 1,4-naphthoquinone. For this reason, decay rates were determined up to 7.5 minutes. The pseudo-first-order decay rates up to 7.5 minutes were 1.98 x 10^{-3} s^{-1} (R^2=0.89), 2.34 x 10^{-3} s^{-1} (R^2=0.94), and 2.57 x 10^{-3} s^{-1} (R^2=0.93) at 10, 20, and 30 ^{o}C, respectively.

Consistent with screening results, ASA represented the most significant product formed, representing one major fragment of the original MET following the fragmentation of the thiol functionality. ASA demonstrated temperature-dependent formation most significantly at 10 ^{o}C, while less variation was observed for 20 and 30°C. The Δ[ASA] over the experiment was 15.30 μM, 16.40 μM, and 16.40 μM at 10, 20, and 30 ^{o}C, respectively. Relative to the change in MET concentration, the formation of ASA at 15 minutes accounted for 83%, 76%, and 70% of decay at 10, 20, and 30 ^{o}C, respectively. On average over the time-scale, ASA accounted 77 ± 3%, 76 ± 1%, and 73 ± 2% of MET decay at 10, 20, and 30 ^{o}C, respectively. The second major product, MSA, represented a significant fraction of the fragmented thiol functionality from the original MET molecule.
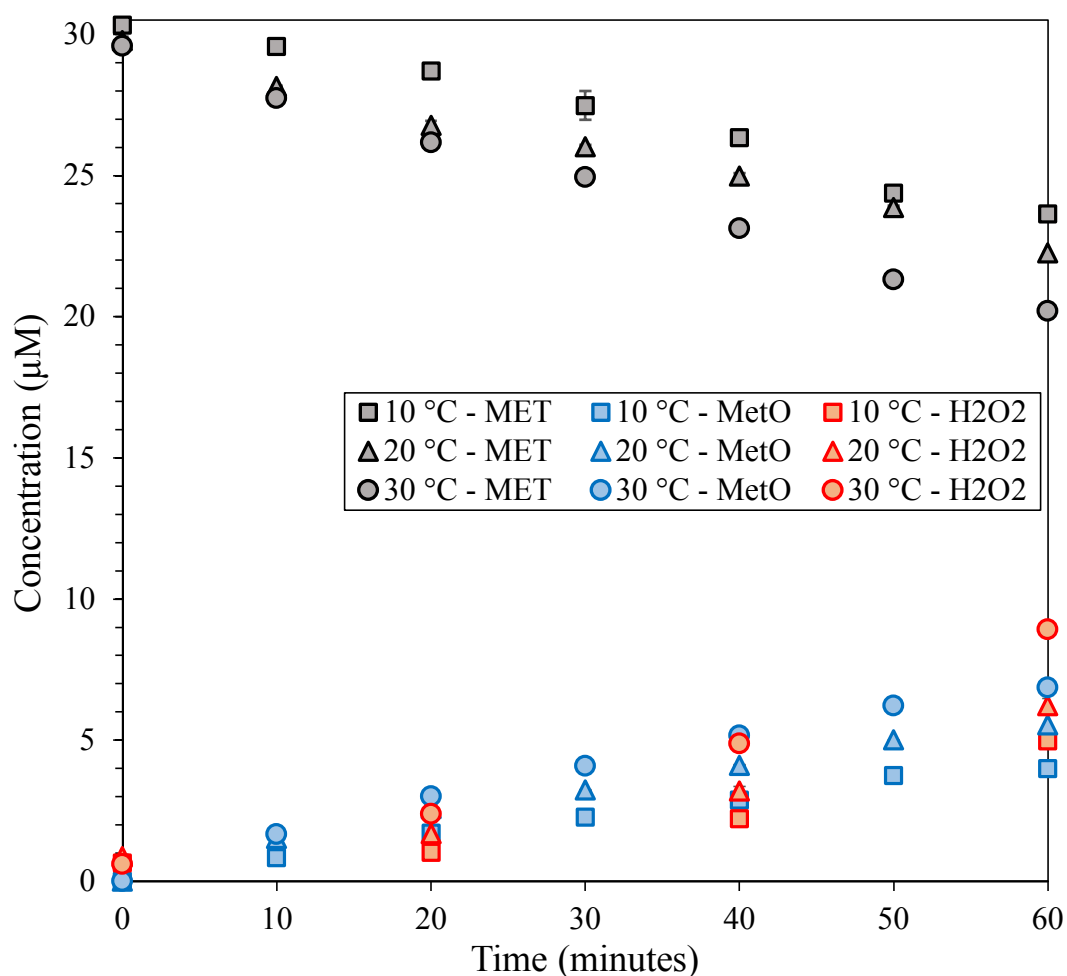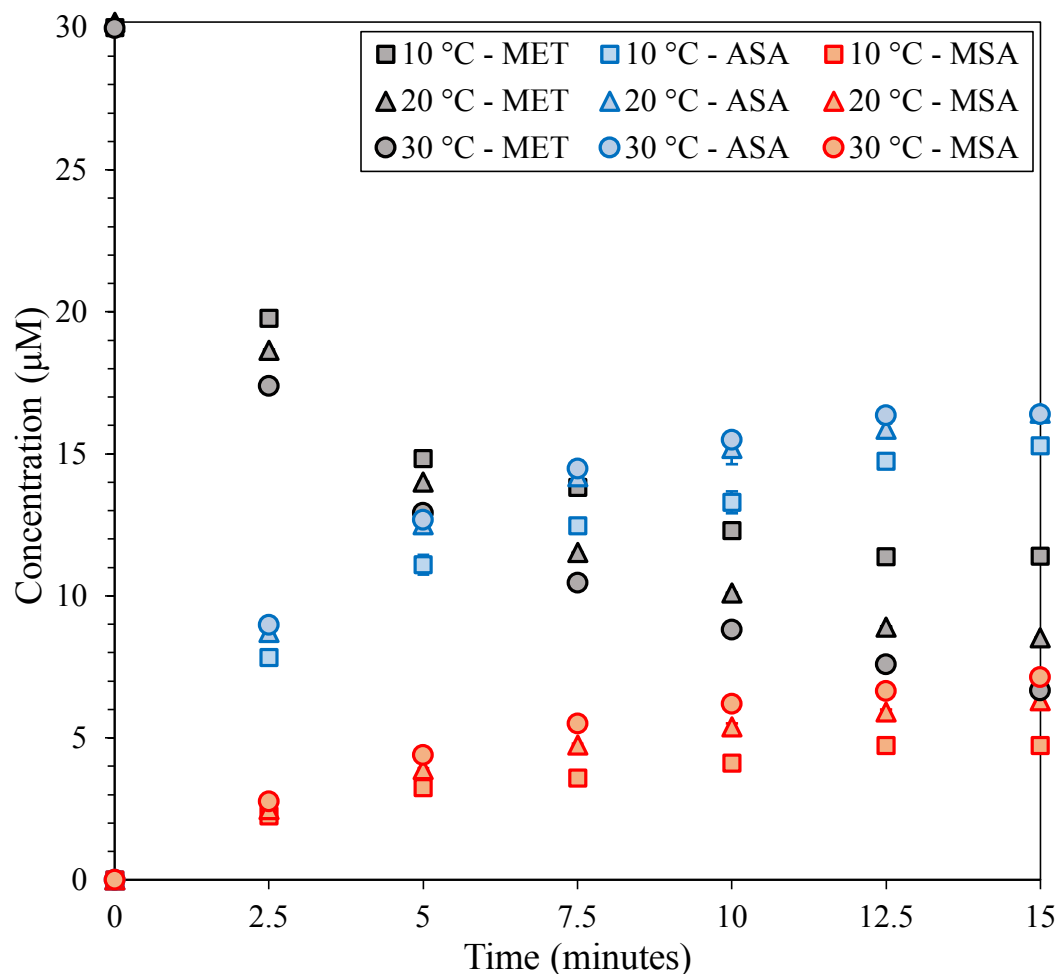
Figure 29. Time-dependent concentration profiles for MET and the major photo-transformation products produced in 1,4-naphthoquinone solutions at 10, 20, and 30 ℃. Error bars represent the standard deviation of triplicate measurements.

Over the 15 minutes, the MSA concentration increases to 4.70 µM, 6.30 µM, and 7.10 µM at 10, 20, and 30 ℃, respectively. These concentrations of MSA account for 25%, 29%, and 31% of MET decay at 10, 20, and 30 ℃, respectively. On average over the time-scale of the experiment, MSA accounted 23 ± 2%, 26 ± 3%, and 28 ± 3% of MET decay at 10, 20, and 30 ℃, respectively. The significant formation of ASA and MSA suggest they are two co-products that represent major fragments of MET that has undergone cleavage of the S − C bond. While MSA is not as abundant as ASA, this was anticipated due to the low

boiling point of methanethiol (6 °C), suggesting that some portions of the S-containing fragment may be lost to volatilization. To our knowledge, this is the first time that ASA has been reported quantitatively and verifies previously proposed oxidation products in proteins.[33,65] The observed MSA formation is in agreement with literature-reported production from MET in the presence of Dismal Swamp Water.[13] In addition to these products, we observed formation of other volatile sulfur compounds, amino acids, and inorganic compounds.

The minor photo-transformation products measured in 1,4-naphthoquinone are shown in Figure 30 at 10, 20, and 30 °C. Significant photo-ammonification was observed in 1,4-naphthoquinone, demonstrating temperature-dependent formation (Figure 30A). Over 15 minutes, the NH_4^+ concentration increased by 3.80 μM, 4.50 μM, and 4.90 μM at 10, 20, and 30 °C, respectively. The increases in NH_4^+ at 15 minutes accounted for 21 ± 0.1% on average between the three temperatures. On average over the time-scale of the experiment, the formation of NH_4^+ accounted for 21 ± 2%, 23 ± 2%, and 20 ± 1% of MET decay at 10, 20, and 30 °C, respectively. Considering that photo-ammonification of MET has been previously associated with methional production in the literature,[36,37,41] it was anticipated that it would form to a similar order of magnitude. Methional formation demonstrated no discernible temperature-dependence of formation, with tendencies to increase initially up to 5 minutes followed by decreasing concentrations up to 15 minutes (Figure 30B). Over the 15 minutes, the methional concentration increased by 2.30 μM, 1.20 μM, and 1.70 μM at 10, 20, and 30 °C, respectively. These concentrations accounted for 12%, 5%, and 7% of MET decay at 10, 20, and 30 °C, respectively.
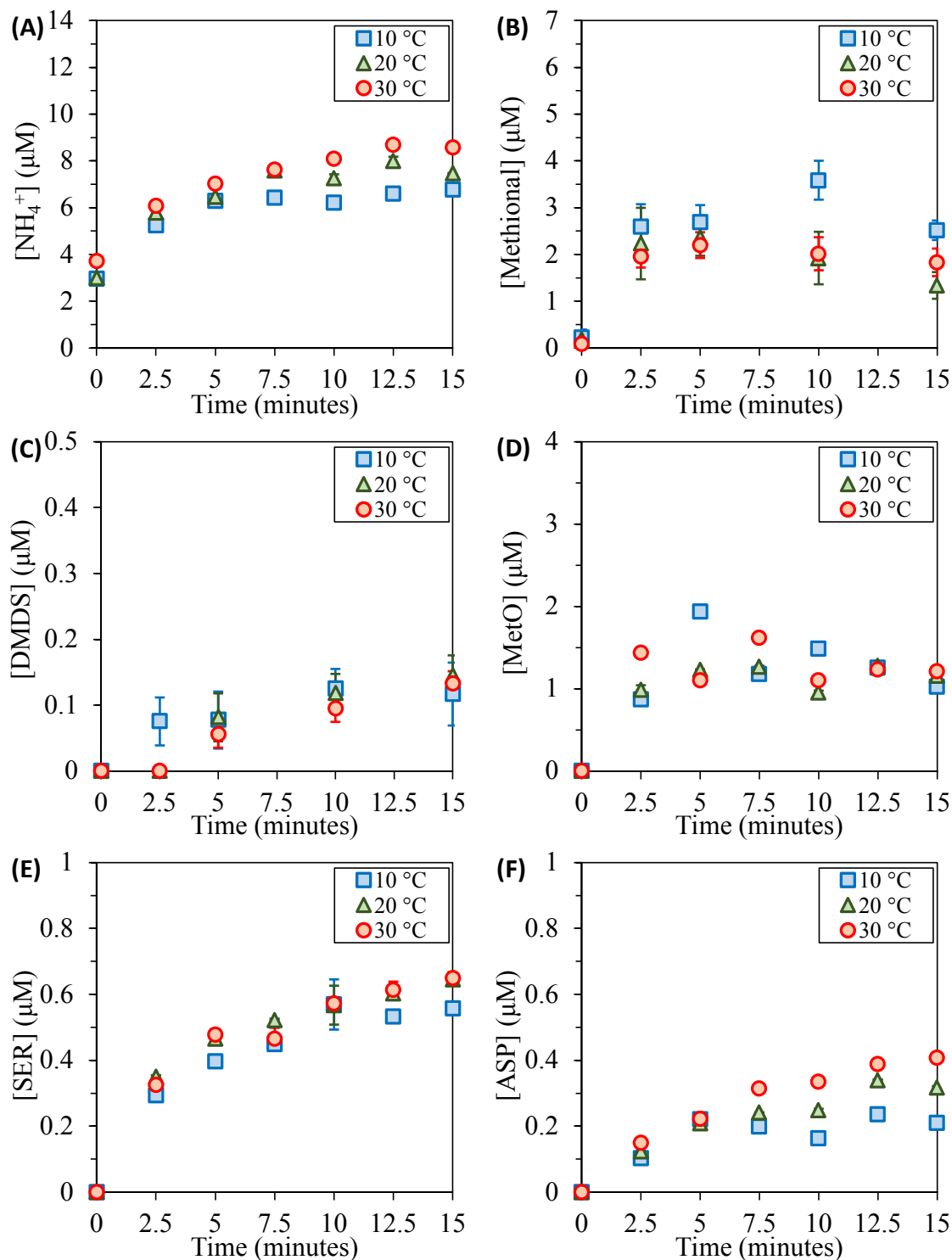
Figure 30. Time-dependent concentration profiles of minor photo-transformation products measured in 1,4-naphthoquinone at 10, 20, and 30 °C: (A) NH_4^+, (B) Methional, (C) DMDS, (D) MetO, (E) SER, and (F) ASP. Error bars show ± SD of measurements.

On average over the time-scale of the experiment, the formation of methional accounted for 17 ± 5%, 11 ± 5%, and 11 ± 3% of MET decay at 10, 20, and 30 ℃, respectively. Clearly, the formation of NH_4^+ exceeds that of methional formation at 15 minutes and on average over the time-scale, suggesting the instability of methional as a product reported in the literature.[36,37] Focusing on the initial increases of methional in the 2.5 minute samples, the ratio of methional to NH_4^+ ([Methional]:[NH_4^+]) was determined to be 1.03, 0.74, and 0.78 at 10, 20, and 30 ℃, respectively. This result indicates they are initially formed in similar proportions predominantly at 10 ℃, which may be owed to higher stability of volatile methional at lower temperatures. DMDS was also formed at all three temperatures, although only to low concentrations with no temperature-dependence (Figure 30C). At 60 minutes, the [DMDS] only increased by 0.12 μM, 0.15 μM, and 0.13 μM at 10, 20, and 30 ℃, respectively. On average over time and between the temperatures, the formation of DMDS accounted for 0.5 ± 0.2%, suggesting little variation between temperatures and with time. Nevertheless, the presence of DMDS is indicative of MeSH radical formation. The observed instability of methional suggests further degradation to MeSH as proposed in the literature,[36,37] providing a pathway for volatilization and formation of MSA. It should be noted that MeSH could not be quantified due to its high boiling point and instability.

Consistent with the results for non-targeted screening, other amino acid products were formed, including MetO, ASP, and SER (Figure 30D-F). As expected, the formation of MetO was less significant in 1,4-naphthoquinone and demonstrated no clear temperature-dependence (Figure 30D). Furthermore, the trends in concentration appear to show increasing and decreasing with time, suggesting potential instability of MetO in 1,4-

naphthoquinone solutions. On average over time, MetO formation accounted for 8 ± 3%, 7 ± 1%, and 7 ± 3% of MET decay at 10, 20, and 30 °C, respectively. Fragmented amino acid products, ASP and SER, formed less than 1 µM over the course of irradiation, with SER demonstrating higher formation than ASP (Figure 30E,F). Interestingly, ASP demonstrates clear temperature dependence despite lower formation while SER does not. On average over time and between temperatures, ASP formation accounted for 1.3 ± 0.2% while SER accounted for 2.8 ± 0.2% of MET decay. The formation of ASP is in agreement with ASA formation due to previous notions that ASP is the final oxidation product.[65]

The time-dependent concentration profiles for organic acids (i.e., formic acid, acetic acid, oxalic acid) and sulfate are depicted in Figure 31. Of the organic acids, formic acid (Figure 31A) and acetic acid (Figure 31B) demonstrated enhanced formation relative to 1,4-naphthoquinone photolysis (Figure 11; Section 3.1.1.3). Following correction procedure (Section 2.4.1), the change in formic acid concentration associated to MET decay was 0.80 µM, 1.80 µM, and 2.20 µM at 10, 20, and 30 °C, respectively. For acetic acid, the change in concentration associated to MET decay was 0.30 µM, 0.50 µM, and 0.20 µM at 10, 20, and 30°C, respectively. On average over time, formic acid accounted for 5.0 ± 3.0%, 6.0 ± 2.0%, and 7.0 ± 2.0% of MET decay at 10, 20, and 30 °C, respectively. Acetic acid accounted for 0.7 ± 0.7%, 1.6 ± 0.3%, and 0.9 ± 0.6% of MET decay at 10, 20, and 30 °C, respectively. The enhanced production of formic acid with MET present is indicative of literature-reported decay of methional to produce MeSH, formic acid, and ethylene.[36,37]
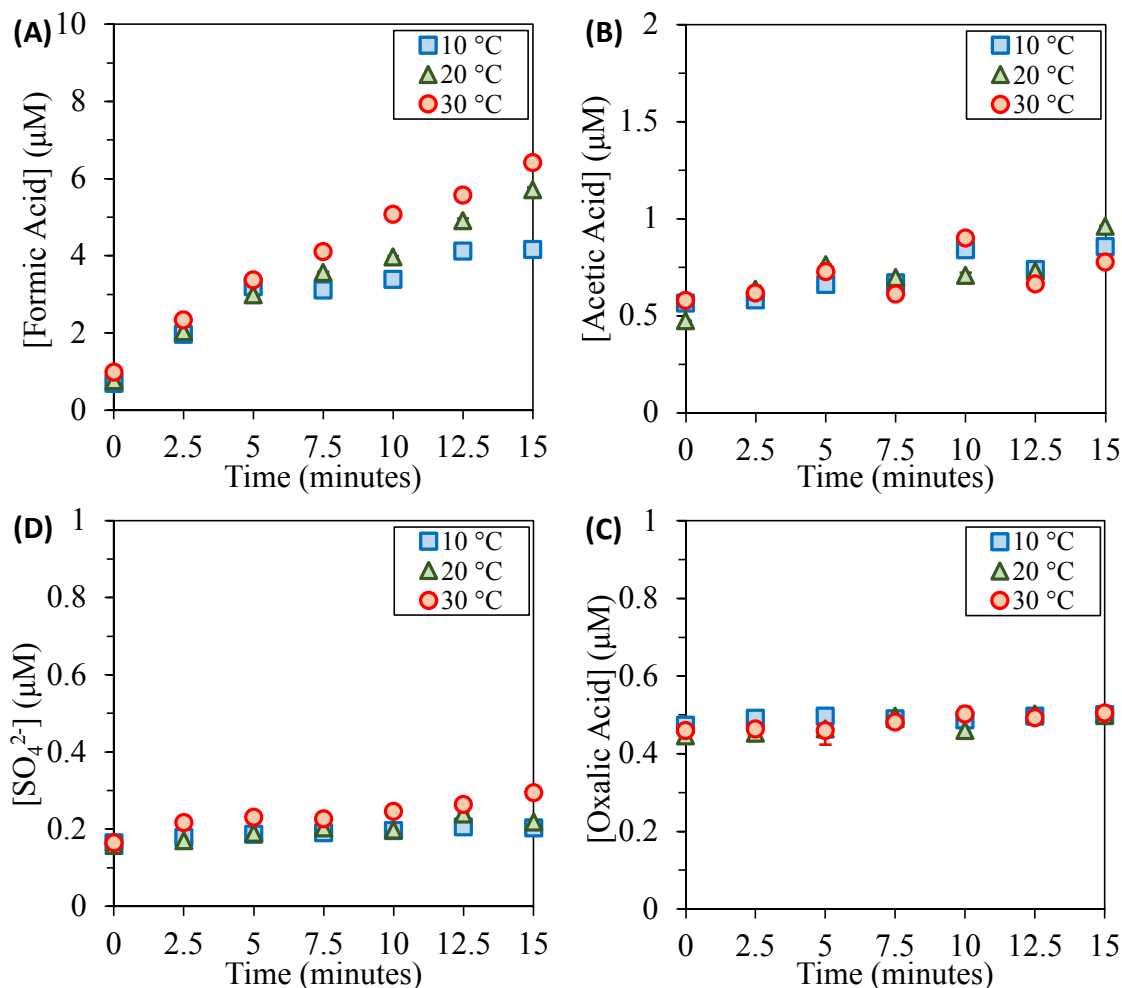
Figure 31. Time-dependent concentration profiles for organic acids and sulfate measured in 1,4-naphthoquinone at 10, 20, and 30 °C: (A) Formic Acid, (B) Acetic Acid, (C) Oxalic Acid, and (D) SO_4^{2-}.

Oxalic acid was not formed in 1,4-naphthoquinone solutions (Figure 31C). The photo-mineralization of organic S to sulfate was generally not observed in 1,4-naphthoquinone (Figure 31D), consistent with previous results for 2-naphthaldehyde. On average over time and between temperatures, sulfate formation only accounted for $0.3 \pm 0.1\%$ of MET decay.

The relatively low formation and unstable concentration trends observed for MetO indicated that it may be susceptible to further degradation in the presence of 1,4-naphthoquinone, particularly since $^1O_2$ production was highly efficient. To test this

hypothesis, we employed 30 µM of MetO as the parent compound and quantified the major and minor products observed with MET. Volatile compounds were not quantified in this experiment. The time-dependent concentration profiles for MetO, major products, and minor products are shown in Figure 32 for 1,4-naphthoquinone at 20 °C.
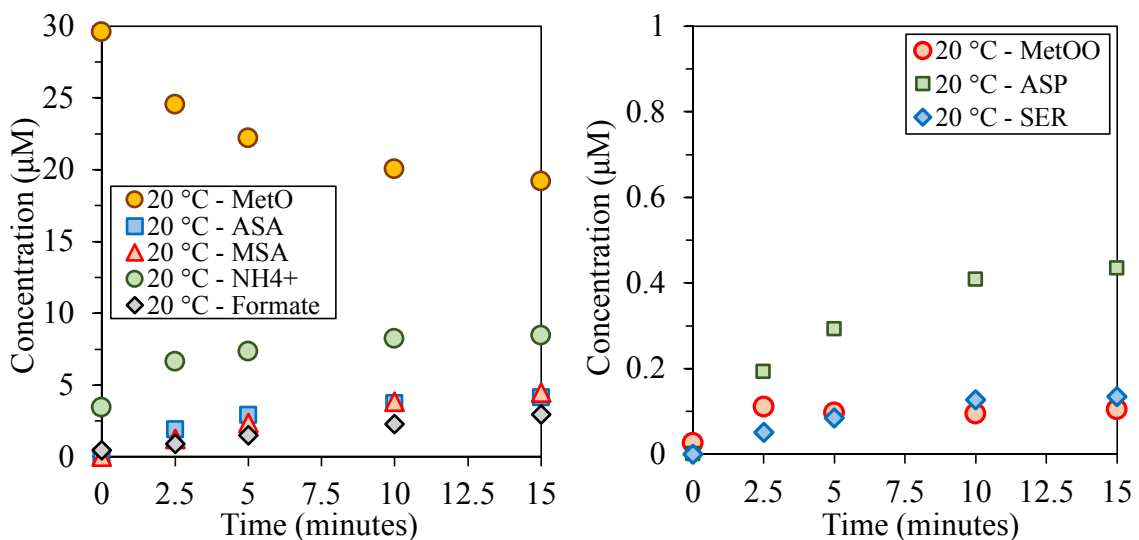
Figure 32. Time-dependent concentration profiles for MetO and major products (left) and minor products (right) produced in 1,4-naphthoquinone at 20 °C.

MetO decay was observed over the 15 minute experiment, degrading to 65% of its initial concentration and verifying the hypothesis that it is unstable in 1,4-naphthoquinone solutions. The pseudo-first-order decay rate up to 5 minutes was 1.01×10^{-3} s^{-1} ($R^2 = 0.96$), which is approximately 2.3 times lower than what was observed for MET. Production of ASA, MSA, NH_4^+, ASP, SER, and formic acid were observed in solutions with MET and MetO as the parent compound; however, key differences in product distributions were observed. Conversely to MET, the most abundant product produced was NH_4^+, accounting for $54 \pm 6\%$ of MetO decay on average. Importantly, ASA and MSA were formed to similar proportions, accounting for $39 \pm 1\%$ and $35 \pm 8\%$ of MetO decay, respectively. These

results imply that the oxygen addition to the S-atom in MetO provides a more stable pathway to MSA following the cleavage of the S − C bond, whereas with MET more volatile losses may likely occur. For example, if we compare [MSA]$_{15\ min}$ with that of the sum of concentrations of fragmented products (i.e., ASA, ASP, and SER), the MSA concentration accounts for 95% of fragmented product concentration in MetO solution. With MET as the parent compound, the MSA concentration only accounts for 36% of the fragmented product concentration. Furthermore, it seems that oxygen addition to the S-atom induces preferential photo-ammonification. Both ASP and SER were measured at increasing concentrations; however, we observed more significant formation of ASP and less significant SER formation when using MetO as the parent compound. ASP and SER account for 4.0 ± 0.2% and 1.0 ± 0.2% of MetO degradation on average. Formic acid production was also enhanced with MetO as the parent compound, accounting for 7 ± 3% of MetO decay. Lastly, we observed the formation of methionine sulfone (MetOO) only in solutions with MetO as the parent compound, suggesting that when [MetO] is high, it is subject to further oxidation whereas this was not observed in MET solutions with 1,4-naphthoquinone. MetOO accounted for 1.0 ± 0.5% of MetO degradation in 1,4-naphthoquinone.

The photo-transformation products of MET in 1,4-naphthoquinone solution demonstrated the strong activity of ^{3}NQ* and minor involvement of ^{1}O$_2$. The summarized reaction pathways and products for MET in the presence of 1,4-napthoquinone are shown in Figure 33 with percent conversions for each product. The significant production of CHNO-containing amino acids (i.e., ASA, ASP, SER) and small S-containing products

70

(i.e., MSA, DMDS) indicated that cleavage of the S – C bond in MET was a primary reaction pathway induced by ^{3}NQ*. As a secondary pathway involving ^{3}NQ*, decarboxylation and deamination of MET lead to the production of methional and NH_4^+. The unstable concentrations of methional and production of formic acid indicated further decay of methional to produce MeSH, ethylene, and formic acid in agreement with proposed decay in the literature.[36,37] While $^1O_2$ was active and produced MetO, it was found to be further susceptible to degradation producing similar products but at different proportions than with MET.
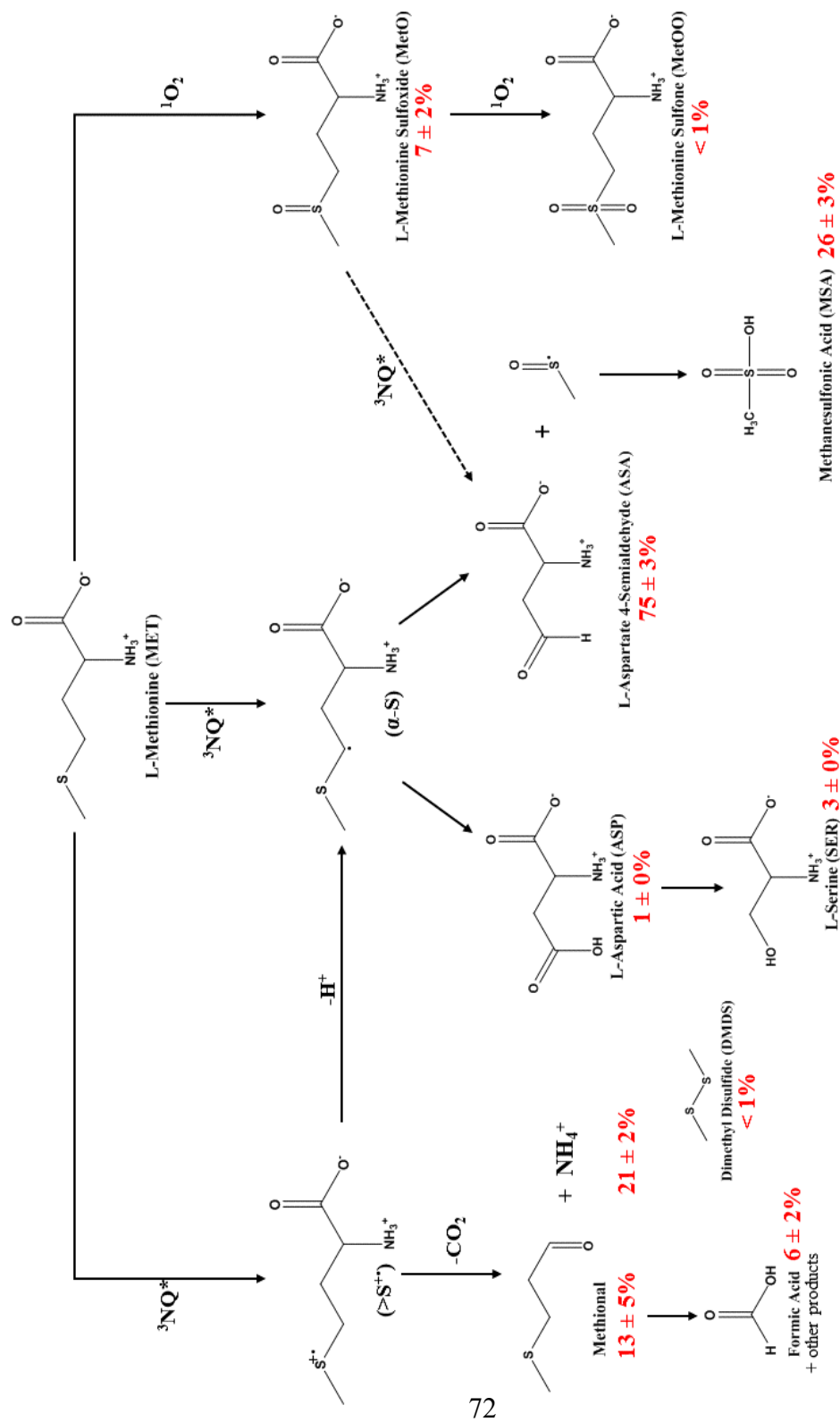
Figure 33. Summary of reaction pathways and products from MET in the presence of 1,4-naphthoquinone. Percent conversion shown in red with standard deviations between temperatures.

72

3.2.3 Product Formation in Standard Isolate DOM Solutions

In order to put the results depicted in surrogate DOM solutions into perspective, the same photo-transformation products observed in the surrogate DOM solutions were then calibrated and measured for the degradation of MET in the presence of two standard isolate DOM solutions at 20 °C: (1) Suwannee River Humic Acid (SRHA) and (2) Elliott Soil Humic Acid (ESHA). These two isolate DOM solutions were chosen as they represent two different environmental DOM (i.e., aqueous and soil DOM) with varying carbon content as well as differences in reactivity observed by probe compound decay.

3.2.3.1 Suwannee River Humic Acid (SRHA)

The observed MET decay in SRHA solution followed pseudo-first-order kinetics, decreasing to 79% of the initial MET concentration of 30 μM over the 480 minute experiment. The pseudo-first-order decay rate was 8.30 x 10^{-6} s^{-1} (R^2 = 0.99), approximately one order of magnitude lower than in 2-naphthaldehyde. The time-dependent concentration profiles for MET and major products produced in 10 mg C/L SRHA solution at 20 °C are depicted in Figure 34. Consistent with 2-naphthaldehyde, MetO production was significant and represented the predominant product observed in SRHA solution. Over the course of the experiment, MetO increased by 3.60 μM and accounted for 60 ± 2% of the observed MET degradation on average. Given the predominance of MetO and literature-reported mechanisms for $^1O_2$, the production of DHM and H_2O_2 was expected. The production of H_2O_2 was enhanced relative to what was produced in SRHA photolysis (Figure 15; Section 3.1.2.2). Specifically, formation of H_2O_2 at 480 minutes was 9.80 μM in SRHA photolysis and 10.90 μM with MET present in

solution. On average over time, the corrected results demonstrate an increase of H_2O_2 associated with MET decay on the order of 2.20 ± 0.80 μM.
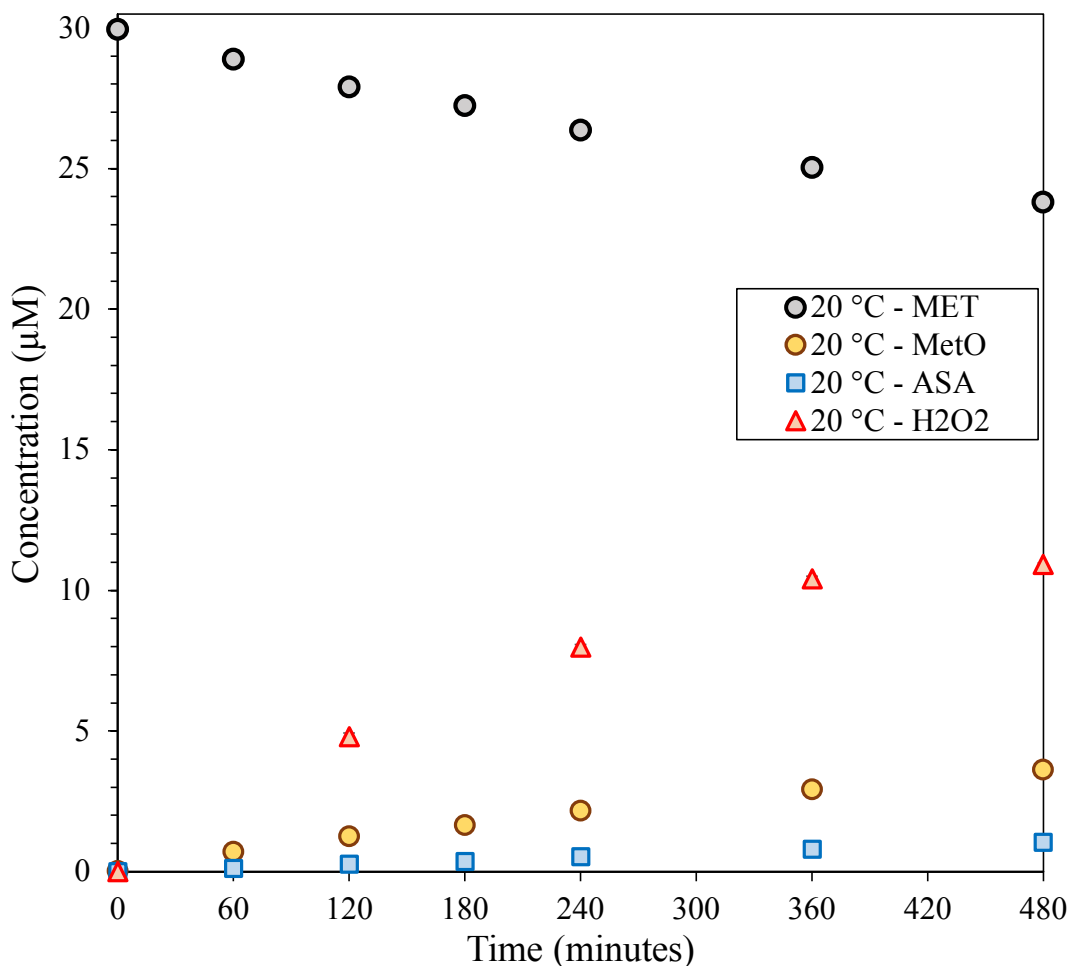
Figure 34. Time-dependent concentration profiles for MET and the major photo-transformation products produced in 10 mg C/L SRHA solution at 20 °C. Error bars represent the standard deviation of triplicate measurements.

The relatively high variation in corrected H_2O_2 concentrations potentially indicates the contribution of H_2O_2 to MET decay over the time-scale of the experiment. We experimentally investigated the H_2O_2-induced oxidation of 30 μM MET in the dark at 20 °C using 1 mM H_2O_2 to promote pseudo-first-order kinetics. Over the 6 hour experiment, MET degraded to 87% of the initial concentration and conversion to MetO was $80 \pm 3\%$.

The pseudo-first-order decay rate was 6.68 x 10^{-6} s^{-1} (R^2 = 1.00), corresponding to an apparent second-order rate constant (k_{app, H_2O_2}) was 6.68 x 10^{-3} $M^{-1}s^{-1}$. Taking into account the $[H_2O_2]_{480min}$ of 10.90 μM yields a pseudo-first-order rate of 7.30 x 10^{-8} s^{-1}, two orders of magnitude lower than the overall MET decay rate in SRHA. This confirms that H_2O_2 produced in SRHA photolysis and with MET present will not contribute significantly to MET decay, even at the longer experimental time-scales used for standard isolate DOM.

The results thus far suggest that $^1O_2$ is largely responsible for the degradation of MET in SRHA solutions, yet $^3CDOM*$-induced reactions cannot be ignored due to the formation of fragmented products. The time-dependent concentration profiles for minor products are shown in Figure 35 for 10 mg C/L SRHA at 20 °C. Importantly, ASA demonstrated formation SRHA solution, demonstrating an increase of 1.00 μM over the 480 minute experiment. While formed to a lesser extent than MetO, ASA still accounts for a significant fraction of MET decay over the experiment. On average, ASA accounted for 14 ± 2% of the observed MET decay. While other CHNO-containing amino acids observed in 1,4-naphthoquinone solutions were detected, their formation was relatively insignificant in SRHA solution. For example, ASP demonstrated very little changes in concentration with an average of 0.10 ± 0.01 μM. The minimal increases in [ASP] corresponded to less than 1% of MET decay on average. SER was only statistically detectable past 360 minutes and for this reason, it can be considered effectively negligible, accounting for less than 1% of MET decay on average. Consistent with observed formation of CHNO-containing amino acids in 1,4-naphthoquinone, the formation of MSA was also observed in SRHA solution.

MSA only forms approximately 0.30 µM over the 480 minutes and accounts for 4 ± 1% of MET decay on average.

Figure 35. Time-dependent concentration profiles for the minor photo-transformation products produced in 10 mg C/L SRHA solution at 20 °C. Error bars represent the standard deviation of triplicate measurements.

MSA only forms approximately 0.30 µM over the 480 minutes and accounts for 4 ± 1% of MET decay on average. For comparison, the ratio of Δ[MSA] to change in CHNO-containing amino acid concentration (i.e., ASA, ASP, and SER) yields a value of 0.27 in SRHA solution while for 1,4-naphthoquinone the ratio was 0.36 at 20 °C. This suggests that formation of MSA relative to CHNO-containing amino acids was in similar proportion

between the 1,4-naphthoquinone and SRHA. The slightly decreased ratio may indicate that the complex, macromolecular structure of SRHA may inhibit formation of MSA following S – C cleavage.

The time-dependent concentration profiles for organic acids (i.e., formic acid, acetic acid, and oxalic acid) and inorganic compounds (i.e., NH_4^+, SO_4^{2-}) are shown in Figure 36. Consistent with SRHA photolysis, formic acid demonstrated the most significant formation with MET present in solution. Comparing the organic acids, the amount of formation observed in order of decreasing significance was: formic acid (2.20 µM) > acetic acid (1.70 µM) > oxalic acid (0.60 µM). The formation of organic acids with MET present did not deviate significantly from SRHA photolysis (Figure 16; Section 3.1.2.3), indicating that their production was largely driven by the photolysis of SRHA. For example, the change in formic acid and oxalic acid concentration was 2.10 µM and 0.50 µM in SRHA photolysis, respectively. Acetate deviates from this demonstrating higher formation when MET was spiked into solution. Specifically, acetic acid increases by 0.70 µM in SRHA photolysis and 1.70 µM with MET present in solution over the 480 minute experiment. The corrected values associated with MET decay accounted for 5 ± 6%, 17 ± 14%, and 3 ± 3% for formic acid, acetic acid, and oxalic acid, respectively. The production of inorganic compounds of N and S were generally minimal in both SRHA photolysis and with MET present in solution. Photo-ammonification with MET present in SRHA solution is observed to very small degree, with an increase of 0.20 µM over the experiment. We previously observed higher photo-ammonification in the photolysis of SRHA, forming approximately 0.50 µM over the experiment; however, this may be owed to error in the initial sample measurement. Thus, it can be concluded that little to no photo-

ammonification is observed and that volatile products such as methional may not be formed.

Figure 36. Time-dependent concentration profiles for organic acids and inorganic compounds produced in 10 mg C/L SRHA solution at 20 °C. Error bars represent the standard deviation of triplicate measurements.

Sulfate formation was not significant in either SRHA photolysis or with MET present. Sulfate demonstrates highly similar trends in the photolysis of SRHA and when MET is present in solution, suggesting that the increases observed are associated with SRHA photolysis and not MET decay. This is consistent with results obtained for surrogate DOM solutions.

The results depicted for SRHA indicate that $^1O_2$-mediated oxidation of MET is the dominant pathway for decay as observed with 2-naphthaldehyde, yet the formation of fragmented byproducts indicate ^{3}CDOM* involvement that cannot be ignored. Furthermore, the proportions of key ^{3}CDOM*-induced fragmentation products were similar to that of 1,4-naphthoquinone as indicated by the ratio of MSA formation relative to CHNO-containing amino acids formation. The production of H_2O_2 was in agreement with the $^1O_2$ mechanisms for formation of MetO and DHM. While non-targeted screening was not applied to the standard isolate DOM, it is expected that a significant portion of MET decay that isn't accounted for is likely associated with DHM formation in SRHA solution.

3.2.3.2 Elliott Soil Humic Acid (ESHA)

In ESHA solution, the observed MET decay was much more significant than in SRHA solution, decreasing to just 42% of the initial MET concentration over the experiment. The pseudo-first-order decay rate was 3.17 x 10^{-5} s^{-1} (R^2 = 0.98), approximately four times faster than in SRHA and more comparable to 2-naphthaldehyde. The time-dependent concentration profiles for MET and major products produced in 10 mg C/L ESHA solution at 20 ºC are depicted in Figure 37.
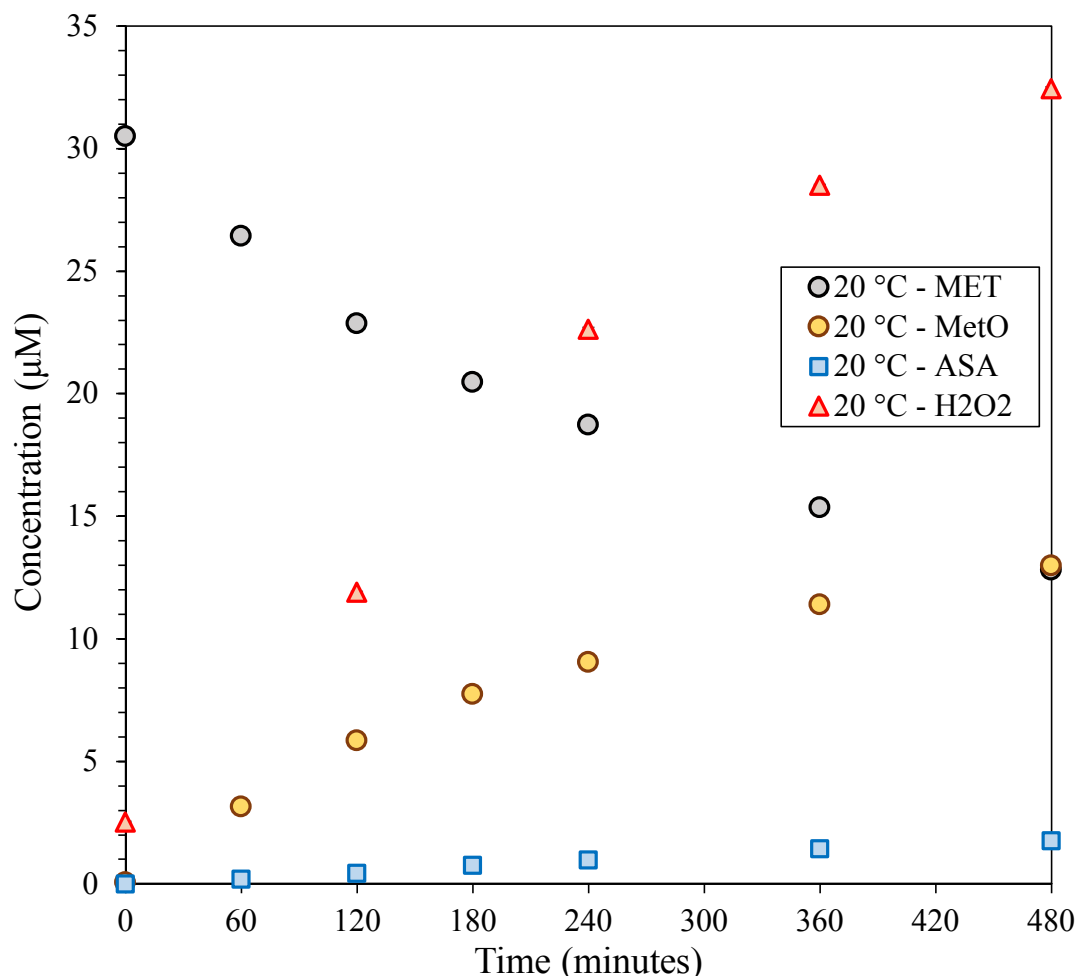
Figure 37. Time-dependent concentration profiles for MET and the major photo-transformation products produced in 10 mg C/L ESHA solution at 20 °C. Error bars represent the standard deviation of triplicate measurements.

Relative to SRHA, the enhanced MET decay in ESHA agrees with increased probe compound decay for both ^{3}CDOM* and $^1O_2$ probes (Section 3.1.2.2). As a result of enhanced $^1O_2$ production, the formation of MetO was significant and comprised a major fraction of MET transformation. Specifically, 13.00 μM of MetO was formed over the course of the experiment, accounting for 76 ± 1% of the observed MET decay on average. The production of H_2O_2 was significantly enhanced relative to what was produced in ESHA photolysis (Figure 15; Section 3.1.2.2). For example, formation of H_2O_2 at 480 minutes

80

was 12.00 μM in ESHA photolysis and 29.90 μM with MET present in solution. On average over time, the corrected results demonstrate increase of H_2O_2 associated with MET decay on the order of 9.90 ± 7.50 μM and a maximum increase of 17.90 μM at 480 minutes. Despite significantly higher formation of H_2O_2, the concentration formed is still not significant enough to contribute to significant decay of MET as with SRHA. Such high production is likely a strong indicator for the formation of DHM in ESHA solution.

Consistent with SRHA, the results so far indicate the dominant activity of $^1O_2$ in the transformation of MET. Production of MetO and H_2O_2 was significant and MetO accounted for a larger fraction of MET decay compared to SRHA. Given the enhanced production of $^3CDOM^*$ in ESHA, it was also expected that production of fragmented products would be increased relative to SRHA. The time-dependent concentration profiles for minor products are shown in Figure 35 for 10 mg C/L ESHA at 20 ^oC. As expected, the production of ASA was higher than what was observed in SRHA, forming 1.80 μM over the course of the experiment and accounting for 10% of MET decay. On average, $8 \pm 2\%$ of decay was accounted for by ASA formation. Other CHNO-containing amino acids were detected, yet their formation was insignificant as observed with SRHA. While ASP and SER concentrations were within detection limits, the minimal increases in concentration accounted for less than 1% of MET decay combined. Consistent with the formation of ASA in both 2-naphthaldehyde and SRHA, MSA production was observed in ESHA solution.
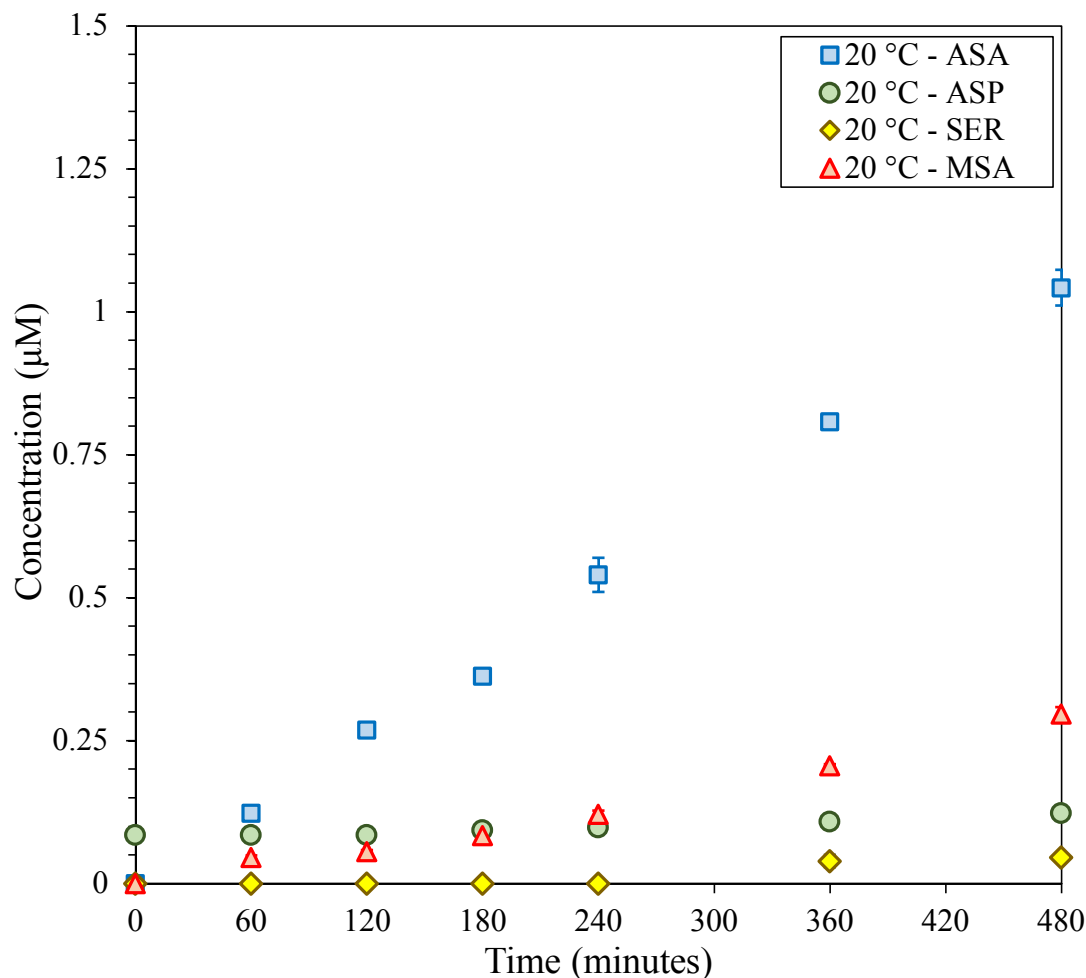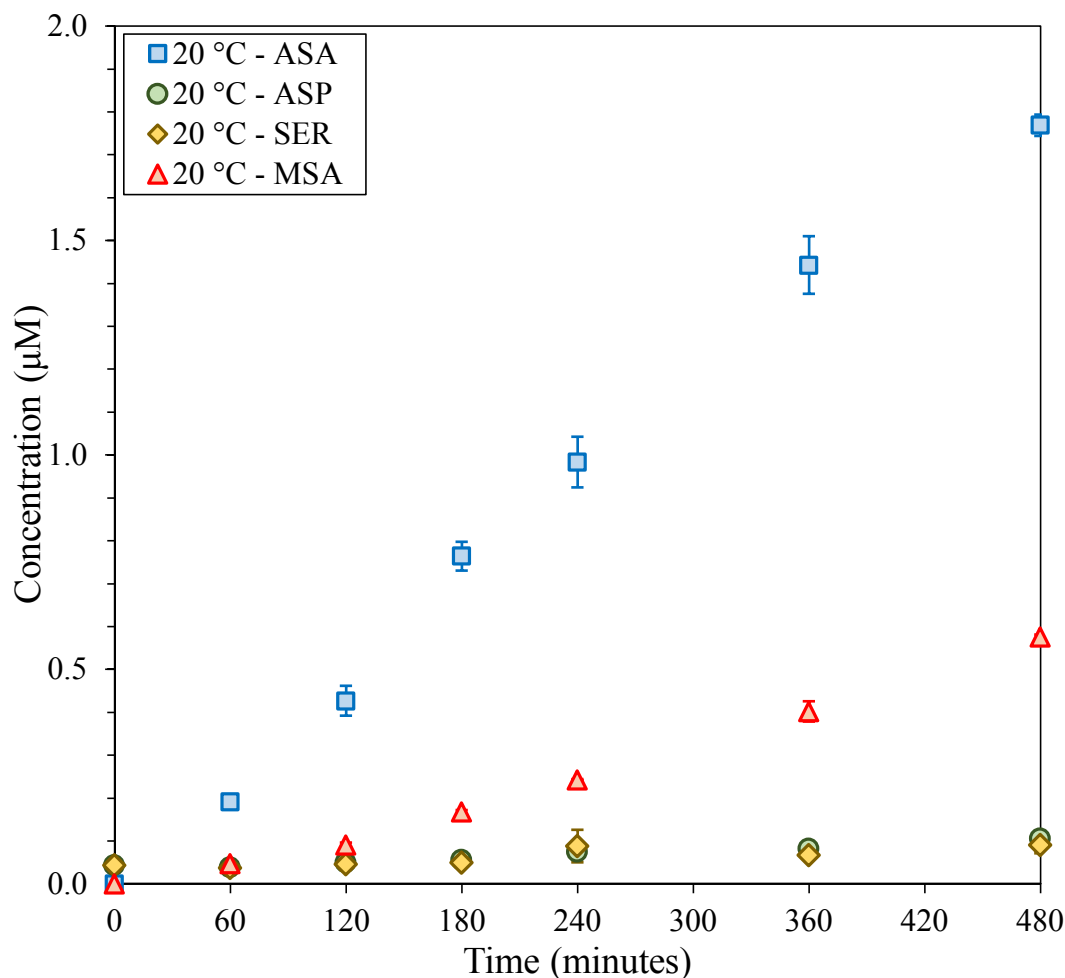
Figure 38. Time-dependent concentration profiles for the minor photo-transformation products produced in 10 mg C/L ESHA solution at 20 °C. Error bars represent the standard deviation of triplicate measurements.

MSA formation was higher in ESHA, forming 0.58 μM over the 480 minutes; however, the relative significance as a product was less than with SRHA. Specifically, MSA formation accounted for $2 \pm 1\%$ of MET decay on average. While ASA and MSA formation was increased in ESHA, the relative significance as a transformation product was lesser than in SRHA due to the rapid MET decay and MetO formation observed. Applying the same comparison as with SRHA, the ratio of Δ[MSA] to change in CHNO-containing amino acid concentration (i.e., ASA, ASP, and SER) yields a value of 0.31 compared to

0.27 for SRHA and 0.36 for 1,4-naphthoquinone. This suggests that formation of MSA relative to CHNO-containing amino acids was in similar proportion between the 1,4-naphthoquinone and both standard isolate DOM. On average between the surrogate and standard isolate DOM, the ratio was 0.31 ± 0.05. Furthermore, this result indicates that there is likely some loss of the fragmented thiol group due to volatilization. Considering the high activity of $^{1}O_2$ in both 1,4-naphthoquinone and ESHA, the higher ratios may be associated with increased production of MetO and subsequent reaction with $^{3}CDOM^*$, which was demonstrated to produce MSA and CHNO-containing amino acids in near 1:1 proportions (Figure 32; Section 3.2.2.2).

The time-dependent concentration profiles for organic acids (i.e., formic acid, acetic acid, and oxalic acid) and inorganic compounds (i.e., NH_4^+, SO_4^{2-}) are shown in Figure 39. Comparing the organic acids, the amount of formation observed in order of decreasing significance was: formic acid (1.30 µM) > acetic acid (0.90 µM) > oxalic acid (0.30 µM). Formic acid demonstrated less formation when MET was present in solution compared to ESHA photolysis. Similar to SRHA, acetic acid formation was enhanced in the presence of MET, accounting for 1 ± 1% of MET decay on average. Formic acid and oxalic acid accounted for less than 1% of MET decay, suggesting their formation is likely owed to the photolysis of ESHA and not transformation of MET.
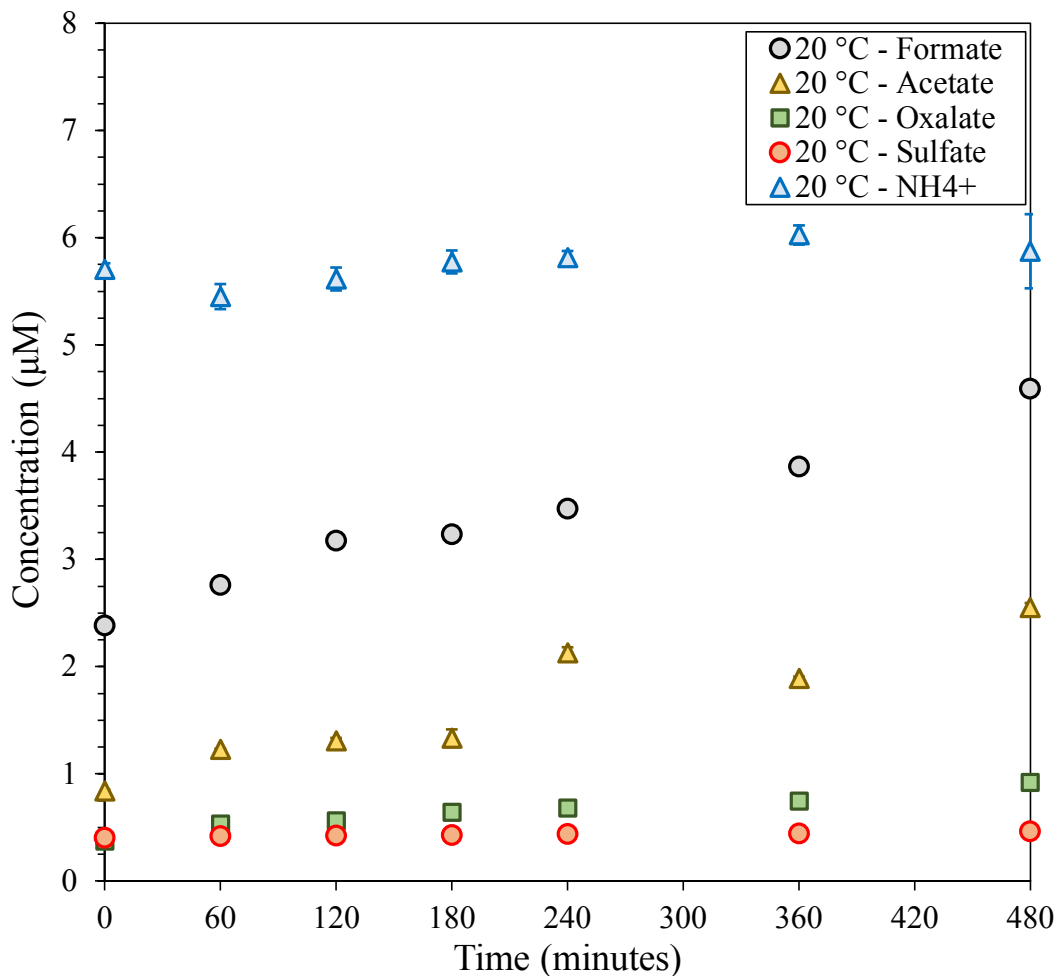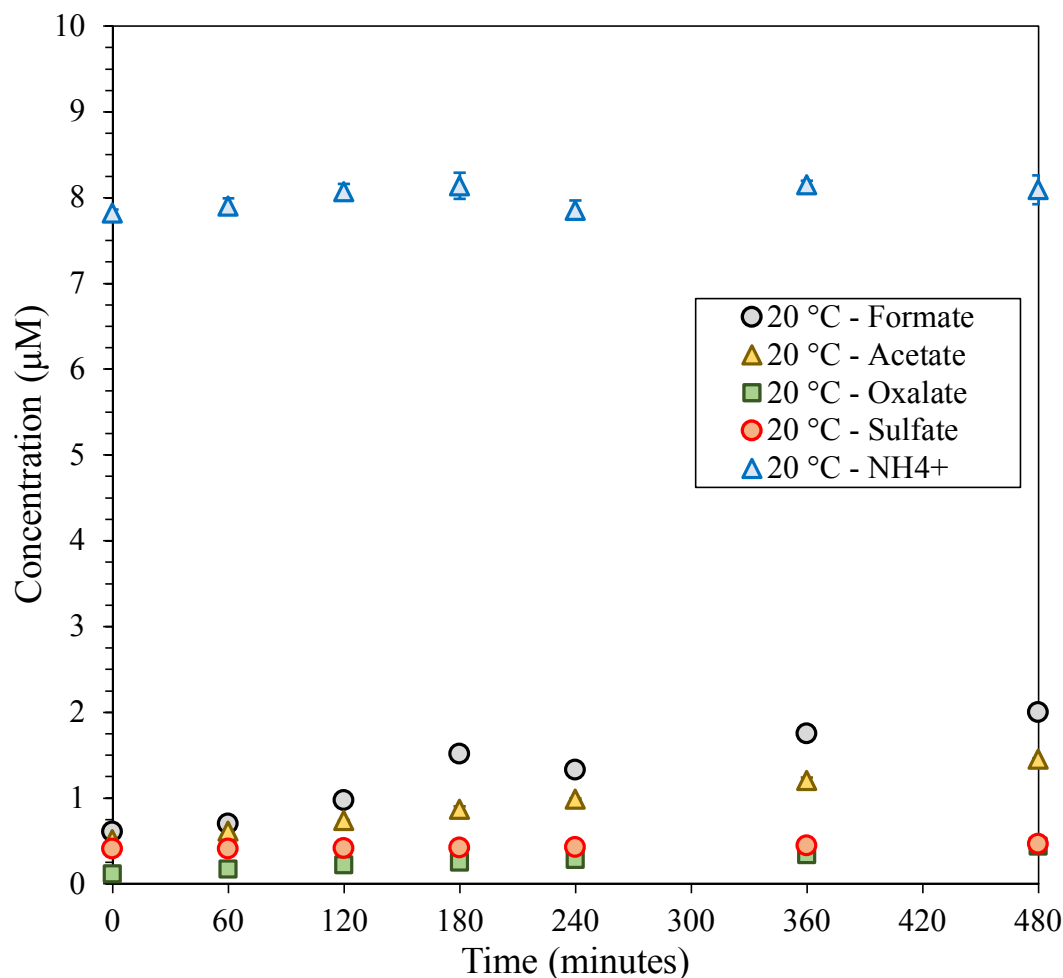
Figure 39. Time-dependent concentration profiles for organic acids and inorganic compounds produced in 10 mg C/L ESHA solution at 20 °C. Error bars represent the standard deviation of triplicate measurements.

The photo-mineralization of N and S was not observed in ESHA solution with or without MET present to a significant degree. Photo-ammonification with MET present was observed with generally increasing concentrations throughout the experiment, albeit only amounting to 0.30 μM of formation. In ESHA photolysis, [NH$_4^+$] remained stable until 480 minutes, where an increase of 0.50 μM is observed. This is consistent with what was observed with SRHA, yet the relatively steady increasing trends in ESHA suggest a degree

of enhancement with MET present. On average, photo-ammonification accounts for 2 ± 2% of MET decay. Sulfate formation was not significant in either SRHA photolysis or with MET present. Similar trends were observed for sulfate formation in SRHA photolysis and with MET is present in solution, suggesting that the increases observed are driven by SRHA photolysis and not MET decay.

The standard isolate DOM tested in this study demonstrated major formation of $^1O_2$-mediated transformation products consistent with those observed in 2-naphthaldehyde solution. Despite this, the minor transformation products indicated $^3CDOM^*$ involvement that contributed significantly to MET decay as observed in 1,4-naphthoquinone solutions. Furthermore, the production of MSA in standard isolate DOM relative to CHNO-containing amino acids was observed in similar proportions to that 1,4-naphthoquinone solutions, indicating similar $^3CDOM^*$-induced decay mechanisms occurred. The production of H_2O_2 in both SRHA and ESHA further agrees with $^1O_2$ mechanisms for the production of DHM and MetO. While non-targeted screening was not applied to the standard isolate DOM, it is expected that a significant portion of MET decay that isn't accounted for is likely associated with DHM formation.

3.2.4 Mass Balances & Conversion of Carbon, Nitrogen, & Sulfur

3.2.4.1 Dissolved Organic Carbon

The mass balance for dissolved organic carbon (DOC) was evaluated according to procedure described in Section 2.4.2. DOC concentrations, both measured and calculated based off quantified products in surrogate DOM solutions, are depicted in Figure 40.
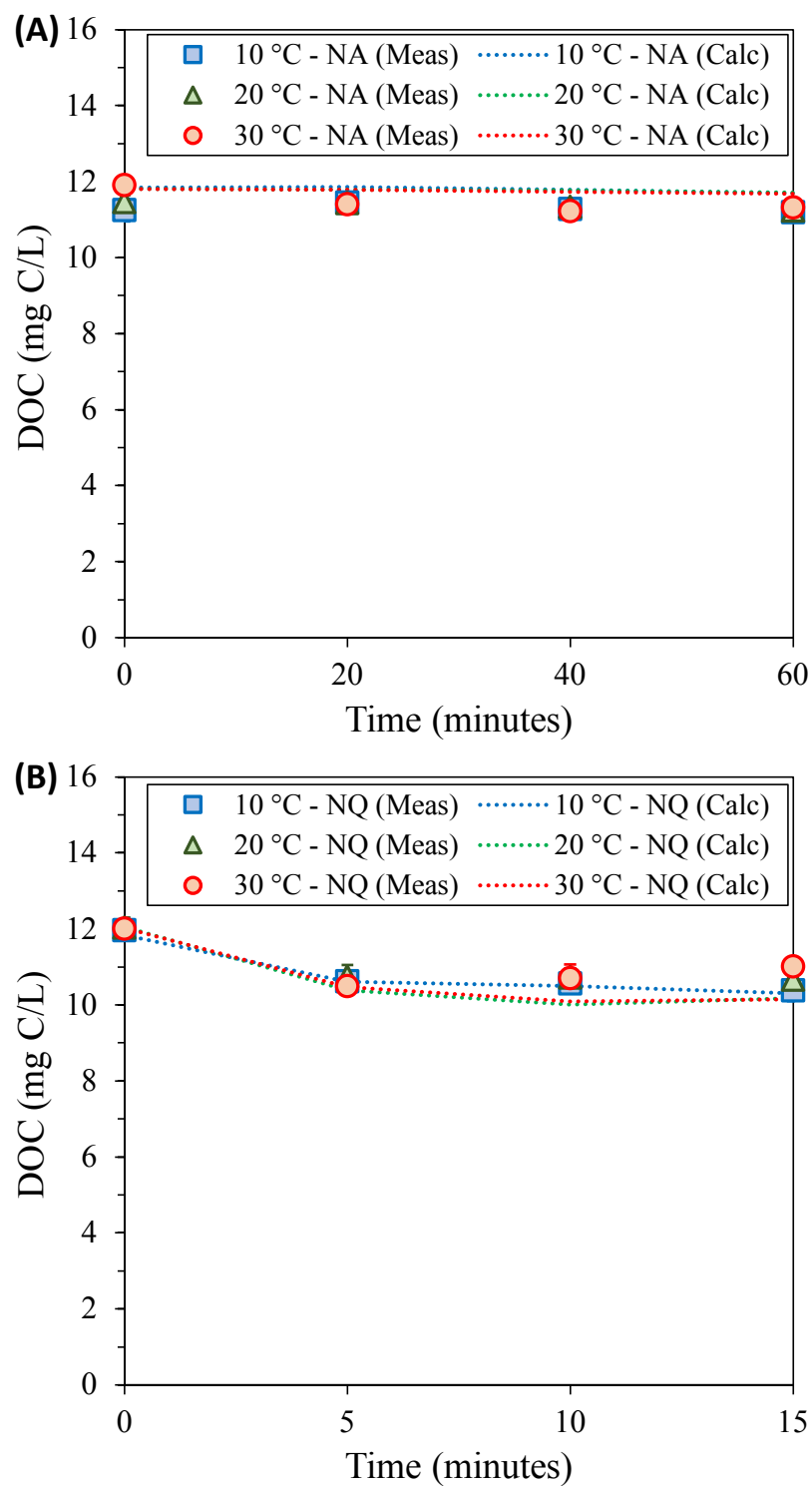
Figure 40. Time-dependent dissolved organic carbon (DOC) concentrations directly measured (markers) and calculated (lines) based on quantified products: (A) 2-naphthaldehyde and (B) 1,4-naphthoquinone.

Compounds accounted for in the calculated DOC for 2-naphthaldehyde included: MET, MetO, MSA, formic acid, acetic acid, and oxalic acid (Figure 40A). For 1,4-naphthoquinone, the compounds included in addition to those used for 2-naphthaldehyde were: ASA, ASP, SER, methional, and DMDS (Figure 40B). Consistent with low photo-transformation of 2-naphthaldehyde and high conversion to MetO, little changes in measured DOC were observed. Conversely, loss of DOC in all three solutions was observed in the first 5 minutes of irradiation in 1,4-naphthoquinone. The average loss of DOC at 15 minutes was 1.80 ± 0.20 mg C/L for all three temperatures. This was anticipated given the production of methional via MET-decarboxylation in addition to the production of other volatile species (ie., DMDS, MeSH) that can be lost from solution. Furthermore, the rapid photo-transformation of 1,4-naphthoquinone significantly contributed to loss of DOC, with an average loss of 1.60 ± 0.10 mg C/L at 15 minutes between the three temperatures. Taking the difference, approximately 0.20 ± 0.10 mg C/L of DOC lost is associated with MET decay corresponding to $11 \pm 6\%$ of the total loss observed. Thus, loss of DOC was predominantly driven by 1,4-naphthoquinone photolysis. The calculated DOC concentrations based on product concentrations fit the measured values well for both surrogate DOM. In 2-naphthaldehyde, the calculated DOC accounted for $104 \pm 1\%$, $104 \pm 1\%$, and $103 \pm 2\%$ of the measured DOC at 10, 20, and 30 ºC on average, respectively. Similar results were obtained for 1,4-naphthoquinone, where the calculated DOC accounted for $99 \pm 1\%$, $96 \pm 3\%$, and $97 \pm 4\%$ of the measured DOC at 10, 20, and 30 ºC on average, respectively. Generally, these results indicate that the C-containing products measured in each surrogate DOM solution accounted for significant fractions of DOC transformation.

87

The measured and calculated DOC concentrations for standard isolate DOM at 20 ºC are depicted in Figure 41. Calculated values of DOC in standard isolate DOM included the following compounds: MET, MetO, ASA, ASP, SER, MSA, formic acid, acetic acid, and oxalic acid. It is worthy to note that initial DOC concentrations were less than 10 mg C/L for standard isolate DOM due to the presence of inorganic and purgeable organic components present in standard isolate DOM.

Figure 41. Time-dependent dissolved organic carbon (DOC) concentrations directly measured (markers) and calculated (lines) based on quantified products in SRHA (blue) and ESHA (red) solutions at 20 ºC.

In SRHA solution, changes in DOC concentration were minimal throughout the experiment. The average measured DOC was 8.70 ± 0.20 mg C/L and reached a maximum at 480 minutes of 9.00 mg C/L. Similarly, the measured DOC concentration in SRHA photolysis demonstrated an average of 6.90 ± 0.20 mg C/L and reached a maximum at 480

minutes of 7.20 mg C/L. Conversely, decreases in the measured DOC concentration were observed throughout the experiment in ESHA solution. At 480 minutes, the loss of DOC was 1.20 mg C/L. In ESHA photolysis, the measured DOC showed an initial increase of up to 120 minutes followed by decreasing DOC concentrations up to 480 minutes. Relative to the initial 7.40 mg C/L at 0 minutes, the overall decrease of 0.40 mg C/L at 480 minutes corresponds to 33% of DOC loss associated with ESHA photolysis. From the maximum of 7.70 mg C/L at 120 minutes, the decrease of 0.70 mg C/L corresponds to approximately 60% of DOC loss associated with ESHA photolysis. The calculated values of DOC demonstrated good fits with measured values, consistent with surrogate DOM solutions. On average over time, calculated DOC based on measured products accounted for $100 \pm 1\%$ and $100 \pm 1\%$ of the measured DOC concentrations in SRHA and ESHA solution, respectively. Consistent with results for surrogate DOM, the standard isolate DOM demonstrated that the quantified C-containing transformation products accounted for significant fractions of DOC transformation, suggesting DOC was balanced well with measured products.

To further evaluate the transformation of C in surrogate and standard isolate DOM solutions, the conversion of MET to measured transformation products in terms of mg C/L was determined using the procedure described in Section 2.4.1. Compounds were grouped into classes, including: (1) MetO, (2) amino acids (i.e., ASA, ASP, and SER), (3) organic acids (i.e., MSA, formic acid, acetic acid, and oxalic acid), and (4) volatiles (i.e., methional and DMDS). MetO was evaluated separate from the amino acid class given the generally high conversion observed in 2-naphthaldehyde and standard isolate DOM solutions. The distribution of these classes in each solution is shown in Figure 42 at 20 ºC.
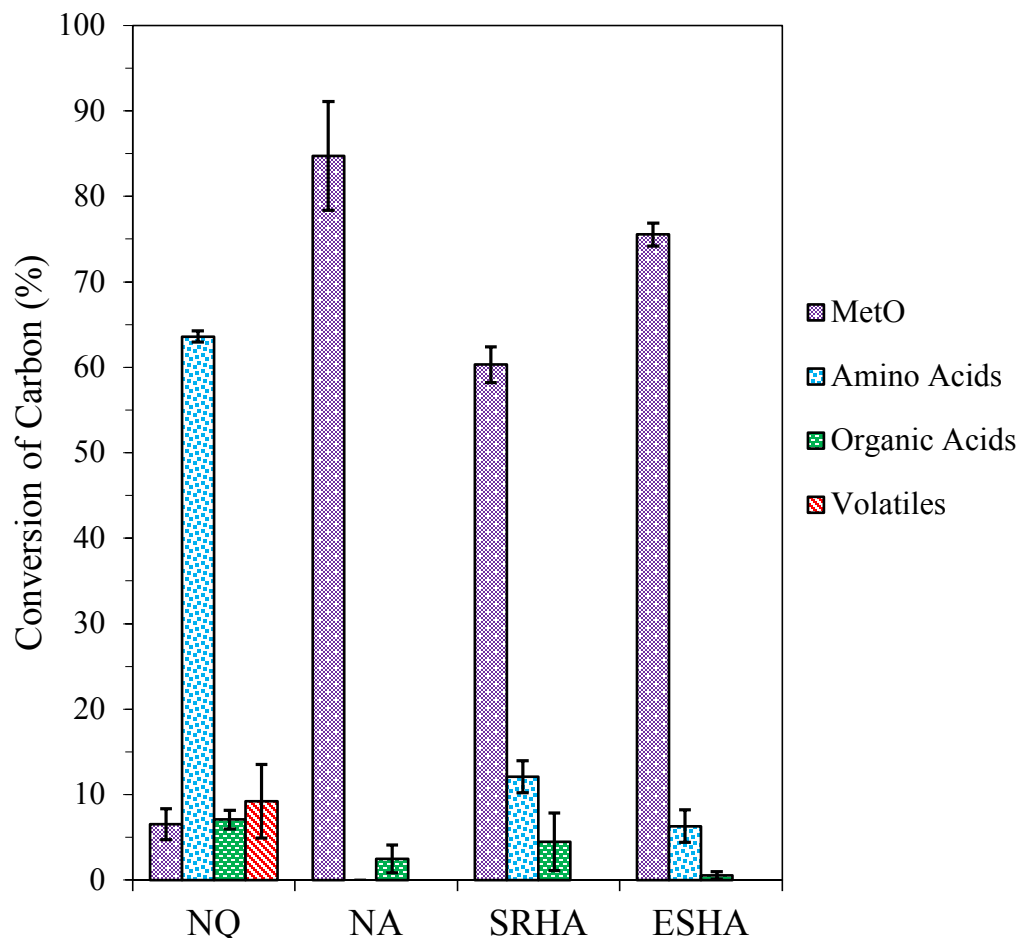
Figure 42. Distribution of quantified photo-transformation products based on conversion of carbon in surrogate and standard isolate DOM solutions at 20 ℃. Error bars represent the standard deviations of conversion over time for each compound class.

The total conversion of C accounted for by products measured was determined to be 86 ± 8% and 87 ± 8% in 2-naphthaldehyde and 1,4-naphthquinone, respectively. For standard isolate DOM, total conversion of C was determined to be 77 ± 7% and 82 ± 4% in SRHA and ESHA, respectively. Generally, the conversion of C was accounted for significantly by the quantified changes in products concentrations; however, important differences in distributions of each class were observed. Firstly, the production of MetO accounted for significant conversion of C in 2-naphthaldehyde and both standard isolate DOM. The

relative significance of MetO formation in decreasing order was: 2-naphthaldehyde (85 ± 6%) > ESHA (76 ± 1%) > SRHA (60 ± 2%) > 1,4-naphthoquinone (7 ± 2%). Secondly, production of other amino acids was dominant in 1,4-naphthoquinone and also observed to a lesser degree in standard isolate DOM solutions. The relative significance of amino acid production in decreasing order was: 1,4-naphthoquinone (64 ± 1%) > SRHA (12 ± 6%) > ESHA (6 ± 2%) > 2-naphthaldehyde (0%). For organic acids, the relative significance of formation in decreasing order was: 1,4-naphthoquinone (7 ± 1%) > SRHA (4 ± 3%) > 2-naphthaldehyde (2 ± 2%) > ESHA (<1%). Lastly, volatile formation observed in 1,4-naphthoquinone contributed significantly to conversion of C, accounting for 9 ± 4%.

Generally, it can be concluded that the product distributions in terms of C in standard isolate DOM closely resemble those observed in 2-naphthaldehyde. The significant production of MetO in these solutions accounted for the majority of C-conversion and verify the significant importance of $^1O_2$. Despite this, the production of CHNO-containing amino acids constituted a fraction of conversion that cannot be in ignored in standard isolate DOM solutions. Strong ^{3}CDOM-induced transformation was observed in 1,4-naphthoquinone and the production formation of ASA and MSA in standard isolate DOM suggests involvement of ^{3}CDOM.

3.2.4.2 Total Nitrogen

The mass balance on total nitrogen (TN) was evaluated following a same procedure as used for DOC (Section 2.4.2). Measured and calculated TN concentrations based on quantified product concentrations are depicted in Figure 43 for the surrogate DOM solutions at all three temperatures.
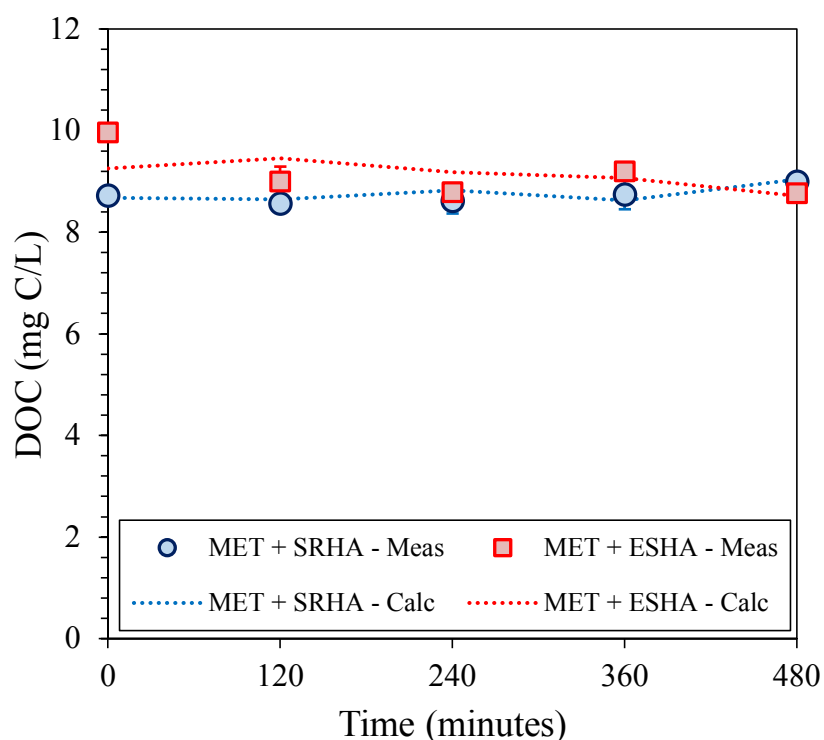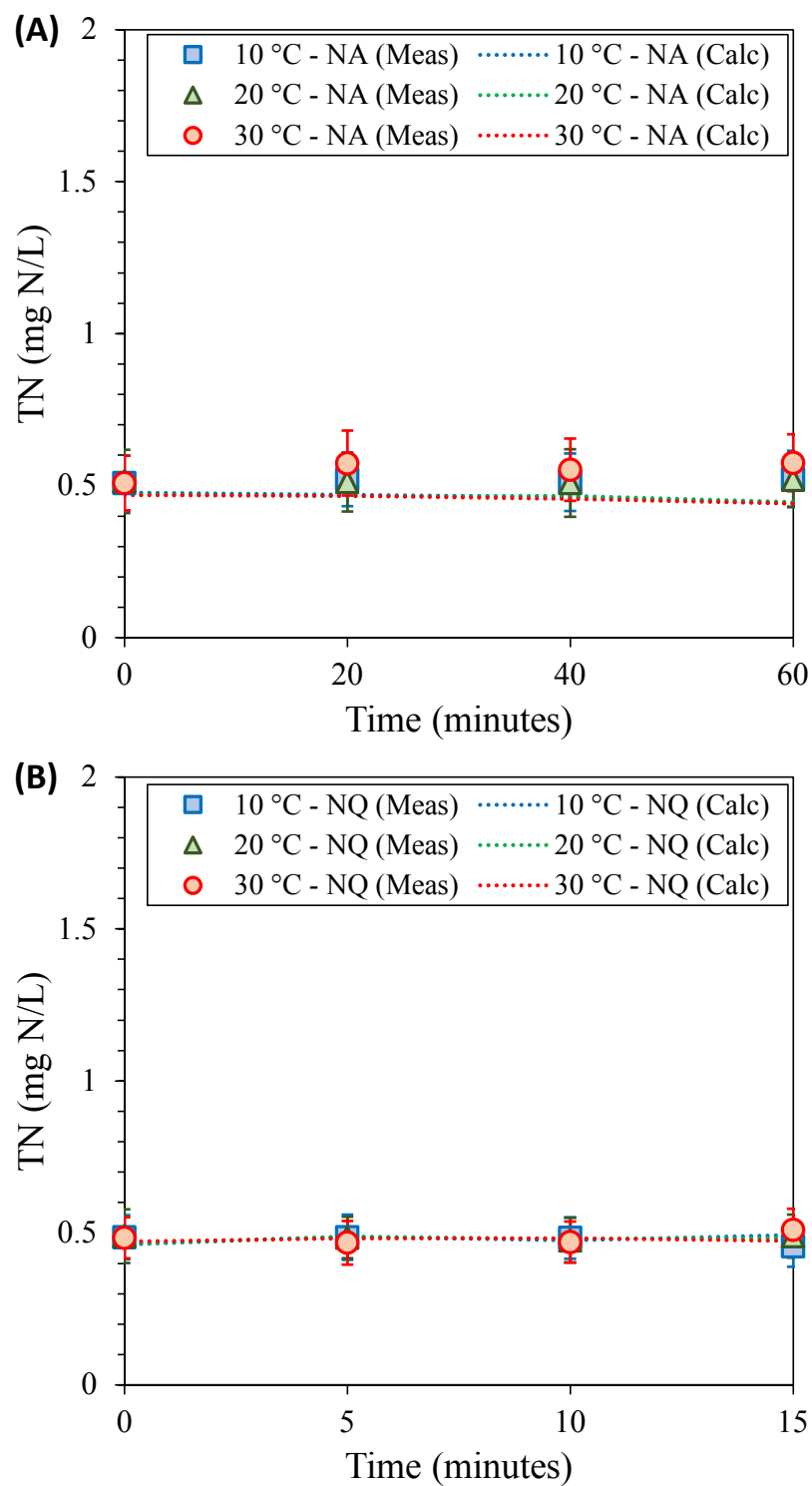
Figure 43. Time-dependent total nitrogen (TN) concentrations directly measured (markers) and calculated (lines) based on quantified products: (A) 2-naphthaldehyde and (B) 1,4-naphthoquinone.

92

Compounds accounted for in the calculation of TN for 2-naphthaldehyde included: MET, MetO, and NH_4^+ (Figure 43A). For 1,4-naphthoquinone, the compounds utilized in the calculation of TN included: MET, MetO, ASA, ASP, SER, and NH_4^+ (Figure 43B). Generally, it was anticipated that very little changes in measured TN concentration would be observed in surrogate DOM solutions, which is observed visually in Figure 43. In addition, the average measured TN concentration across time and temperature was 0.53 ± 0.03 mg N/L and 0.48 ± 0.01 mg N/L showing little variation for 2-naphthaldehyde and 1,4-naphthquinone, respectively. The calculated TN concentrations based on product concentrations provided good fits of the measured TN concentrations for both surrogate DOM. In 2-naphthaldehyde, the calculated TN accounted for $90 \pm 4\%$, $90 \pm 3\%$, and $83 \pm 6\%$ of the measured TN at 10, 20, and 30 ºC on average, respectively. Similar yet slightly improved results were obtained for 1,4-naphthoquinone, where the calculated TN accounted for $100 \pm 5\%$, $99 \pm 3\%$, and $99 \pm 5\%$ of the measured TN at 10, 20, and 30 ºC on average, respectively. The production of significant CHNO-containing amino acids, NH_4^+, and MetO seem to provide a better balance of TN in 1,4-naphthoquinone while the lack of DHM concentrations may account for the lesser balance of TN in 2-naphthaldehyde. Overall, the results demonstrate that the N-containing products measured in surrogate DOM solutions account for a significant fraction of the measured TN concentrations.

The measured and calculated TN concentrations for standard isolate DOM at 20 ºC are depicted in Figure 41. In standard isolate DOM, the calculated values of TN included the following compound concentrations: MET, MetO, ASA, ASP, SER, and NH_4^+.
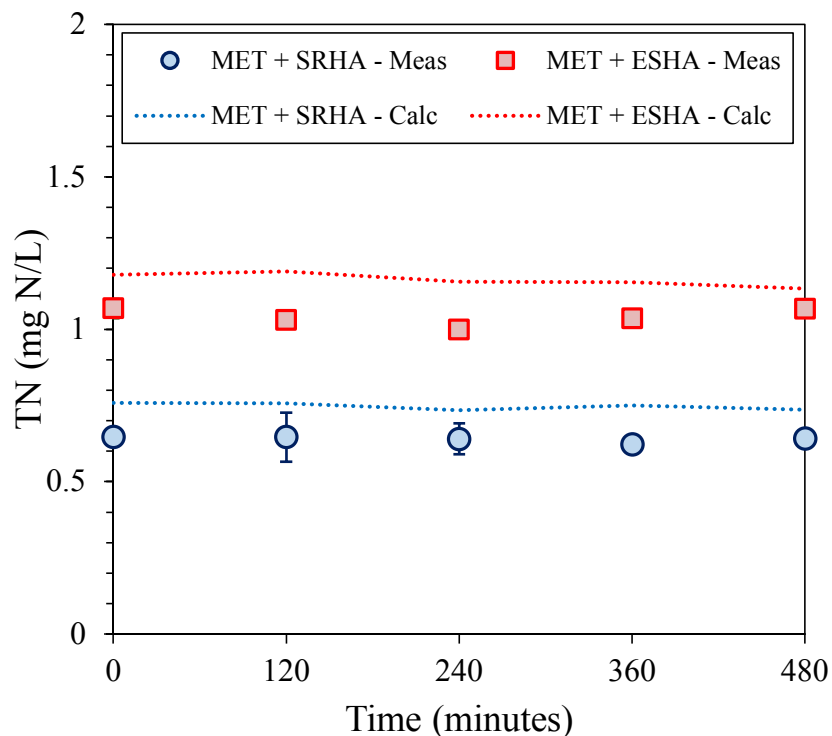
Figure 44. Time-dependent total nitrogen (TN) concentrations directly measured (markers) and calculated (lines) based on quantified products in SRHA (blue) and ESHA (red) solutions at 20 °C.

Consistent with surrogate DOM, the measured TN concentrations demonstrated very little changes over the experiment. The average TN concentrations over time were 0.64 ± 0.01 mg N/L and 1.04 ± 0.03 mg N/L for SRHA and ESHA, respectively. The average background concentrations of TN were 0.26 ± 0.01 mg N/L and 0.64 ± 0.01 mg N/L for the photolysis of SRHA and ESHA, respectively. The calculated TN concentration was generally higher than the measured TN concentration. Specifically, the calculated values of TN accounted for $117 \pm 2\%$ and $112 \pm 4\%$ of the measured TN concentration on average for SRHA and ESHA, respectively. While overestimated, these results generally agree with surrogate DOM in that N-containing compounds measured in experiments account for the measured TN concentrations and consequently the transformation of TN in solution.

To directly evaluate the conversion of N in MET to products measured, the same approach used for DOC was utilized (Section 2.4.1). Compounds were grouped into classes, including: (1) MetO, (2) amino acids (i.e., ASA, ASP, and SER), and (3) inorganic N (i.e. NH_4^+). Similar to DOC, MetO was evaluated as its own class due to the significant conversion observed in 2-naphthaldehyde and both standard isolate DOM solutions. The distribution of these classes in surrogate and standard isolate DOM solutions are shown in Figure 45 at 20 ºC.

Figure 45. Distribution of quantified photo-transformation products based on conversion of nitrogen in surrogate and standard isolate DOM solutions at 20 ºC. Error bars represent the standard deviations of conversion over time for each compound class.

The total conversion of N accounted for by products measured was determined to be $88 \pm 9\%$ and $110 \pm 4\%$ in 2-naphthaldehyde and 1,4-naphthquinone, respectively. For standard isolate DOM, total conversion of N was determined to be $78 \pm 7\%$ and $85 \pm 5\%$ in SRHA and ESHA, respectively. Consistent with the conversion of C, a significant fraction of N in MET was accounted for by the measured products, particularly regarding the formation of MetO. The relative significance of MetO formation for N-conversion in decreasing order was: 2-naphthaldehyde ($85 \pm 6\%$) > ESHA ($76 \pm 1\%$) > SRHA ($60 \pm 2\%$) > 1,4-naphthoquinone ($6 \pm 1\%$). For the production of other amino acids observed in 1,4-naphthoquinone and the standard isolate DOM, the relative significance to N-conversion in decreasing order was: 1,4-naphthoquinone ($80 \pm 1\%$) > SRHA ($15 \pm 2\%$) > ESHA ($8 \pm 2\%$) > 2-naphthaldehyde (0%). The photo-mineralization of N in MET was only significantly observed in 1,4-naphthoquinone. The relative significance of inorganic N (i.e. NH_4^+) to the conversion of N in decreasing order was: 1,4-naphthoquinone ($23 \pm 2\%$) > 2-naphthaldehyde ($3 \pm 2\%$) = SRHA ($3 \pm 2\%$) > ESHA ($1 \pm 1\%$).

Consistent with conversion of C, the product distributions in terms of N for standard isolate DOM further resemble that observed in 2-naphthaldehyde, with the exception of formation of CHNO-containing amino acids observed in standard isolate DOM. This agrees with previous conclusions that $^1O_2$-induced oxidation of MET to MetO dominates in standard isolate DOM solutions; however, $^3CDOM*$-induced transformation cannot be ignored as it contributes a significant fraction of transformation. The lack of MET photo-ammonification observed in 2-naphthaldehyde and standard isolate DOM further agree with minimal contributions of $^1O_2$ as speculated by Zhang et al. 2021 using rose bengal as a $^1O_2$ sensitizer.[49] The high photo-ammonification of MET observed in 1,4-

naphthoquinone agrees with the work by Zhang et al. 2021 using anthraquinone-2-sulfonate to evaluate contribution of ^{3}CDOM, suggesting quinones play an important role.[49] Despite this, discrepancies exist between the results described here and in the literature for standard isolate DOM. Tarr et al. 2000 reported significant photo-ammonification of 100 µM MET in the presence of 37 mg C/L SRHA on the order of 20 µM over 6 hours; however, this group did not employ strict temperature control of their solutions.[20] Zhang et al. 2021 reported photo-ammonification of 100 µM MET in natural water samples from various sources in China ranging from 11 – 16 µM over 6 hours, with reported solution temperature control at 25 ± 5 °C.[49] Beyond the lack of strict temperature control in these studies and higher MET and DOM concentrations, no clear differences can be attributed to the discrepancies identified. From a mechanistic standpoint, the production of S – C cleaved products (i.e., ASA, MSA) in standard isolate DOM may indicate preferential ^{3}CDOM*-induced reaction pathways with MET as observed for 1,4-naphthoquinone. Furthermore, the wide array of triplets with varying energies and triplet reduction potentials present in complex DOM may influence the availability of ^{3}CDOM* that can react with MET. The majority of triplets may undergo energy transfer with $^3O_2$ to produce $^1O_2$, which can shorten lifetimes of ^{3}CDOM* consequently reducing their concentration.[49]

3.2.4.3 Conversion of Sulfur

The conversion of S present in MET was evaluated similarly to the conversion previously discussed for C and N (Section 2.4.1). Compounds were group into classes, including: (1) MetO, (2) MSA, (3) Inorganic S (i.e. sulfate), and (4) Volatiles (i.e.,

methional and DMDS). MetO and MSA were evaluated as their own classes given their significance as transformation products in surrogate and standard isolate DOM solutions. The distribution of these classes in surrogate and standard isolate DOM solutions are shown in Figure 46 at 20 °C.
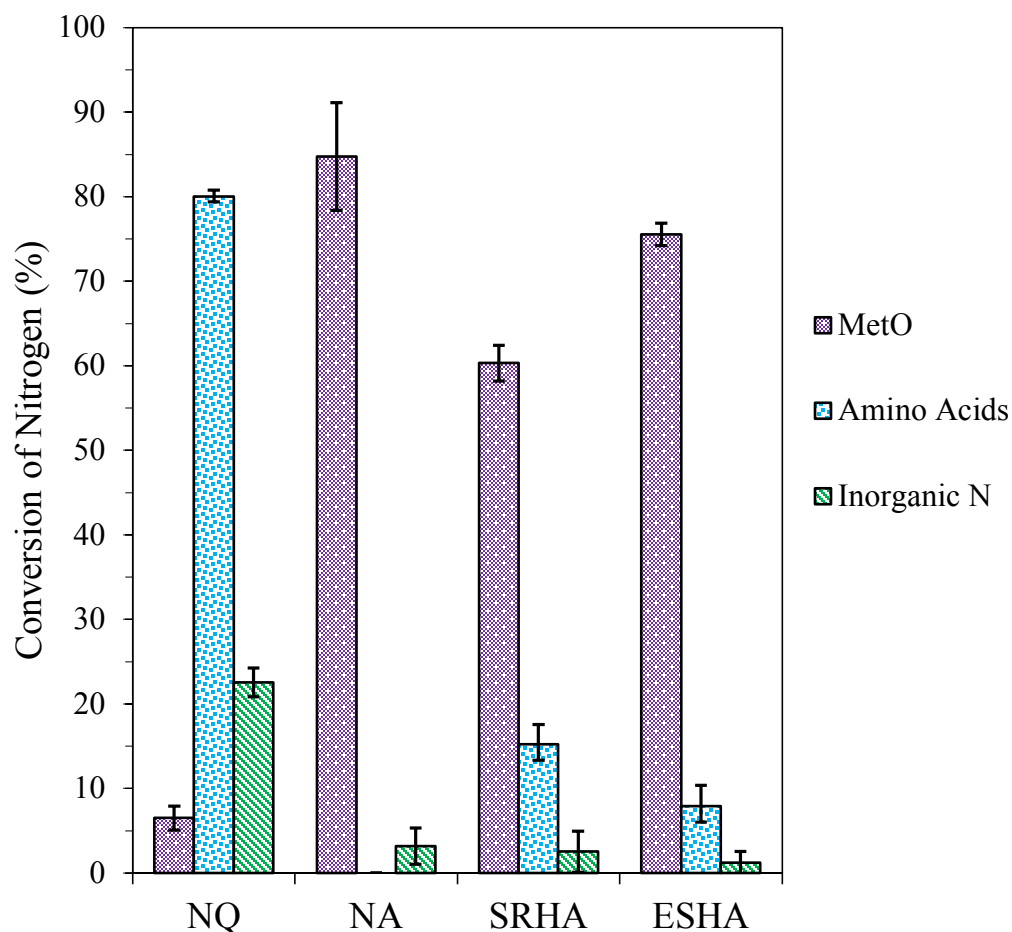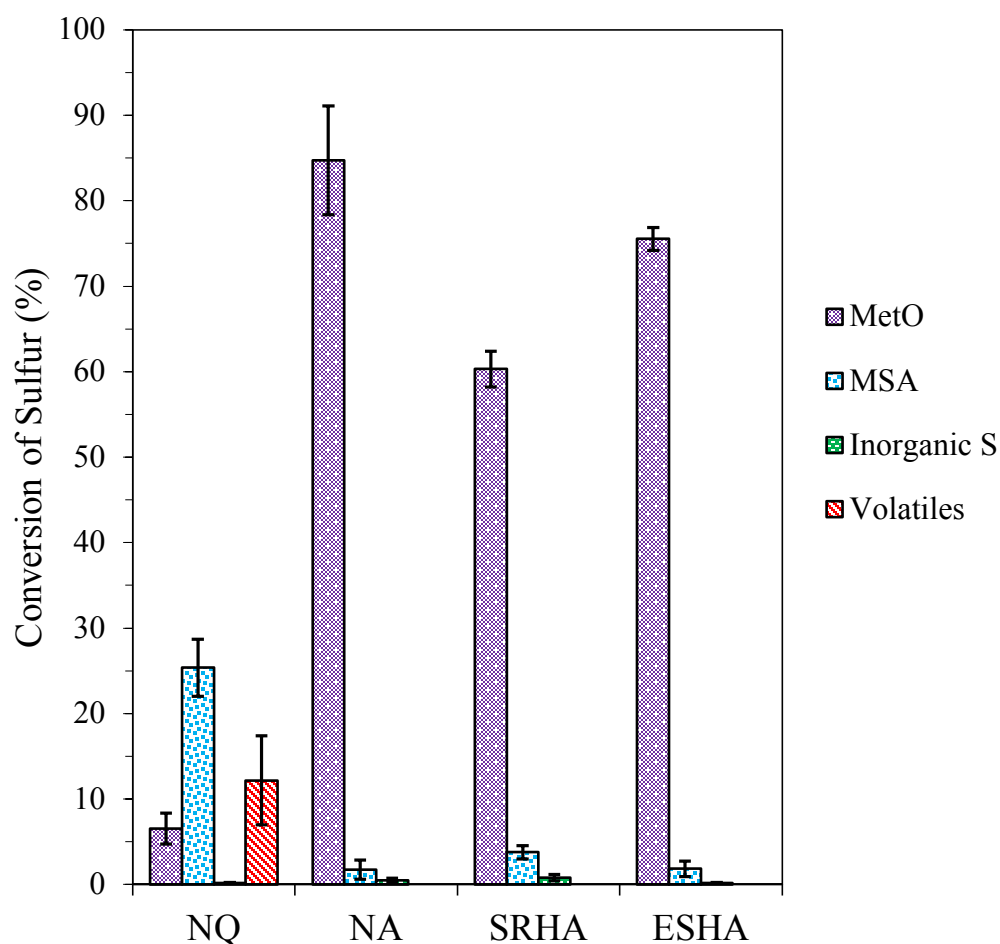

Figure 46. Distribution of quantified photo-transformation products based on conversion of sulfur in surrogate and standard isolate DOM solutions at 20 °C. Error bars represent the standard deviations of conversion over time for each compound class.

The total conversion of S accounted for by products measured was determined to be 87 ± 8% and 44 ± 10% in 2-naphthaldehyde and 1,4-naphthquinone, respectively. In standard isolate DOM solutions, the conversion of S accounted for by products measured was 65 ±

3% and 76 ± 2% for SRHA and ESHA, respectively. Similar to conversion of C and N, a significant fraction of the S-conversion was accounted for by oxidation to MetO in 2-naphthaldehyde and both standard isolate DOM. Specifically, the relative significance of MetO formation for S-conversion in decreasing order was: 2-naphthaldehyde (85 ± 6%) > ESHA (76 ± 1%) > SRHA (60 ± 2%) > 1,4-naphthoquinone (6 ± 2%). MSA formation was observed in all solutions to varying degrees and the relative significance for S-conversion in decreasing order was: 1,4-naphthoquinone (25 ± 3%) > SRHA (4 ± 1%) > ESHA (2 ± 1%) = 2-naphthaldehyde (2 ± 1%). The photo-mineralization of S present in MET to inorganic S (i.e. sulfate) was negligible in surrogate and standard isolate DOM solutions, with conversion values accounting for less than 1% of MET transformation. In 1,4-naphthoquinone, the conversion of S accounted for by products was low and the predominant S-products were MSA and volatile sulfur compounds. The production of volatiles in 1,4-naphthoquinone accounted for 12 ± 5% of the S-conversion.

The product distributions in terms of S-conversion demonstrates clear differences associated with the ^{3}CDOM*- and ^{1}O$_2$-induced transformation of MET. Consistent with both conversion of C and N, the S-conversion provides further demonstrates the similarities of 2-naphthaldehyde and the standard isolate DOM. The ^{1}O$_2$-mediated oxidation of MET to MetO is the predominant transformation pathway present in 2-naphthaldehyde and standard isolate DOM solutions, yet consistent observations of products indicative of S – C cleavage in MET provides evidence for ^{3}CDOM* involvement in standard isolate DOM. Interestingly, the production of MSA was observed in 2-naphthaldehyde despite the lack of formation of CHNO-containing amino acids as observed with 1,4-naphthoquinone, SRHA, and ESHA. This suggests a small degree of ^{3}CDOM*-induced transformation in 2-

naphthaldehyde and agrees with distributions observed for SRHA and ESHA. The observed production of volatile sulfur compounds indicates that loss of S to the atmosphere likely occurs in the [3]CDOM-induced transformation of MET. This is in agreement with the lower S-conversion accounted for in 1,4-naphthoquinone solutions and literature reported production of volatiles (e.g., methional, DMDS, MeSH).[34,36-38,48] Despite reported photo-mineralization of S in the literature for both the photolysis of various types of naturally-derived DOM and in the presence of MET,[13] we consistently observed negligible amounts of sulfate formation in surrogate and standard isolate DOM solutions. The works by Ossola et al. 2019 measured the production of MSA and sulfate from various DOS compounds, including thiols, thioethers, sulfonic acids and sulfate esters.[13] This group reported production of both MSA and sulfate from 50 µM MET in the presence of a naturally-derived sensitizer (dismal swamp water), forming approximately 1.90 µM of sulfate and 2.00 µM of MSA over 2 hours.[13] The production of MSA was only observed in methylated thioethers such as MET, suggesting that these compounds are the main precursors to MSA. Sulfate production from MET is indicative of $S-C$ cleavage and demethylation; however, Ossola et al. 2019 demonstrated the photo-stability of MSA with no production of sulfate, suggesting MSA is not subject to further oxidation.[13] Thiols such as cysteine appear to be more conducive to sulfate formation which agrees with the lack of observed MSA production when employing thiols as the parent compound. Even under highly oxidative conditions observed in 1,4-naphthoquinone, no sulfate production was observed from MET or MetO and the results generally suggest MSA is the dominant S-containing product followed by volatile sulfur compounds. The only clear difference between the works by Ossola et al. 2019 and this study is the utilization of a strict temperature control method

and mechanistic differences remain unclear. In general, more attention should be payed to solution temperature in studies of aquatic photochemistry to better replicate environmentally-relevant conditions.

4 Environmental Implication

Amino acids, both free and combined, represent important sources of key macronutrients providing the building blocks for protein synthesis and energy for microbial growth in natural waters. The abiotic transformation of amino acids has received considerable attention given their significant contributions to bacterial nitrogen demand and to DON pools in engineered and natural waters. The major sinks of amino acids include biological uptake, photochemical transformation, and abiotic adsorption.[67-70] During photosynthetic processes, organisms such as algae produce exudates of organic matter both actively and passively.[71,72] Notably, dissolved free and combined amino acids have been identified as primary algal exudates that are selectively and rapidly taken up by heterotrophic bacteria.[11,73,74] While all amino acids intrinsically relate to cycling of DOC and DON, S-containing amino acids and DOS in general have received less attention. In oxygenated surface waters, labile dissolved S species are assimilated by microorganisms to achieve cellular requirements of S and the formation of critical S-containing amino acids (e.g., cysteine and MET) for protein synthesis.[11,72] Concentrations of S-containing amino acids are low, representing less than 5% of the total amino acid pool; however, higher concentrations in cells further suggest rapid cycling in biota.[1,11] The relative contribution to the total DOS pool in the Eastern Atlantic indicated approximately 2% is derived from proteins, suggesting S-containing amino acids represent an important fraction of DOS subject to transformation in the ocean.[24] Understanding the abiotic sinks of S-containing amino acids has important implications for global cycling of C, N, and S.

Evaluating the relative magnitudes of abiotic sinks for S-containing amino acids is critical in natural waters. In the Atlantic Ocean, Zubkov et al. 2008 reported biological uptake rates for MET of 23 pmol L^{-1} h^{-1} ([MET] = 200 pmol L^{-1}) in temperate Atlantic waters, 12 pmol L^{-1} h^{-1} ([MET] = 410 pmol L^{-1}) in the Atlantic gyre, and 32 pmol L^{-1} h^{-1} ([MET] = 690 pmol L^{-1}) in the equatorial waters of the Atlantic.[75] These microbial uptake rates and concentrations yield half-lives ($t_{1/2}$) of 6 hours in the temperature regions, 24 hours for the gyre regions, and 15 hours in the equatorial waters of the Atlantic Ocean. Evaluating the observed pseudo-first-order decay rates of MET in 10 mg C/L SRHA (0.03 h^{-1}) and ESHA (0.11 h^{-1}), the corresponding $t_{1/2}$ values would be 23 hours for SRHA and 6 hours for ESHA. This suggests that photo-transformation in surface waters of the Atlantic Ocean have a high potential to impact bioavailability of MET. Recently, Brailsford et al. 2020 evaluated the heterotrophic bacterial uptake of isotopically labeled MET and cysteine in upland oligotrophic and lowland mesotrophic river samples.[11] The decay rates observed were 0.89 h^{-1} and 2.36 h^{-1} in upland oligotrophic and lowland mesotrophic river samples, respectively. These rates correspond to much more rapid $t_{1/2}$ values, just 0.3 hours and 0.8 hours for upland oligotrophic and lowland mesotrophic samples, respectively. While this suggests a much lesser impact on bioavailability, the rates of decay in SRHA and ESHA constitute $1 - 3\%$ and $5 - 13\%$ of the observed biological depletion rates, respectively. Consequently, photo-transformation is still likely to have an impact on bioavailability in these waters. Furthermore, this highlights the importance of the characteristics of the DOM present as well as the relative productivity in natural waters. For example, if we compare rates of decay in ESHA with that determined for the river samples, the photo-transformation rate constitutes 5% in mesotrophic waters and increases to 13% in

103

oligotrophic waters. This suggests the importance of photo-transformation as a sink increases in less biologically productive systems, such arctic lakes and rivers.[75]

While photo-transformation processes for MET are of clear importance to its bioavailability in natural waters, the ability of biota to utilize the transformation products is key to understanding the fate of MET in sunlit surface waters. In this study, we identified multiple classes of transformation products including oxidized forms of MET (i.e. MetO), fragmented CHNO-containing amino acids (i.e., ASA, ASP, and SER), DOS compounds (i.e., MSA, methional, and DMDS), and photo-mineralized inorganic compounds (i.e. NH_4^+). The predominant conversion of MET to MetO is one of the few transformations that is known to be biologically reversible through MSRs.[34,35] In cellular proteins, MET residues can act as antioxidants where MSRs can access the residue to reverse the oxidative damage whereas when bound in the core of proteins, the oxidation to MetO can lead to loss of protein function due to decreased hydrophobicity.[34,35] The irreversible oxidation of MET to CHNO-containing amino acids suggest a lesser impact on availability of DOC and DON but has potential to impact the bioavailability of S. Indeed, the production of volatile species could yield a flux of DOS into the atmosphere, yet uptake and incorporation of volatile DOS compounds into proteins has been reported in the literature for compounds such as MeSH, a further degradation product of methional.[77] Furthermore, MSA has been shown to be utilized by microorganisms as a source for C, S, and energy in various environments, with particular importance in marine environments.[13] Uptake of inorganic forms of S (i.e. sulfate) and N (i.e. NH_4^+) are the predominant forms utilized in the synthesis of proteins, yet these processes are more energy intensive.[1,11] The lack of photo-

mineralized S observed in this study suggests S remains bound in organic forms that may be utilized by microorganisms or lost to the atmosphere through volatile production.

While this study identified various products produced from both triplet-state dissolved organic matter and $^1O_2$, further research should be completed to evaluate of specific functional groups found in naturally-derived dissolved organic matter. More research comparing the differences in structural components of naturally-derived dissolved organic matter is likely needed. Furthermore, more attention should be payed to the energetic feasibility of triplet-states in the transformation of methionine and evaluating the different energetic pools found in naturally-derived dissolved organic matter. The work here highlights the importance of quinones and their high oxidizing capabilities and future work should give focus to such functional groups and their role in irreversible oxidative damage to proteins and free amino acids. Future studies should employ stricter temperature-control to better replicate environmentally-relevant surface water conditions to elucidate whether or not DOS such as MET is photo-mineralized to sulfate. Furthermore, the quantification of the transformation products detailed in this study should be expanded to other surrogate and naturally-derived DOM in photo-sensitized experiments to further elucidate the understanding of different reactive species in their production and the roles of specific functional groups.

5 Reference List

1. Lundeen, R. A.; Janssen, E. M. L.; Chu, C.; McNeill, K., Environmental photochemistry of amino acids, peptides and proteins. *Chimia* **2014,** *68,* (11), 812-824.

2. Cui, X.; Choo, K.-H. Natural Organic Matter Removal and Fouling Control in Low-Pressure Membrane Filtration for Water Treatment. *Environmental Engineering Research* **2014**, *19* (1), 1–8.

3. Michael-Kordatou, I.; Michael, C.; Duan, X.; He, X.; Dionysiou, D.; Mills, M.; Fatta-Kassinos, D. Dissolved Effluent Organic Matter: Characteristics and Potential Implications In Wastewater Treatment and Reuse Applications. *Water Research* **2015**, *77*, 213-248.

4. Gonsior, M.; Zwartjes, M.; Cooper, W. J.; Song, W.; Ishida, K. P.; Tseng, L. Y.; Jeung, M. K.; Rosso, D.; Hertkorn, N.; Schmitt-Kopplin, P. Molecular Characterization of Effluent Organic Matter Identified by Ultrahigh Resolution Mass Spectrometry. *Water Research* **2011**, *45* (9), 2943–2953.

5. Rice, J.; Westerhoff, P., Spatial and Temporal Variation in De Facto Wastewater Reuse in Drinking Water Systems across the U.S.A. *Environmental Science & Technology* **2014,** *49* (2), 982-989.

6. Boreen, A. L.; Edhlund, B. L.; Cotner, J. B.; McNeill, K., Indirect photodegradation of dissolved free amino acids: The contribution of singlet oxygen and the differential reactivity of DOM from various sources. *Environmental Science and Technology* **2008,** *42*, (15), 5492-5498.

7. Pehlivanoglu-Mantas, E.; Sedlak, D. L., Measurement of dissolved organic nitrogen forms in wastewater effluents: Concentrations, size distribution and NDMA formation potential. *Water Research* **2008,** *42*, (14), 3890-3898.

8. Bronk, D. A. Dynamics of DON. *Biogeochem. Mar. Dissolved Org. Matter* **2002**, 153–247.

9. Keil, R. G.; Kirchman, D. L. Contribution of dissolved free amino acids and ammonium to the nitrogen requirements of heterotrophic bacterioplankton. *Mar. Ecol.: Prog. Ser.* **1991**, *73* (1), 1–10.

10. Middelboe, M.; Borch, N. H.; Kirchman, D. L. Bacterial utilization of dissolved free amino acids, dissolved combined amino acids and ammonium in the Delaware Bay estuary: effects of carbon and nitrogen limitation. *Mar. Ecol.: Prog. Ser.* **1995**, *128* (1 to 3), 109–120.

11. Brailsford, F. L.; Glanville, H. C.; Wang, D.; Golyshin, P. N.; Johnes, P. J.; Yates, C. A.; Jones, D. L. Rapid Depletion of Dissolved Organic Sulphur (DOS) in Freshwaters. *Biogeochemistry* **2020**, *149* (1), 105–113.

12. Chu, C.; Lundeen, R. A.; Remucal, C. K.; Sander, M.; McNeill, K., Enhanced indirect photochemical transformation of histidine and histamine through association with chromophoric dissolved organic matter. *Environmental Science and Technology* **2015,** *49*, (9), 5511-5519.

13. Ossola, R.; Tolu, J.; Clerc, B.; Erickson, P. R.; Winkel, L. H. E.; McNeill, K. Photochemical Production of Sulfate and Methanesulfonic Acid from Dissolved Organic Sulfur. *Environmental Science and Technology.* **2019**, *53* (22), 13191 − 13200.

14. Ossola, R.; Clerc, B.; McNeill, K. Mechanistic Insights into Dissolved Organic Sulfur Photo-mineralization through the Study of Cysteine Sulfinic Acid. *Environmental Science & Technology* **2020**, *54* (20), 13066–13076.

15. McNeill, K.; Canonica, S., Triplet state dissolved organic matter in aquatic photochemistry: Reaction mechanisms, substrate scope, and photophysical properties. *Environmental Science: Processes and Impacts* **2016,** *18*, (11), 1381-1399.

16. Appiani, E.; Ossola, R.; Latch, D. E.; Erickson, P. R.; McNeill, K., Aqueous singlet oxygen reaction kinetics of furfuryl alcohol: effect of temperature, pH, and salt content. *Environmental Science: Processes & Impacts* **2017**, *19* (4), 507-516.

17. Hubig, S. T., Bockman, T. M., and Kochi, J. K., Identification of Photexcited Singlet Quinones and Their Ultrafast Electron-Transfer vs Intersystem Crossing Rates. *Journal of the American Chemical Society* **1997**, *119* (12), 2926-2935

18. Canonica, S.; Jans, U. R. S.; Stemmler, K.; Hoigne, J., Transformation Kinetics of Phenols in Water: Photosensitization. *Environmental Science & Technology* **1995**,

29, (7), 1822-1831.

19. Mopper, K.; Kieber, D. J.; Stubbins, A. Chapter 8 – Marine Photochemistry of Organic Matter: Processes and Impacts A2 - Hansell, Dennis A. In Biogeochemistry of Marine Dissolved Organic Matter, 2nd ed.; Carlson, C. A., Ed.; Academic Press: Boston, **2015**; pp 389−450.

20. Tarr, M., Wang, W., Bianchi, T., Engelhaupt, E. Mechanisms of ammonia and amino acid photoproduction from aquatic humic and colloidal matter. *Water Research* **2001**, *35* (15), pp.3688-3696.

21. Holmer, M. and Storkholm, P. Sulphate reduction and sulphur cycling in lake sediments: a review. *Freshwater Biology* **2001**, 46(4), pp.431-451.

22. Hornak, K.; Schmidheinv, H.; Pernthaler, J. High throughput determination of dissolved free amino acids in unconcentrated freshwater by ion-pairing liquid chromatography and mass spectrometry. *Journal of Chromatography A* **2016**, *1440*, 85-93

23. Ho, T.; Quigg, A.; Finkel, Z.; Milligan, A.; Wyman, K.; Falkowski, P.; Morel, F. THE ELEMENTAL COMPOSITION OF SOME MARINE PHYTOPLANKTON. *Journal of Phycology* **2003**, *39* (6), 1145-1159.

24. Ksionzek, K.; Lechtenfeld, O.; McCallister, S.; Schmitt-Kopplin, P.; Geuer, J.; Geibert, W.; Koch, B., 2016. Dissolved Organic Sulfur In The Ocean: Biogeochemistry Of A Petagram Inventory. *Science* **2016**, *354* (6311), 456-459.

25. Gomez-Saez, G. V.; Pohlabeln, A. M.; Stubbins, A.; Marsay, C. M.; Dittmar, T. Photochemical Alteration of Dissolved Organic Sulfur from Sulfidic Porewater. *Environmental Science & Technology* **2017**, *51*, 14144− 14154.

26. Stubbins, A.; Dittmar, T. Illuminating the Deep: Molecular Signatures of Photochemical Alteration of Dissolved Organic Matter from North Atlantic Deep *Water Marine Chemistry* **2015**, *177*, 318−324.

27. Antony, R.; Willoughby, A. S.; Grannas, A. M.; Catanzano, V.; Sleighter, R. L.; Thamban, M.; Hatcher, P. G. Photo-Biochemical Transformation of Dissolved Organic Matter on the Surface of the Coastal East Antarctic Ice Sheet.

Biogeochemistry **2018**, *141*, 229−247.

28. Herzsprung, P.; Hertkorn, N.; Friese, K.; Schmitt-Kopplin, P. Photochemical Degradation of Natural Organic Sulfur Compounds (CHOS) from Iron-Rich Mine Pit Lake Pore Waters–an Initial Understanding from Evaluation of Single-Elemental Formulae Using Ultra-High Resolution Mass Spectrometry. *Rapid Commun. Mass Spectrum.* **2010**, *24* (19), 2909−2924.

29. Du, Q.; Mu, Y.; Zhang, C.; Liu, J.; Zhang, Y.; Liu, C. Photochemical Production of Carbonyl Sulfide, Carbon Disulfide and Dimethyl Sulfide in a Lake Water. *Journal of Environmental Science* **2017**, *51*, 146−156

30. Uher, G.; Pillans, J. J.; Hatton, A. D.; Upstill-Goddard, R. C. Photochemical Oxidation of Dimethylsulphide to Dimethylsulphoxide in Estuarine and Coastal Waters. *Chemosphere* **2017**, 186, 805−816.

31. Hoffmann, E. H.; Tilgner, A.; Schrödner, R.; Bräuer, P.; Wolke, R.; Herrmann, H. An Advanced Modeling Study on the Impacts and Atmospheric Implications of Multiphase Dimethyl Sulfide Chemistry. *Proceedings of the National Academy of Sciences of the U.S.A.* **2016**, *113* (42), 11776−11781.

32. Houle, T.; Carignan, R.; Lachance, M and Dupont, J. Dissolved organic carbon and sulfur in southwestern Quebec lakes: Relationships with catchment and lake properties. *Limnology and Oceanography*, **1995**, *40* (4), 710-717

33. Hawkins, C. L.; Davies, M. J. Detection, Identification, and Quantification of Oxidative Protein Modifications. *Journal of Biological Chemistry* **2019**, *294* (51), 19683–19708.

34. Schöenich, C. Methionine oxidation by reactive oxygen species: reaction mechanisms and relevance to Alzheimer's disease. *Biochemica et Biophysica Acta (BBA) – Proteins and Proteomics* **2005,** *1703* (2), 111-119.

35. Liu, F.; Lu, W.; Yin, X.; Liu, J. Mechanistic and Kinetic Study of Singlet O2 Oxidation of Methionine by on-Line Electrospray Ionization Mass Spectrometry. *Journal of the American Society for Mass Spectrometry* **2015**, *27* (1), 59–72.

36. Asaduzzaman, M.; Scampicchio, M.; Biasioli, F.; Bremer, P. J.; Silcock, P.

Methanethiol Formation during the Photochemical Oxidation of Methionine-Riboflavin System. *Flavour and Fragrance Journal* **2019**, *35* (1), 34–41.

37. Furet, A.; Sicello, A.; Guillemat, B.; Absalon, C.; Langleron, E.; Bassani, D. M. Revisiting the Mechanism Responsible for the Light-Struck Flavor in White Wines and Champagnes. *Food Chemistry* **2022**, *372*, 131281.

38. Fracassetti, D.; Limbo, S.; Pellegrino, L.; Tirelli, A. Light-Induced Reactions of Methionine and Riboflavin in Model Wine: Effects of Hydrolysable Tannins and Sulfur Dioxide. *Food Chemistry* **2019**, *298*, 124952.

39. Fracassetti, D.; Tirelli, A.; Limbo, S.; Mastro, M.; Pellegrino, L.; Ragg, E. M. Investigating the Role of Antioxidant Compounds in Riboflavin-Mediated Photo-Oxidation of Methionine: A 1H-NMR Approach. *ACS Omega* **2020**, *5* (40), 26220–26229.

40. Sysak, P. K.; Foote, C. S.; Ching, T. Y., CHEMISTRY OF SINGLET OXYGEN—XXV. PHOTOOXYGENATION OF METHIONINE*. *Photochemistry and Photobiology* **1977,** *26*, (1), 19-27.

41. Castaño, C.; Thomas, A. H.; Lorente, C. Type I Photosensitized Oxidation of Methionine. *Photochemistry and Photobiology* **2020**, *97* (1), 91–98.

42. Peskin, A. V.; Turner, R.; Maghzal, G. J.; Winterbourn, C. C.; Kettle, A. J. Oxidation of Methionine to Dehydromethionine by Reactive Halogen Species Generated by Neutrophils. *Biochemistry* **2009**, *48* (42), 10175–10182.

43. Beal, J. L.; Foster, S. B.; Ashby, M. T.; Hypochlorous Acid Reacts with the N-terminal Methionines in Proteins to Give Dehydromethionine, a Potential Biomarker for Neutrophil-Induced Oxidative Stress. *Biochemistry* **2009,** *48* (46), 11142-11148

44. Nascimento, R. O.; Prado, F. M.; Massafera, M. P.; Di Mascio, P.; Ronsein, G. E. Dehydromethionine Is a Common Product of Methionine Oxidation by Singlet Molecular Oxygen and Hypohalous Acids. *Free Radical Biology and Medicine* **2022**, *187*, 17–28.

45. Barrios, B.; Mohrhardt, B.; Doskey, P. V.; Minakata, D. Mechanistic Insight into the Reactivities of Aqueous-Phase Singlet Oxygen with Organic Compounds. *Environmental Science & Technology* **2021**, *55* (12), 8054–8067.

46. Ossola, R.; Jönsson, O. M.; Moor, K.; McNeill, K. Singlet Oxygen Quantum Yields in Environmental Waters. *Chemical Reviews* **2021**, *121*, 4100-4146

47. Marcinak, B. and Bobrowski, K. Photo- and Radiation-Induced One-Electron Oxidation of Methionine in Various Structural Environments Studied by Time-

Resolved Techniques. *Molecules* **2022**, *27*, 1028

48. Spasojevic, I.; Bogdanovic, P.; Vujisic, L.; Spasic, M., The reaction of methionine with hydroxyl radical: reactive intermediates and methanethiol production. *Amino Acids* **2012**, *42*, 2439-2445

49. Zhang, Y.; Zhang, R,; Li, S-L.; Mostofa, K. M. G.; Fu, X.; Ji, H.; Liu, W.; Sun, P., Photo-ammonification of low molecular weight dissolved organic nitrogen by direct and indirect photolysis. *Science of the Total Environment* **2021**, *764*,

50. Görner, H., Electron transfer from aromatic amio acids to triplet quinones. *Journal of Photochem. & Photobiol. B* **2007**, *88*, 83-89

51. International Humic Substances Society (IHSS), https://humic-substances.org (accessed Aug 2, 2022).

52. Kibler, R., Initial Transformation of Photo-Viable Free Amino Acids in the Presence of Surrogate and Standard Dissolved Organic Matter Under Sunlit Irradiation. *Open Access Master's Theses, Michigan Technology University,* **2020.**

53. Moor, K. J.; Schmitt, M.; Erickson, P. R.; McNeill, K., Sorbic Acid as a Triplet Probe: Triplet Energy and Reactivity with Triplet-State Dissolved Organic Matter via $^1O_2$ Phosphorescence. *Environmental Science & Technology* **2019**, *53*, 8078-8086

54. Rosario-Ortiz, F. L.; Canonica, S., Probe compounds to assess the photochemical acitivity of dissolved organic matter. *Environmental Science & Technology* **2016**, *50* (23), 12532-12547

55. Agilent Technologies, Inc., Application Compendium: Amino Acid Analysis. https://www.agilent.com/cs/library/applications/compendium-%20aminoacidadvancebio-5994-0033EN-us-agilent.pdf (accessed Aug 2, 2022).

56. Dziekońska-Kubczak, U.; Pielech-Przybylska, K.; Patelski, P.; Balcerek, M. Development of the Method for Determination of Volatile Sulfur Compounds (VSCs) in Fruit Brandy with the Use of Hs–SPME/GC–MS. *Molecules* **2020**, *25* (5), 1232.

57. SEAL Anatytical, AQ2 Environmental Methods List Rev. 5 (USEPA). https://www.seal-analytical.com/Methods/Discrete-Methods/AQ2-EPA-Methods (accessed Aug 2, 2022).

58. Schum, S. K.; Brown, L. E.; Mazzoleni, L. R., MFAssignR: Molecular formula assignment software for ultrahigh resolution mass spectrometry analysis of environmental complex mixtures. *Environmental Research* **2020**, *191*, 110-114

59. Kosaka, K.; Yamada, H.; Matsui, S.; Echigo, S.; Shishida, K., Comparison amont

the Methods for Hydrogen Peroxide Measurements To Evaluate Advanced Oxidation Processes: Application of a Spectrophotometric Method Using Copper (II) Ion and 2,9-Dimethyl-1,10-phenanthroline. *Environmental Science & Technology* **1998**, *32*, 3821-3824

60. Brahmia, O. and Richard, C., Phototransformation of 1,4-naphthoquinone in aqueous solution. *Photochem. Photobiol. Sci.* **2003**, *2*, 1038-1043

61. Gay, C.; Collins, J.; Gebicki, J. M., Hydroperoxide Assay with the Ferric-Xylenol Orange Complex. *Analytical Biochemistry* **1999**, *273*, 149-155

62. Standard Methods Committee of the American Public Health Association, American Water Works Association, and Water Environment Federation. 5310 total organic carbon In: Standard Methods For the Examination of Water and Wastewater. **2018**. Lipps WC, Baxter TE, Braun-Howland E, editors. Washington DC: APHA Press.

63. Parker, K. M. and Mitch, W. A., Halogen radicals contribute to photooxidation in coastal and estuarine waters. *Proceedings of the National Academy of Sciences of the U.S.A.* **2016**, *113* (21), 5868-5873

64. Qu, S.; Kolodziej, E. P.; Cwiertny, D. M., Phototransformation Rates and Mechanisms for Synthetic Hormone Gorwth Promoters Used in Animal Agriculture. *Environmental Sicence and Tehcnology* **2012**, *46* (24), 13202-13211

65. Zhang, Z.; Chow, S.-Y.; De Guzman, R.; Joh, N. H.; Joubert, M. K.; Richardson, J.; Shah, B.; Wikström, M.; Zhou, Z. S.; Wypych, J. A Mass Spectrometric Characterization of Light-Induced Modifications in Therapeutic Proteins. *Journal of Pharmaceutical Sciences* **2022**, *111* (6), 1556–1564.

66. Viola, R. E. The Central Enzymes of the Aspartate Family of Amino Acid Biosynthesis. *Accounts of Chemical Research* **2001**, *34* (5), 339–349.

67. Veuger, B.; Middelburg, J. J., Incorporation of nitrogen from amino acids and urea by benthic microbes: role of bacteria versus algae and coupled incorporation of carbon. *Aquatic microbial ecology: international journal* **2007**, *48*, (1), 35-46.

68. Berman, T.; Bronk, D. A., Dissolved organic nitrogen: a dynamic participant in aquatic ecosystems. *Aquatic microbial ecology: international journal* **2003**, *31*, 279-305.

69. Bronk, D. A.; See, J. H.; Bradley, P.; Killberg, L., DON as a source of bioavailable nitrogen for phytoplankton. *Biogeosciences* **2007**, *4* (3), 283-296.

70. Hansell, D. A.; Carlson, C. A., Biogeochemistry of Marine Dissolved Organic Matter. *In Academic Press: US*, **2002**.

71. Bjørrison, P., Phytoplankton Exudation of Organic Matter: Why Do Healthy Cells Do it?. *Limnology and Oceanography* **1998**, *33* (1), 151-154

72. Giordano, M.; Norici, A.; Hell, R., Sulfur and Phytoplankton: Acquisition, Metabolism, and Impact on the Environment. *New Phytologist* **2005**, *166* (2), 371-382

73. Rosenstock, B.; Simon, M. Use of Dissolved Combined and Free Amino Acids by Planktonic Bacteria in Lake Constance. *Limnology and Oceanography* **1993**, *38* (7), 1521-1531

74. Sarmento, H.; Romera-Castillo, C.; Lindh, M.; Pinhassi, J.; Sala, M.; Gasol, J.; Marrase, C.; Taylor, G., Phytoplankton Species-Specific Release Of Dissolved Free Amino Acids And Their Selective Consumption By Bacteria. *Limnology and Oceanography* **2013**, *58* (3), 1123-1135.

75. Zubkov, M. V.; Tarran, G. A.; Mary, I.; Fuchs, B. M. Differential Microbial Uptake of Dissolved Amino Acids and Amino Sugars in Surface Waters of the Atlantic Ocean. *Journal of Plankton Research* **2007**, *30* (2), 211–220.

76. Cory, R. M.; Ward, C. P.; Crump, B. C.; Kling, G. W. Sunlight Controls Water Column Processing of Carbon in Arctic Fresh Waters. *Science* **2014**, *345* (6199), 925–928.

77. Kiene, R. P.; Linn, L. J.; González José; Moran, M. A.; Bruton, J. A. Dimethylsulfoniopropionate and Methanethiol Are Important Precursors of Methionine and Protein-Sulfur in Marine Bacterioplankton. *Applied and Environmental Microbiology* **1999**, *65* (10), 4549–4558.